Electric Technology U.S.S.R.

ЭЛЕКТРИЧЕСТВО

Volume 4, December, 1959

Selected papers from
Elektrichestvo Nos. 10, 11 and 12, 1958

blished by

ERGAMON PRESS NEW YORK LONDON OXFORD PARIS LOS ANGELES

for Pergamon Institute, Washington and Oxford

ELECTRIC TECHNOLOGY, U.S.S.R.

PERGAMON INSTITUTE

A DIVISION OF PERGAMON INTERNATIONAL CORPORATION, OPERATED IN THE PUBLIC SERVICE FOR THE FURTHERANCE AND DISSEMINATION OF SCIENTIFIC KNOWLEDGE

President of the Scientific Advisory Council:
Sir Robert Robinson, O.M., F.R.S.

Executive Director: Captain I. R. Maxwell, M.C.

Scientific Secretary: Dr. D. J. Hughes

1404 New York Avenue, N.W., WASHINGTON, 5, D.C. (Telephone No. Metropole No. 8-5382)

Headington Hill Hall, OXFORD. (Telephone No. Oxford 64881)

Pergamon Institute can occasionally use additional translators for science and engineering material to assist with this programme of translation from Russian and other Slavonic languages.

Scientists and engineers who have a knowledge of Russian, and who are willing to assist with this work, should apply to the Administrative Secretary of the Institute. They should write to either Washington, D.C., or Oxford for rates of payment and other details.

Financial assistance has also been received from A.S.E.A., Sweden

---

Four volumes per annum. Approximately 700 pages per annum.
Annual Subscription Rate £20 ($56).
Single volumes may be purchased for £6 ($14).

Orders should be sent to the distributors at either of the following addresses

4 & 5 Fitzroy Square, London W.1
122 East 55th Street, New York 22, N.Y.

PUBLISHED BY

PERGAMON PRESS LTD.

NEW YORK · LONDON · OXFORD · PARIS · LOS ANGELES

February 1960

EDDY CURRENTS IN SYNCHRONOUS AND ASYNCHRONOUS MACHINES WITH UNLAMINATED ROTORS*

I.M. POSTNIKOV

Kiev

(Received 17 April 1958)

In synchronous machines with unlaminated rotors it is very important to know the losses, caused in the rotor by higher harmonics of the m.m.f. of the armature, and also losses due to the fundamental harmonic during asynchronous running. These losses are sometimes called surface losses, since it is assumed that eddy currents only penetrate the rotor surface to a small depth. In fact, the depth of penetration depends on the frequency and magnetic properties of the rotor material, and may be very considerable.

The methods, which are widely used for calculating eddy currents, in many important cases give considerably different results and lead to exagerations. For example, in one recent work [1], we find an erroneous determination of the induction of the rotor surface due to eddy currents, and in consequence a greatly exaggerated value of losses was obtained. The application of the usual formulae to machines with a small air gap or for various materials and frequencies also leads to incorrect results. The reasons why the formulae of individual authors lead to widely divergent answers, are explained by a different evaluation of the screening effect and variable permeability.

As will be shown later, it is possible to obtain a method of calculating losses due to eddy currents, by which all the main factors that influence the magnitude of these losses are accounted for. The method discussed in this article may also serve for designing electromagnetic couplings, brakes, high-frequency heating etc.

We shall first analyse the phenomena connected with propagation with respect to the rotor surface of any one single sinusoidal wave of the armature m.m.f. of the order ν_1. The result is obtained by the summation of all possible harmonics (we assume that the superposition of results due to individual harmonics is admissible).

* *Elektrichestvo* No. 10, 7–14, 1958.

When the sinusoidal current flows in a three phase stator winding with an integral number of slots per pole and phase, a series of space waves of the order ν_1 is induced in the stator; these waves move in various directions; $\nu_1 = 6k + 1$, i.e. is equal to 1,5,7,11 and so on, ($k = 0, \pm 1, \pm 2, \pm 3$ etc.) During synchronous running, the fifth harmonic rotates in the opposite direction to the fundamental wave, the seventh harmonic rotates in the same direction as the fundamental wave. Therefore, the fifth and seventh harmonics during synchronous running induce harmonics in the rotor, the order of which is $\nu = \nu_1 - 1 = \pm 6$.

In a similar way, the 11th and 13th harmonics induce the 12th order harmonic and so on. Harmonics ν_1 which are multiples of 3, are absent. For the slip $s \neq 0$, $\nu = \nu_1 - (1 + s_1)$.
For windings with a fractional number of slots per pole and phase

$$q = b + \frac{c}{d} = \frac{bd + c}{d} = \frac{N}{d};$$

the order of the stator harmonics [2] for the six-zone windings is

$$\nu_1 = \frac{6k}{d} + 1$$

where k is any arbitrary integer, positive or negative, including zero; for the three-zone windings $\nu_1 = \frac{3k}{d} + 1$. In this case the fractional values of the m.m.f. order ν_1 appear in the stator, and $\nu = \nu_1 - 1$ in the rotor. Moreover, harmonic ripples appear, the order of which is $\nu_1 = k \frac{Z_1}{p} + 1$; since $\nu = \nu_1 - (1 + s\,\nu_1)$ then

for S = 0

$$\nu = k \frac{Z_1}{p}$$

where Z_1 is the number of the stator slots;
p is the number of pole pairs;
k is any arbitrary positive or negative integer.
when $k = \pm 1$, we have two fundamental ripple harmonics: direct and reverse. Both these harmonics induce in the rotor rotating at a synchronous speed a harmonic of the order of frequency $\nu = \frac{Z_1}{p}$
The fundamental harmonic $\nu_1 = 1$ during a synchronous running determines, in the rotor, the slip frequency $\nu = s$.

For a non-sinusoidal current, every current harmonic of the i-th time order produces its own series of space harmonics.

The frequency in the rotor will be $\nu_1 = i\,\nu$

Calculation of losses

In order to calculate the losses, it is necessary to determine the resultant induction in the rotor produced by a propagating wave of the stator m.m.f. of the order of ν_1. If we denote a co-ordinate that rotates together with the wave in question by X, then the amplitude of the m.m.f. wave $F_{\nu\,im}$ is equal to the integral of the linear load $A_{\nu\,im} \sin \frac{\pi}{\tau_{\nu_1}} x$ at the middle of the pole spacing $\frac{\tau_{\nu_1}}{2}$

$$F_{\nu im} = \int_0^{\frac{\tau_{\nu 1}}{2}} A_{\nu im} \sin \frac{\pi}{\tau_{\nu 1}} x \; dx = \frac{\tau_{\nu 1}}{\pi} A_{\nu im}. \tag{1}$$

The rotating wave of the linear load of the order of ν_1 can be represented in this form:

$$A_{\nu i} = A_{\nu im}\, e^{j\left(\frac{\pi \nu_1}{\tau} x' - \omega_i t\right)} = A_{\nu im}\, e^{j\frac{\pi \nu_1}{\tau} x}, \tag{2}$$

where $\tau_{\nu_1} = \frac{\tau}{\nu_1}$;

$\omega_i = \omega_1\, \nu_i$ is the angular frequency of the supply current (or angular frequency of rotation of the wave of the excitation current in the case of d.c. excitation).

The m.m.f. wave of the order of ν_1 induces in the rotor a corresponding m.m.f. due to induced currents of frequency

$$\omega_\nu = \omega_1 \nu i, \tag{3}$$

where νi – multiple of the frequency ω_1.

For $i = 1$, $\nu = [\nu_1 (1 - s) \pm 1]$; for $s = o$, $\nu = \nu_1 - 1$; for $\nu_1 = 1$, $\nu = s$,

(for a non-sinusoidal current $\nu_1 = i\nu$ for the current harmonic of the order of ν; further we assume $i = 1$, i.e. we assume a sinusoidal current).

The resultant field in the gap on the rotor surface and inside its body can be determined by solving Maxwell's differential equations for vectors of the magnetic field strength $H = \frac{B}{\mu}$, of the electric field $E = S'\rho$, and of the current density s μ if the permeability μ remains constant, i.e.

$$\text{rot}\,\dot{H} = \dot{s} = \frac{\dot{E}}{\rho}; \tag{4}$$

$$\text{rot}\,\dot{E} = -\frac{\partial \dot{B}}{\partial t} = -\mu \frac{\partial \dot{H}}{\partial t}. \tag{5}$$

In the majority of cases we can neglect the curvature of the rotor surface and consider it as a plane x-z (z is the direction of the rotor axis). The radial direction corresponds to y, ($y = o$ at the surface of the stator circle, $y = -\delta$ on the rotor

Constants α and α_1 are determined by substituting equation (10) into (8), i.e.

$$-\left(\frac{\pi\nu_1}{\tau}\right)^2+\alpha^2-\alpha_1^2+2j\alpha\alpha_1=-j\omega_\nu\frac{\mu}{\rho}, \tag{19}$$

where we get the set:

$$\left.\begin{aligned}\alpha^2-\alpha_1^2-\left(\frac{\pi\nu_1}{\tau}\right)^2&=0;\\ 2\alpha\alpha_1&=-\frac{\omega_\nu\mu}{\rho}.\end{aligned}\right\} \tag{20}$$

Solving (20) we get:

$$\left.\begin{aligned}\alpha&=\frac{1}{\sqrt{2}}\frac{\pi\nu_1}{\tau}\sqrt{1+\sqrt{1+\left(\frac{\omega_\nu\mu}{\rho}\frac{\tau^2}{\pi^2\nu_1^2}\right)^2}};\\ \alpha_1&=\frac{1}{\sqrt{2}}\frac{\pi\nu_1}{\tau}\sqrt{-1+\sqrt{1+\left(\frac{\omega_\nu\mu}{\rho}\frac{\tau^2}{\pi^2\nu_1^2}\right)^2}}.\end{aligned}\right\} \tag{21}$$

Except for very high values of ν_1, very low frequencies ω_ν and small values of μ, which have no practical significance, the quantity $\left(\frac{\omega_\nu\mu}{\rho}\cdot\frac{\tau^2}{\pi^2\nu_1^2}\right)^2$ is considerably greater than unity, and consequently

$$\alpha=\alpha_1=\sqrt{\frac{\mu\omega_\nu}{2\rho}}=\frac{1}{\Delta_\nu}, \tag{22}$$

where the quantity, which is the reciprocal of the conventional depth of penetration, is given by:

$$\Delta_\nu=\sqrt{\frac{2\rho}{\mu\omega_\nu}}. \tag{23}$$

In this case equations (17) and (18) assume the following form:

$$H_x=\frac{B_{\nu 0}\tau}{j\mu\pi\nu_1\Delta_\nu}(1+j)e^{\frac{\mu+\delta}{\Delta_\nu}}e^{j\left(\frac{\pi\nu_1}{\tau}x+\frac{\mu+\delta}{\Delta_\nu}\right)}; \tag{24}$$

$$H_y=\frac{B_{\nu 0}}{\mu}e^{\frac{\mu+\delta}{\Delta_\nu}}e^{j\left(\frac{\pi\nu_1}{\tau}x+\frac{\mu+\delta}{\Delta_\nu}\right)}. \tag{25}$$

Determination of constants C_1 and C_2 and induction on the rotor surface $B_{\nu 0}$

1. Normal components of the induction on the surface of separation should vary continuously.

The tangential components of the magnetic field strength vary continuously in the

surface, in the rotor centre we can assume $y = -\infty$). We assume that the rotor surface is smooth since the influence of slots in cylindrical rotors or of interpole spaces in salient pole rotors is to a certain degree compensated by the losses on the slot walls, on the metal wedges or on the radial surfaces of the poles shoes. Moreover, we neglect at first the influence of frontal parts, i.e. we assume that all currents flow in the axial direction, and, consequently, we have:

$$E_x = E_y = 0, \quad E_z = E, \quad \frac{\partial E}{\partial z} = \frac{\partial^2 E}{\partial z^2} = 0.$$

Under these conditions, applying the operation:

$$\text{rot rot } \dot{E} = -\nabla^2 \dot{E},$$

for the solenoidal vector E from (4) and (5) we get:

$$\frac{\partial^2 \dot{E}}{\partial x^2} + \frac{\partial^2 \dot{E}}{\partial y^2} = \frac{\mu}{\rho} \frac{\partial \dot{E}}{\partial t}. \tag{6}$$

Similar equations are obtained for vectors H and s.

For the region of the air gap the right-hand side of equation (6) is zero. The solution of equation (6) for cases when E is a periodic function of x of the form:

$$f(x) = \cos \frac{\pi \nu_1}{\tau} x; \quad f(x) = \sin \frac{\pi \nu_1}{\tau} x,$$

or in a complex form, $\exp\left(-j \frac{\pi \nu_1}{\tau} x,\right)$ it is:

$$E = \varphi(y) e^{j \frac{\pi \nu_1}{\tau} x} =$$

$$= \left(C_1 e^{-j \frac{\pi \nu_1}{\tau} y} + C_2 e^{j \frac{\pi \nu_1}{\tau} y}\right) e^{j \frac{\pi \nu_1}{\tau} x}. \tag{7}$$

For the rotor body, equation (6) for a field varying sinusoidally with time $E = E(x, y) \cdot \exp(-j W_\nu t)$ is of this form:

$$\frac{\partial^2 E}{\partial x^2} + \frac{\partial^2 E}{\partial y^2} = -j\omega_\nu \frac{\mu}{\rho} E. \tag{8}$$

This equation is satisfied by the function

$$E = (C_3 e^{\beta y} + C_4 e^{-\beta y}) e^{j \frac{\pi \nu_1}{\tau} x}, \tag{9}$$

where $\beta = a + j a_1$ is a complex number, which is determined by substituting (9) into (8).

Since, for $y = -\infty$, $E = o$, then the second solution $C_4 \exp(-\beta y)$ has no meaning and should be made equal to zero.

Putting on the rotor surface $y = -\delta$ and assuming the value of the E on the surface $E_{\nu 0} = -B_{\nu 0} U_\nu$, where $B_{\nu 0}$ and U_ν are the induction and the wave tangential speed on the surface, we get

$$E = E_{v0} e^{\dot{\beta}(y+\delta)} e^{-j\frac{\pi v_1}{\tau}x} =$$

$$= B_{v0} v_v e^{\dot{\beta}(y+\delta)} e^{-j\frac{\pi v_1}{\tau}x}; \tag{10}$$

$$v_v = \frac{\omega_v \tau}{\pi v_1}; \tag{11}$$

$$C_3 = -\frac{\omega_v B_{v0} \tau}{\pi v_1}. \tag{12}$$

Equations for the magnetic field strength H in the gap and inside the rotor body can be obtained from (7) and (10) by using equation (5). For a field varying sinusoidally with time, the equation assumes the form:

$$\text{rot}\,\dot{E} = -\mu\frac{\partial \dot{H}}{\partial t} = j\omega_v \mu \dot{H};$$

$$\text{rot}_x \dot{E} = \frac{\partial E_z}{\partial y} - \frac{\partial E_y}{\partial z} = \frac{\partial E}{\partial y} \quad \text{(since } \frac{\partial E_y}{\partial z} \text{ is by assumption zero, } E_z = E\text{)}$$

$$\text{rot}_y \dot{E} = \frac{\partial E_x}{\partial z} - \frac{\partial E_z}{\partial x} = -\frac{\partial E}{\partial x} \quad \text{(since } \frac{\partial E_x}{\partial z} \text{ is by assumption zero).}$$

Therefore:

$$H_x = \frac{1}{j\omega_v \mu}\frac{\partial E}{\partial y}; \tag{13}$$

$$H_y = -\frac{1}{j\omega_v \mu}\frac{\partial E}{\partial x}. \tag{14}$$

Taking partial derivatives of (7) and (10) we get for the region of the air gap:

$$H_x = -\frac{\pi v_1}{j\omega_v \mu_0 \tau}\left(C_1 e^{-\frac{\pi v_1}{\tau}y} - C_2 e^{\frac{\pi v_1}{\tau}y}\right) e^{j\frac{\pi v}{\tau}x}; \tag{15}$$

$$H_y = -\frac{\pi v_1}{\omega_v \mu_0 \tau}\left(C_1 e^{-\frac{\pi v_1}{\tau}y} + C_2 e^{\frac{\pi v_1}{\tau}y}\right) e^{j\frac{\pi v_1}{\tau}x}, \tag{16}$$

and for the region of the rotor body:

$$H_x = \frac{1}{j\omega_v \mu}\cdot\frac{\partial E}{\partial y} =$$

$$= -\frac{B_{v0}\tau}{j\mu\pi v_1}(\alpha + j\alpha_1) e^{(\alpha+j\alpha_1)(y+\delta)} e^{j\frac{\pi v_1}{\tau}x}; \tag{17}$$

$$H_y = \frac{B_{v0}}{\mu} e^{(\alpha+j\alpha_1)(y+\delta)} e^{j\frac{\pi v_1}{\tau}x}. \tag{18}$$

absence of surface currents (we consider the rotor currents as distributed inside the rotor body, and not confined to the surface).

The first condition causes equation (25), for $y = -\delta$, multipled by μ to become:

$$-\frac{\pi\nu_1}{\omega_\nu\tau}\left(C_1 e^{\frac{\pi\nu_1}{\tau}\delta}+C_2 e^{-\frac{\pi\nu_1}{\tau}\delta}\right)=B_{\nu 0}. \tag{26}$$

The second condition causes equation (24), for $y = -\delta$, to be equivalent to equation (15) for $y = -\delta$, i.e.

$$-\frac{\pi\nu_1}{j\omega_\nu\mu_0\tau}\left(C_1 e^{\frac{\pi\nu_1}{\tau}\delta}-C_2 e^{-\frac{\pi\nu_1}{\tau}\delta}\right)=-\frac{B_{\nu_0}\tau}{j\pi\mu'\nu_1\Delta_\nu}(1+j). \tag{27}$$

From these two conditions we get:

$$C_1=-\frac{1}{2}\frac{B_{\nu_0}\omega_\nu\tau}{\pi\nu_1}\left[1-\frac{\tau(1+j)}{\pi\mu'\nu_1\Delta_\nu}\right]e^{-\frac{\pi\nu_1}{\tau}\delta}; \tag{28}$$

$$C_2=-\frac{1}{2}\frac{B_{\nu 0}\omega_\nu\tau}{\pi\nu_1}\left[1+\frac{\tau(1+j)}{\pi\mu'\nu_1\Delta_\nu}\right]e^{\frac{\pi\nu_1}{\tau}\delta}, \tag{29}$$

where $\mu_1=\frac{\mu}{M_0}$ is the relative permeability of the rotor material.

The third condition is that on the rotor surface i.e. for $y = o$, according to the law of the total current the tangential component H_x of the field strength from equation (15) should be equal to the linear load $A_{\nu 1m}$ (we neglect the field strength in the stator steel).

$$-\frac{\pi\nu_1}{j\omega_\nu\mu_0\tau}(C_1-C_2)=A_{\nu 1m}. \tag{30}$$

Substituting the values of the constants C_1 and C_2 obtained in this way, we get the value of the induction on the surface:

$$\dot{B}_{\nu 0}=\frac{\mu_0 A_{\nu 1m}}{\sinh\frac{\pi\nu_1}{\tau}\delta+(1+j)\frac{\tau}{\nu_1\mu'\pi\Delta_\nu}\operatorname{ch}\frac{\pi\nu_1}{\tau}\delta}, \tag{31}$$

or

$$B_{\nu 0}=\frac{\mu_0 A_{\nu 1m}}{\sqrt{\left(\sinh\frac{\pi\nu_1}{\tau}\delta+\frac{\tau}{\mu'\nu_1\pi\Delta_\nu}\operatorname{ch}\frac{\pi\nu_1}{\tau}\delta\right)^2+\left(\frac{\tau}{\mu'\nu_1\pi\Delta_\nu}\operatorname{ch}\frac{\pi\nu_1}{\tau}\delta\right)^2}} \tag{32}$$

In the absence of currents in the rotor, we would have:

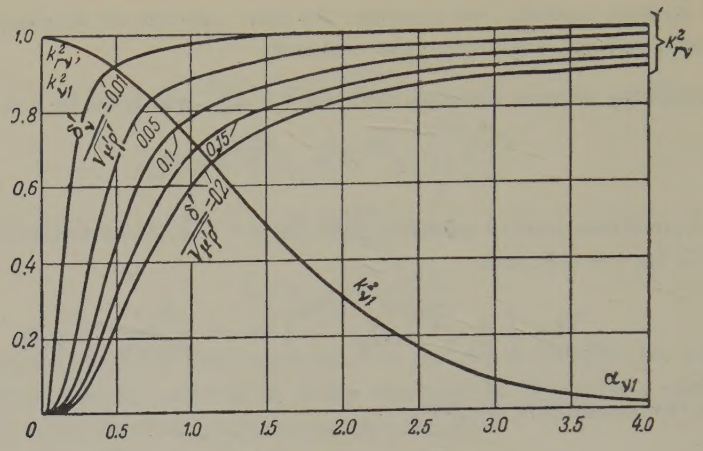

FIG. 1.

$$B_{v0} = \frac{\mu_0 A_{v1m}}{\sinh \frac{\pi \nu_1}{\tau} \delta}, \tag{33}$$

and for small values of $\frac{\pi \nu_1}{\tau} \delta$, when we can put:

$$\sinh \frac{\pi \nu_1}{\tau} \delta \approx \frac{\pi \nu_1}{\tau} \delta,$$

we have:

$$B_{v0} = \frac{\mu_0 A_{v1m} \tau}{\pi \nu_1 \delta} = \frac{\mu_0 F_{v1m}}{\delta}. \tag{34}$$

It is expedient to introduce two factors:

$$k_{v1} = \frac{\alpha_{v1}}{\sinh \alpha_v}; \tag{35}$$

$$k_{rv} = \frac{1}{\sqrt{\left(1 + \frac{\tau}{\Delta_v \mu' \nu_1 \pi \operatorname{th} \alpha_{v1}}\right)^2 + \left(\frac{\tau}{\Delta_v \mu' \nu_1 \pi \operatorname{th} \alpha_{v1}}\right)^2}}, \tag{36}$$

where

$$\alpha_{v1} = \frac{\pi \nu_1 \delta}{\tau}.$$

The first factor accounts for the field attenuation due to the finite gap magnitude, and the second one – the back influence of the rotor currents, i.e. it is equal to the field attenuation factor or to the reaction factor of the rotor currents (Fig. 1). Thus, we obtain the expression for the induction on the surface in this form:

$$B_{v0} = \frac{\mu_0 F_{v1m}}{\delta} k_{v1} k_{rv}. \tag{37}$$

Losses per unit area of the unlaminated rotor due to the harmonic of the order of ν are:

$$w_\nu = \frac{B_{\nu 0}^2 \tau^2 f_1^{1,5} \nu^{1,5}}{\nu_1^2 \sqrt{\pi \mu \rho}} \left[\frac{W}{cm^2}\right]. \tag{38}$$

This expression can be obtained from equations (10) and (24) as the real part of the Umov–Poynting vector:

$$w_\nu = \frac{1}{2} \operatorname{Re} \left| \dot{H} E^* \right| = \frac{1}{2} H_{x0} E_0 . \tag{38a}$$

The imaginary part becomes equal to the real part and is equal to the mean value of the reactive power per unit of the reactor surface. Substituting the value of B_{ν_0} into (38) we get:

$$w_\nu = \frac{\mu_0^2 F_{\nu 1 m}^2 k_{\nu 1}^2 k_{r\nu}^2 \tau^2 f_1^{1,5} \nu^{1,5}}{\delta^2 \nu_1^2 \sqrt{\pi \mu_0 \mu' \rho}} \cdot \left[\frac{W}{cm^2}\right]. \tag{39}$$

The amplitude of the m.m.f. of the stator harmonic of the order of ν_1 can be expressed by means of the m.m.f. of the fundamental wave F_1 in the form:

$$F_{\nu 1 m} = \frac{1}{\nu_1} F_{1m} \frac{k_{w\nu 1}}{k_{w1}}, \tag{40}$$

where

$$F_{1m} = \frac{\sqrt{2}\, m}{\pi p} w I_1 k_{w1} = \frac{\sqrt{2}\, A_1 \tau k_{w1}}{\pi}, \tag{41}$$

$A_1 = \dfrac{F_1 \pi}{\sqrt{2} \tau k_{w1}}$ is the active value of the linear load of the fundamental wave.

Hence, substituting (40) and (41) into (39) we get:

$$w_\nu = \frac{2\mu_0^2 A_1^2 \tau^4 c f_1^{1,5}}{\pi^2 \sqrt{\pi \mu_0 \rho_{Cu}}\, \delta^2 \sqrt{\mu' \rho'}} \left(\frac{k_{w\nu 1}}{\nu_1^2}\right)^2 k_{\nu 1}^2 k_{r\nu}^2 \nu^{1,5} \left[\frac{W}{cm^2}\right], \tag{42}$$

where $\rho' = \dfrac{\rho}{\rho_{Cu}}$; for steel $\rho = 6\text{-}10$.

Taking the sum for all values of ν_1 and ν and multiplying it by the rotor area, we obtain total losses:

$$P_{\nu R} = 4.5 \times 10^{-8} \left(\frac{f_1}{50}\right)^{1.5} \frac{A_1^2 \tau^4 S_R}{\delta^2 \sqrt{\mu' \rho'}} \varphi [W], \tag{43}$$

where $S_R = 2p\tau l$ – the rotor area

$\rho_{Cu} = 1.6 \times 10^{-6}$ ohm.cm.

$$\varphi = \sum_{\nu 1} \left(\frac{k_{w\nu 1}}{\nu_1^2} \right)^2 k_{\nu 1}^2 k_{r\nu}^2 \nu^{1.5} . \tag{44}$$

For the range of frequencies and values of $\sqrt{\mu' \rho'}$, for which we can assume $k^2_{\nu 1} \approx 1$, and the screening factor $k^2_{r\nu} \approx 1$ we have:

$$\varphi = \varphi_1 = \sum_{\nu_1} \left(\frac{k_{w\nu 1}}{\nu_1^2} \right)^2 \nu^{1.5}, \tag{45}$$

ϕ and ϕ_1 as functions of the winding pitch y, expressed in fractions of τ, for windings with an integral number of slots per pole and phase, are represented for higher space harmonics, $\nu = \nu_1 - 1$, in Fig. 2. In this case,

$$k_{w\nu 1} = k_{y\nu 1} \cdot k_{p\nu 1}; \quad k_{y\nu 1} = \sin \nu_1 \frac{\pi}{2} y; \quad k_{p\nu 1} = \frac{\sin 30^\circ}{q \sin \frac{30^\circ}{q} \nu_1}.$$

For six-zone windings, with a fractional number of slots per pole and phase $k_{y\nu 1} = \sin \nu_1 \frac{\pi}{2} y$, the distribution factor when d is even is:

$$k_{p\nu 1} = \frac{\sin 30^\circ}{N \left(\cos \frac{30^\circ}{N} \right) y_w \nu_1 d};$$

when d is odd we have to substitute into the denominator $\sin \frac{30^\circ}{N}$ instead of $\frac{30^\circ}{N}$.

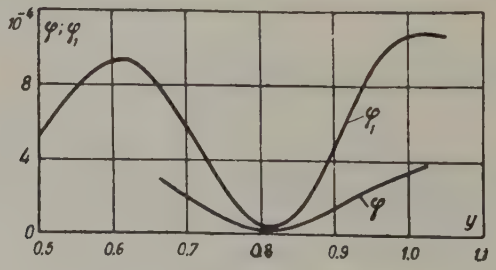

FIG. 2.

Here $N = bd + c$ — numerator of an improper fraction for q;

$y_w = \frac{1 + Ngm}{d}$ is the difference of the numbers of the adjacent rays of the slot star;

g — is the smallest integer ($g > 1$) which makes y_w an integer;

m — is the number of phases.

According to the method discussed in [3] we assume that the factor $k^2_{r\nu}$ is the

same for all harmonics and is equal to $k_d \simeq 0.5-0.6$, the value of $\sqrt{\mu'\rho'}$ being included in the constant k_0. With this method of calculation we may get wrong results if the value of $\sqrt{\mu'\rho'}$ varies. Indeed, from (42) it follows that, for $k^2_{r\nu}$ = const., the losses when $\sqrt{\mu'\rho'}$ decreases. However, with the decrease of $\sqrt{\mu'\rho'}$, due to the screening effect, the factor $k^2_{r\nu}$ might decrease still faster, and the losses will decrease. If we substitute into (36) the value of the depth of penetration Δ_ν (formula (23)) we get:

$$k^2_{r\nu} = \frac{1}{\left(1+\frac{\delta'_\nu}{\sqrt{\mu'\rho'}\cdot\alpha_{\nu 1}\,\mathrm{th}\,\alpha_{\nu 1}}\right)^2+\left(\frac{\delta'_\nu}{\sqrt{\mu'\rho'}\,\alpha_{\nu 1}\,\mathrm{th}\,\alpha_{\nu 1}}\right)^2}, \tag{46}$$

where $\delta'_\nu = \sqrt{\frac{\mu_0\omega_1\nu}{2\rho_{Cu}}}\,\delta.$

For $\rho = \rho_{Cu} = 1.6 \times 10^{-6}$ ohm.cm., $f_1 = 50$ c/s. we get:

$$\delta'_\nu = \sqrt{\nu}\cdot\delta. \tag{47}$$

Graphs of $k^2_{r\nu}$ and $k^2_{r\nu}k^2_{\nu 1}$ as functions of $\alpha_{\nu 1}$ for various values of $\frac{\delta'_\nu}{\sqrt{\mu'\rho'}}$ are shown respectively in Figs. 1 and 3.

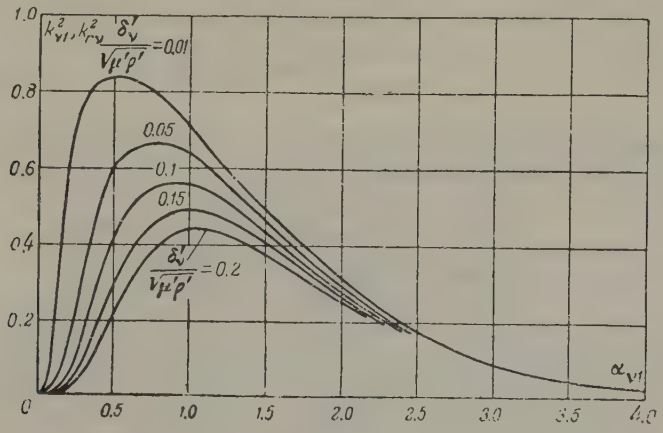

FIG. 3.

Instead of (42) we get

$$w_\nu = \frac{2\mu_0^2}{\sqrt{\pi\mu_0\rho_{Cu}}}\,\frac{A_1^2\tau^2}{\delta}\cdot f_1^{1.5}\left(\frac{k_{\alpha\nu 1}}{\nu_1}\right)^2\varphi_{x\nu\nu}, \tag{48}$$

where $\phi_{x\nu}$ is a function of: the space order ν_1 of the constant $x_\nu = \frac{\sqrt{\nu}\,\delta}{\sqrt{\mu'\rho'}}$ and the frequency in the rotor ν, (Fig. 4):

Taking into consideration (40) and (41) we get:

$$\varphi_{x\nu} = \frac{x_\nu}{\left(\sinh\alpha_{\nu 1} + \frac{x_\nu \operatorname{ch}\alpha_{\nu 1}}{\alpha_{\nu 1}}\right)^2 + \left(\frac{x_\nu \operatorname{ch}\alpha_{\nu 1}}{\alpha_{\nu 1}}\right)^2}. \qquad (48a)$$

Taking into consideration (40) and (41) we get:

$$w_\nu = \frac{(\pi\mu_0 f_1)^{1.5}}{\sqrt{\rho_{Cu}}} \cdot \frac{F_{1m}^2}{\delta} \cdot \psi(\nu,\mu) = 2{,}17 \cdot 10^{-6} \frac{F_{1m}^2}{\delta} \cdot \psi(\nu,\mu),$$

where

$$\psi(\nu,\mu) = \left(\frac{k_{w\nu 1}}{k_{w1}\nu_1}\right)^2 \varphi_{x\nu} \sqrt{\nu}.$$

For small values of $\alpha_{\nu 1}$ it is more convenient to express the function $\phi_{x\nu}$ in this form:

$$\varphi_{x\nu} = \frac{\alpha_{\nu 1}^2}{x_\nu \cosh^2\alpha_{\nu 1}\left[1 + \left(1 + \frac{\alpha_{\nu 1} \operatorname{th}\alpha_{\nu 1}}{x_\nu}\right)^2\right]}. \qquad (49)$$

As can be seen, when the values of $\sqrt{\mu'\rho'}$, $\alpha_{\nu 1}$ and δ'_ν vary, $\phi_{x\nu}$ assumes a certain maximum value $\phi_{x\nu max}$ which is determined from the equation $\partial\phi_{x\nu}/\partial x_\nu = 0$, and in this case $X_\nu = \alpha_{\nu 1}\operatorname{tank}\alpha_{\nu 1}/\sqrt{2}$. Substituting this value of X_ν into (49) we get:

$$\phi_{x\nu max} \approx 0.2 \text{ (Fig. 4).}$$

We can express the formulae for losses per unit area, (42) and (48), for small values of $\alpha_{\nu 1}$ in a more convenient form:

$$\varphi_{x\nu} = \frac{\sqrt{\mu'\rho'}\,\pi^2\delta^2\nu_1^2}{\cosh\alpha_{\nu 1}\sqrt{\nu}\,\delta\tau^2\left[1 + \left(1 + \frac{\alpha_{\nu 1}\operatorname{th}\alpha_{\nu 1}}{x_\nu}\right)^2\right]}. \qquad (50)$$

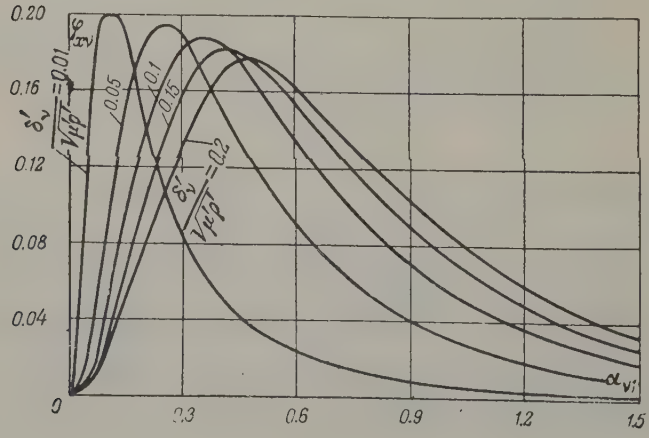

FIG. 4.

Substituting the last expression into (48) we get

$$w_\nu = \frac{1}{\sqrt{2}} \frac{(\mu_0 \omega_1)^{1.5}}{\sqrt{\rho_{Cu}}} A_1^2 C_{\mu\nu}, \tag{51}$$

where

$$C_{\mu\nu} = C'_{\mu\nu} k^2_{w\nu_1} \sqrt{\mu'\rho'} \sqrt{\nu}; \tag{51a}$$

$$C'_{\mu\nu} = \frac{1}{\cosh^2 \frac{\pi\delta\nu_1}{\tau} \left[1 + \left(1 + \frac{\alpha_{\nu 1} \operatorname{th} \alpha_{\nu 1} \sqrt{\mu'\rho'}}{\sqrt{\nu}\,\delta}\right)^2\right]}. \tag{52}$$

The graph of $C'_{\mu\nu}$ as a function of $\alpha_{\nu 1}$ is shown in Fig. 5.

The factor $C_{\mu\nu}$ takes into account: the order of the space harmonic ν_1, the frequency ν of the harmonic induced in the rotor, the distribution factor $k_{w\nu 1}$, the properties of the rotor material ($\sqrt{\mu'\rho'}$) and the ratio $\frac{\delta}{\tau}$. Under these conditions, the losses depend on the product of the square of the linear load by $C_{\mu\nu}$ and by the constant value of the factor $1/(\mu_0 \omega_1)^{1.5-0.5} \rho_{Cu}$; Here, ω_1 is equal to $2\pi\phi_1$ for fields excited by multiphase currents, and for fields excited by d.c. currents it is equal to the angular speed of rotation of the wave of the excitation field $\omega_{rot} = 2\pi\phi_{rot}$.

Summary losses will be:

$$P_{\nu R} = \frac{1}{\sqrt{2}} \frac{(\mu_0 \omega_1)^{1.5}}{\sqrt{\rho_{Cu}}} A_1^2 S_R \sum_\nu C_{\mu\nu} \approx$$
$$\approx 4.34 \cdot 10^{-6} A_1^2\, 2p\tau l \sum_\nu C_{\mu\nu} [\mathrm{W}]. \tag{53}$$

The formulae obtained are universal for all kinds of losses due to eddy currents. In particular they allow the determination of parameters r_2 and x_2 of an unlaminated rotor for the fundamental wave when the frequency in the rotor is $\nu = s$.

In fact, neglecting the magnetizing current, we get:

$$P_\nu = \frac{(\mu_0 \omega_1)^{1.5}}{\sqrt{2\rho_{Cu}}} A_1^2 2p\tau l C_{\mu\nu} = m I_1^2 r'_2. \tag{54}$$

Hence, taking into account that $\nu = s$, $\nu_1 = 1$, $A_1 = \frac{m w_1 I_1}{p\tau}$ we find the resistance reduced to the stator:

$$r'_2 = \frac{(\mu_0 \omega_1)^{1.5} (2\rho_{Cu})^{-0.5} A_1^2 2p\tau l C_{\mu\nu}}{m I_1^2} =$$

$$= \sqrt{2}\,\frac{(\mu_0\omega_1)^{1.5}}{\sqrt{\rho_{Cu}}}\,\frac{lm\,w_1^2 k_{w1}^2 \sqrt{\mu'\rho'}\sqrt{s}}{p\tau\left[1+\left(1+\frac{\pi^2\delta\sqrt{\mu'\rho'}}{\tau^2\sqrt{s}}\right)^2\right]}, \tag{55}$$

and in this case $k_{w\nu 1} = k_{w1}$; $\cos h\, a_{\nu 1} \approx 1$.

It was shown earlier that for $a = a_1$ losses per unit area are equal to the mean value of the power of the magnetic field inside the rotor body, therefore the resistance is equal to the internal reactance:

$$r_2' = r_{2i}' = X_{2i}.$$

To account for the influence of frontal parts, variation of μ with the depth of penetration and hysteresis losses [4 and 8] we introduce the factors:

$$r_2' = a_r k_\delta r_{2i}', \quad x_2' = a_x k_\delta x_{2i}', \tag{56}$$

where

$$a_r \approx 1.4, \quad a_x \approx 0.85.$$

Factor a_r should also be substituted for the evaluation of losses by formula (53). The influence of the frontal parts is approximately accounted for by multiplying r_{2i}' x_{2i}' by the factor

$$k_\delta \approx 1 + \frac{2}{\pi}\cdot\frac{\tau}{l}. \tag{57}$$

The usual formula for r_2' [8] was obtained in this form:

$$r_2' = a_r k_\delta \frac{l}{\tau p}\, 2m\,(w_1 k_{w1})^2 \sqrt{\frac{\mu_0\omega_1\rho}{2}}\cdot\sqrt{\mu' s}.$$

On comparing this formula with (55) and in connexion with (56) and (57) we see that it differs by the factor $k_{\delta s} = \dfrac{2}{1+\left(1+\dfrac{\pi^2\delta\sqrt{\mu'\rho'}}{\tau^2\sqrt{s}}\right)^2}$; for large values of s, $k_{\delta s} \approx 1$.

The influence of the transverse slotting of the surface can be accounted for by introducing the increased value of ρ' equal to $\rho\frac{u}{l}$, where u is the perimeter of the slotted surface along the length; l is the rotor active length.

For the longitudinal slotting or when the slots are not deep we may use the decreased value of $\rho'' = \rho'\dfrac{\pi D_R}{u'}$ where u' is the perimeter of the slotted surface measured on the circumference.

Formulae (42) to (53) can be used for an approximate calculation of losses on the

laminated rotor surface or on the surface of the stator circle by introducing increased values of δ'_r.

$$\rho'_r = \rho'\left(1 + \frac{\tau}{\pi\nu_1\Delta_1}\right), \tag{58}$$

where Δ_1 – thickness of the lamina.
For calculating losses due to the ripple harmonics induced by the armature current, we may use formula (42), after summing the losses due to harmonics $\nu_1 = k\frac{Z_1}{p} + 1$; for this purpose we can assume that $k_{wv} \approx k_{wl}$ is approximately equal to unity.

For the first two harmonics ($k = \pm 1$) we may approximately assume that

$$\left(\frac{\tau}{\nu_1}\right)^4 \approx \left(\frac{\tau p}{Z_1}\right)^4 = \left(\frac{t_1}{2}\right)^4,$$

where $t_1 = \frac{2p\tau}{Z_1}$ – is the pitch of the slot. In this case, according to (42), for the two ripple harmonics of the first order we get:

$$w_{z1} = \frac{2\mu_0 A_1^2 t_1^4 f_1^{1.5}\left(\frac{Z_1}{p}\right)^{1.5} k_{\nu 1}^2 k_{r\nu}^2}{8\pi^2\sqrt{\pi\mu_0\rho_{Cu}}\,\delta^2\sqrt{\mu'\rho'}} \quad [W/cm^2] \tag{59}$$

In summing the series for all harmonics we get approximately twice the value of (59), i.e. for $\rho_{Cu} = 1.6 \times 10^{-6}$ ohm.cm; $\mu_0 = 0.4\,\pi \times 10^{-8}$ H/cm;

$$w_z \approx 1.13 \times 10^{-8}\,\frac{A_1^2 t_1^4\left(\frac{Z_1}{p}\right)^{1.5}}{\delta^2\sqrt{\mu'\rho'}}\left(\frac{f_1}{50}\right)^{1.5} k_{r\nu}^2 k_{\nu 1}^2. \tag{60}$$

It is seen from (60) that for the correct ratio $\frac{t_1}{\delta}$, these losses are considerably smaller than the losses due to the space harmonics.

The influence of the value $\sqrt{\mu'\rho'}$.

As can be seen from (48) there is a value of $\sqrt{\mu'\rho'}$ for which, when a frequency ν_1 a space order ν_1 and ratio $\frac{\delta}{\tau}$ are given, maximum losses occur. The value of μ' is a function of the field strength and depends on the saturation of the steel. The problem of a proper choice of μ' when calculating eddy currents has been investigated in detail in a number of works.

For purposes of approximation, we may assume a certain effective value of μ'. To calculate losses due to higher harmonics in rotors made of mild steel we may assume $\sqrt{\mu'\rho'} = 100$, because of the comparatively small field strength of these harmonics and with regard to the saturation due to the fundamental field.

For a copper surface, $\sqrt{\mu'\rho'} = 1$. For strong saturations which can occur owing to the fundamental wave at the asynchronous start, the value of $\sqrt{\mu'\rho'}$ can amount to 30 or less. The influence of $\sqrt{\mu'\rho'}$ on losses for the given values of ν_1, ν and $\frac{\delta}{\tau}$ can be determined from (49) and (50).

Application of formulae (39) to (52) for calculating losses for non-sinusoidal current.

The formulae can be supplied for any current harmonic of the order i. For this purpose it is sufficient to substitute $A_i = k_i A_l$ instead of A_l, where k_i is the ratio of the amplitude of the i^{th} current harmonic to the amplitude of the fundamental wave, and to substitute $i\nu$ instead of ν. Total losses will be found by the summation of losses due to the time harmonics of all orders.

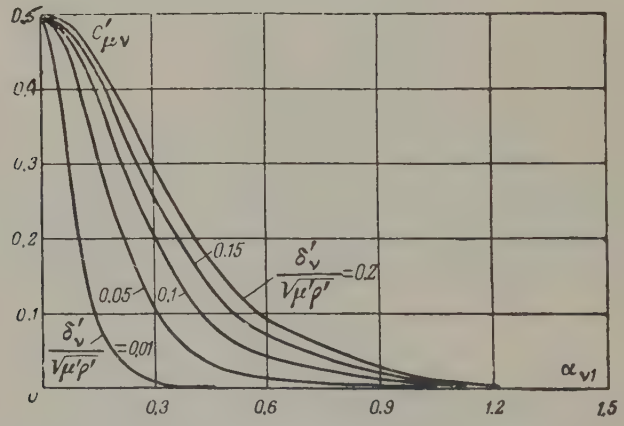

FIG. 5.

EXAMPLE

Data of the turbogenerator of 37, 500 kVA power, 3000 rev/min; $\tau = 137\,cm$, $t_1 = 5.09$ cm; $k_{w1} = 0.9$, $Z_1 = 54$; $A_1 = 814\ A/cm$; $\delta = 3.3\,cm.$; $\gamma = 0.78$. By formula (43) we calculate losses due to higher harmonics:

$$\Sigma w_\nu = 1.4 \cdot 4.5 \cdot 10^{-8} \frac{814^2 \cdot 137^4}{3.3^2 \cdot 100} 0.4 \cdot 10^{-4} = 0.545 \frac{W}{cM^2}.$$

The coefficient 1.4 is introduced to account for the hysteresis losses (R-4) Function $\phi = 0.4 \times 10^{-4}$ is taken from Fig. 2 with the response accounted for. By the method given in [6] neglecting hysteresis losses we get $\Sigma w_\nu = 1.48$ W/cm^2. As can be seen, the first method gives too small a value for losses, the second one – too big a value.

Losses due to the ripple harmonics for the example in question by formula (6)

and for $a_\nu = 1.4$ are:

$$w_z = 1.4 \cdot 1.3 \cdot 10^{-8} \frac{814^2 \cdot 5.09^4 \cdot 0.02 \cdot 54^{1.5}}{3.3^2 \sqrt{100}} = 0\,051 \frac{W}{cM^2};$$

here $k_{r\nu}^2 k_{\nu 1}^2 = 0{,}02$ (Fig. 3) for

$$a_{\nu 1} = \frac{\pi \nu_1 \delta}{\tau} = \frac{\pi Z_1 \delta}{p\tau} = \frac{2\pi\delta}{t_1} = \frac{2\pi \cdot 3{,}3}{5{,}09} = 4{,}06. \qquad (N)$$

As can be seen these losses in our case are considerably smaller than those losses due to higher harmonics.

Translated by S. Szymanski.

REFERENCES

1. G. Barello; *Rev. gen. elect. No. 11 (1955).*
2. T.G. Soroker and Iu. V. Mordvinov; *Sostavlenie skhem i raschet obmotochnykh koeffitsientov obmotok peremennogo toka (Circuit design and calculation of the distribution factors of a.c. windings), VEP,* No. 2 (1955).
3. A.E. Alekseyev and M.P. Kostenko; *Turbogeneratory (Turbogenerators),* Gosenergizdat (1939).
4. L.P. Neiman; *Poverkhnostnyi effekt v ferromagnitnykh telakh (Surface effect in ferromagnetic bodies),* Gosenergizdat (1949).
5. I.A. Syromiatnikov; *Rezhim raboty sinkhronnykh dvigatelei (Operational conditions of synchronous motors),* Gosenergizdat (1952).
6. R. Rikhter; *Elektricheskiye mashiny t.I i II (Electrical machines, vols. I and II),* Gosenergizdat (1936).
7. W.I. Gibbs; *JIEE,* No. 46 (1948).
8. I.M. Postnikov; *Proyektirovanie elektricheskikh mashin (Designing electrical machines),* Gostekhizdat U.S.S.R (1952).

COMPENSATION OF CAPACITIVE CURRENTS IN DIFFERENTIAL PHASE CARRIER PROTECTION OF TRANSMISSION LINES *

E.D. SAPIR

All-Union Scientific and Research Institute of Electroenergetics

(Received 9 September 1957)

Capacitive susceptance in long distance transmission lines makes differential phase carrier protective gear difficult to use on transmission lines [1].

In the case of external short-circuits, this susceptance can cause at the end of the line a flow of currents which differ from one another in magnitude and direction; when two phases are in operation on the line and also when there is a short-circuit on one of the circuits of a double circuit line, a phase shift between currents can occur at the place where a protective gear is located. This can cause faulty operation of the protective gear; in order to prevent this [1 and 2], it was necessary to introduce compensation for the capacitive currents in the differential phase protective gear of the DFZ–400M type on 400 kV lines. The use of this compensation is also necessary in the protective gear of the DFZ–2 type which is widely used in the U.S.S.R. on 220 kV lines with a length over 300 km, [1].

The principles of compensation for line capacitive currents and the design of compensation devices of the DFZ–400 M and DFZ–2 types † for protection are discussed below.

General principles of compensation

In a differential phase protective gear, devices for compensating line capacitive currents can be used in the manipulator with a carrier transmitter and in the current starting device.

In the first device as a general rule, the compensation of capacitive currents of the positive and negative sequences is required, and in the second device of the negative and zero sequences.

In the current starting device, the compensation device is used in those cases when, due to capacitive susceptance during external short-circuits, currents flow at the ends of the line and these differ considerably in magnitude; under these conditions there is a possibility that the protective device will operate wrongly, being triggered at one end of the line only.

† Ing. G.G. Iakubson participated in working out several of the problems discussed in this article.

* *Elektrichestvo* No. 10, 14–20, 1958.

The possibility of the faulty operation of the protective gear under the influence of capacitive currents due to a short-circuit in one of the parallel circuits can be seen by considering Fig. 1, where the line is represented as an equivalent T-network.

When the negative sequence voltages on busbars m and n are equal at both ends of the undamaged line currents $I_{2c}/2$ * flow (I_{2c} is the line capacitive current), which correspond, so far as phase relations are concerned, to the currents flowing during a short-circuit in the protected zone. In this case the probability of the incorrect operation is particularly high in the DFZ–400M protective gear because its starting device responds at short-circuits to negative sequence voltage in the middle of the protected line and consequently, should operate in this case as a rule.

The compensating devices which are discussed below equalize currents in the half-sets of the protective gear at the line ends in magnitude and make them opposite in phase in the cases of: external short-circuits, during two-phase operation of the line and during normal symmetrical conditions of operation irrespective of the magnitude of capacitive susceptance.

In a general case, when the devices discussed are used at both ends of the line, they are connected to the voltage of that phase sequence, the capacitive current which should be compensated.

In this case, the compensation current $\dot{I}_k$ is determined by the expression

$$\dot{I}_k = \dot{U} Y_k, \tag{1}$$

where U is the voltage of the corresponding phase sequence at the point where the protective gear is installed;

Y_k is the compensation device admittance.

In the case of a uniform line, which can be represented by a symmetrical equivalent T-circuit or by a symmetrical four-pole, the admittance Y_k will be equal for both half-sets of the protective gear.

Denoting by $\dot{I}_m$, $\dot{I}_n'$, $\dot{U}_n$ the currents and voltages at the line ends and taking into account that in the presence of an external short-circuit at the substation busbars n, the secondary current of the instrument current transformer of this substation is in the opposite direction to that of the primary current, we can write:

$$\dot{I}_m - \dot{U}_m Y_k = -(-\dot{I}_n - \dot{U}_n Y_k), \tag{2}$$

hence

$$Y_k = \frac{\dot{I}_m - \dot{I}_n}{\dot{U}_m + \dot{U}_n}. \tag{3}$$

* According to custom in the U.S.S.R., complex quantities are denoted by a dot over the symbol.

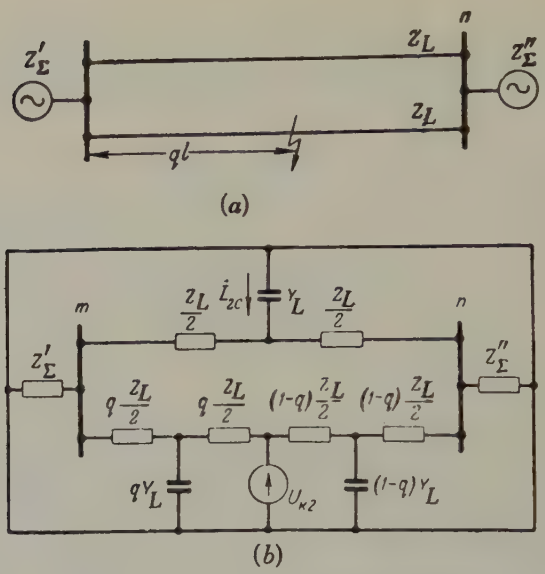

FIG. 1. Equivalent circuit (*b*) for calculating the negative sequence components during short-circuits on one of the parallel circuits (*a*). Circuit capacitive susceptances are accounted for.

Replacing the line by a four-pole and determining the relationship between voltages and currents at the output

$$(\dot{U}_m, \dot{I}_m)$$

and output

$$(\dot{U}_n, \dot{I}_n)$$

by means of expressions:

$$\left.\begin{aligned} \dot{U}_m &= A\dot{U}_n + B\dot{I}_n \\ \dot{I}_m &= C\dot{U}_n + D\dot{I}_n, \end{aligned}\right\} \qquad (4)$$

and

and due to the fact that for a uniform line $A = D$ and $A^2 - BC = 1$, by dividing we get the expression for the determination of Y_k through the four-pole coefficients:

$$Y_k = \frac{A-1}{B}. \qquad (5)$$

Substituting into expression (5) the values of coefficients A and B we may

assume with an accuracy sufficient for practical calculations, that

$$Y_{\kappa} = j\frac{bl}{2}, \tag{6}$$

where b is the capacitive susceptance of the appropriate phase sequence per 1 km of lines;

l is the length of the line, km.

The error in this case for the 400 kV line for the positive and negative sequences is 1.2–2.3 per cent and for the zero sequence it is 2 and 6 per cent. The first figure relates to the line of 250 km length, but the second one to 500 km length. The values of susceptances b_1 for the positive and negative sequences and b_0 for the zero sequence for lines of 220 and 400 kV are given in Table 1.

TABLE 1.

Line voltage, kV	220	400
$b_1, \frac{1}{\Omega\ \text{km}}$	$2.7.10^{-6}$	$3.95.10^{-6}$
$b_0, \frac{1}{\Omega\ \text{km}}$	$1.9.10^{-6}$	$2.72.10^{-6}$

The equivalent T-circuit of a non-uniform line, when, for example, the capacitance of the series compensation device is present at one end of the line, is asymmetrical Fig. 2; admittances Y_{km} and Y_{kn} at the end of this line will be different.

Assuming

$$Y_{\kappa n} = \frac{A-1}{B}$$

and substituting this value of Y_{kn} into equation (2) we get:

$$Y_{\kappa m} = \frac{D-1}{B}.$$

Since the parameters of the elements of the equivalent T-circuit of the line are known in any case, the four-pole coefficients A, B and D, which are needed for the determination of Y_{km} and Y_{kn}, are most easily found from expressions:

$$\left.\begin{aligned} A &= 1 + Z_{1T}Y_T; \\ B &= Z_{1T} + Z_{11T} + Z_{1T}Z_{11T}Y_T; \\ D &= 1 + Z_{11T}Y_T. \end{aligned}\right\} \tag{7}$$

For determination of the parameters of the circuit in Fig. 2b, we may assume for practical calculations that $Y_T = jbl$, and for a uniform line $Z_{IT} = Z_{IIT} = Z_l/2$, where Z_l is the total line impedance neglecting its capacitive susceptance.

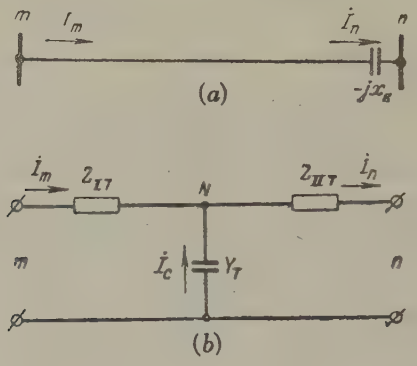

FIG. 2. Circuit of the line with series compensation (*a*) and its equivalent T-circuit (*b*)

$$Z_{IT} = \frac{Z_L}{2};\ Z_{IIT} = \frac{Z_L}{2} - jx_g;\ Y_T = jbl.$$

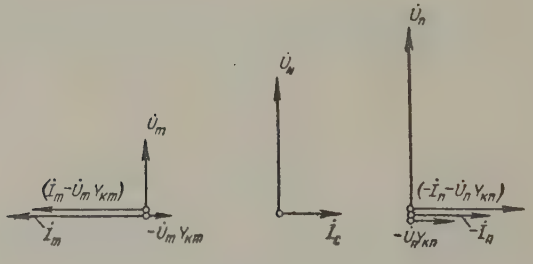

FIG. 3. Vector diagrams of the negative or zero sequences in the presence of an external short-circuit at the busbars of the substation *n* (Fig. 2a) with the compensation of the line capacitive currents accounted for

$$-(\dot{U}_m Y_{Km} + \dot{U}_n Y_{Kn}) = -(\dot{I}_{Km} + \dot{I}_{Kn}) = \dot{I}_C;$$
$$\dot{I}_m - \dot{U}_m Y_{Km} = -(-\dot{I}_n - \dot{U}_n Y_{Kn}).$$

If we neglect the active resistance of the line, then in the case of an external short-circuit, the compensation current will in practice coincide in phase with the secondary current of the current transformers or will be of the opposite phase. In

the case of an asymmetrical short-circuit at the substation busbars n Fig. 2a, the negative and zero sequence components coincide in phase with the secondary current at substation n and are in antiphase with the current in substation m. The sum of currents of the compensation devices at both ends of the line is equal to the capacitive line current of the corresponding phase sequence. The vector diagrams shown in Fig. 3 illustrate this position.

It is necessary to point out that the phase shift compensation between the currents at the end of the line, when it operates in two phases, is only possible, if the voltage transformer is connected directly to the line, since in this case the symmetrical components on the busbars cannot characterize voltages applied to the line capacitive susceptance. For correct operation of the compensation devices it is necessary that, simultaneously with the cutting-off of the line phase, the voltage should be disconnected on both sides from the same phase of the voltage transformer. In this case, the voltage symmetrical components applied to the compensation devices will correspond to the voltage applied at the end of the line to its capacitive elements.

In principle, the compensation of the total capacitive current I_c can be realized only in one of the half-sets of the protective gear. However, the compensation device should be connected not only for voltage but also for the current of the corresponding phase sequence. If compensation is realized, for example, only on the side of the substation m Fig. 2a then the compensation current is:

$$\dot{I}_{Km} = -\dot{I}_C = \dot{U}_N Y_T = (\dot{U}_m - \dot{I}_m Z_{IT})\, Y_T \,. \qquad (8)$$

So far as the manipulator of the high-frequency transmitter is concerned, it is possible in many cases to realize the compensation only on one side of the line, neglecting the component $-I_m\, Z_{IT}\, Y_T$; this is due to the fact that for this device, unlike for the starting device, no equality of the values of the currents at the line ends is needed. The reason is that in the case considered of a short-circuit on one of the parallel circuits or during two-phase operation of the line, when only low power is transmitted and currents are comparatively small, we may neglect the component $-I_m\, Z_{IT}\, Y_T$.

Particular properties of compensation for capacitive currents of the zero sequence

The analysis carried out by the author showed that the method of compensation discussed, when applied to currents of the zero sequence, gives good results for single or two-circuit lines only for short-circuits outside the line.

For short-circuits on one of the parallel circuits, compensation is realized in many cases with considerable error due to mutual induction between circuits, and this should be taken into account for the zero sequence current starting device of the differential phase protective gear concerned.

The usual equivalent circuits [3 and 4] for calculating zero sequence currents

in the case of short-circuits on one of the circuits of a double circuit line do not give a clear idea about the influence of the mutual induction between circuits on the operation of the compensation devices. This can be done more conveniently if, assuming the short-circuit currents to be known, we replace the e.m.f. of the mutual induction by impedances, on which the voltage drops are equal in magnitude and opposite in phase to these e.m.f.

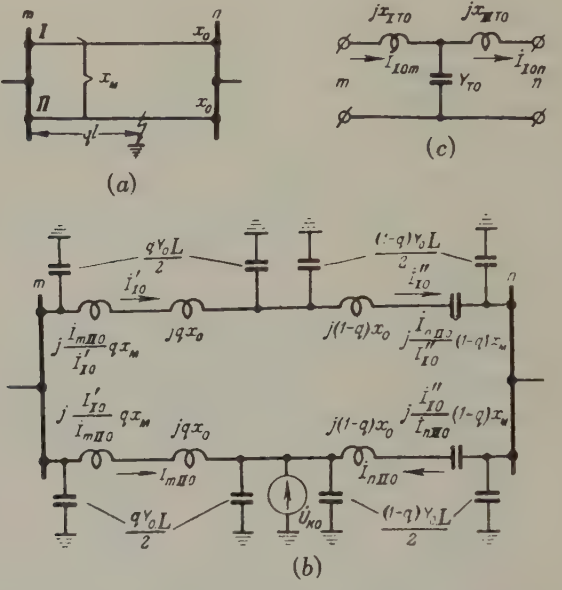

FIG. 4. Equivalent circuit (*b*) of the zero sequence of a double circuit line (*a*) for a fault on one of the circuits; the circuit explains the influence of the mutual induction between the circuits on the accuracy of the compensation of the line capacitive currents in the carrier protective gear; equivalent T-circuit of the undamaged line (*c*).

Such an equivalent circuit, in which the capacitive susceptance of the zero sequence is accounted for, is shown in Fig. 4b, where the lines to the left and right from the place of fault are replaced by an equivalent π-circuit, and active resistances of the network are neglected.

On the section to the right of the fault, where the currents in the lines flow in different directions, and the ratios of the current vectors

$$\dot{I}_{nIIo} | \dot{I}''_{Io} \text{ and } \dot{I}''_{IIo} | \dot{I}_{nIIo}$$

are negative, the e.m.f. of the mutual induction are replaced by inductive reactances.

The circuit shown in Fig. 4b is an approximate one. We can obtain a more accurate result by dividing sections of the line to the left and right from the fault into smaller sections and representing each section by an equivalent π-circuit, in which impedances are introduced that correspond to the mutual-induction e.m.f. of everyone of these sections.

However, calculations show that the circuit shown in Fig. 4b gives a result that is sufficiently accurate in practice.

In Fig. 4c an equivalent T-circuit of the unfaulted circuit I is shown; the circuit shown in Fig. 4b is reduced after transformations to the above equivalent circuit.

The parameters of the circuit shown in Fig. 4c are approximately equal to:

$$\left.\begin{aligned} x_{IT0} &= \frac{x_0}{2} + \frac{q}{2}(2-q)\frac{I_{mII\,0}}{I'_{1\,0}}x_M + \\ &\quad + \frac{(1-q)^2}{2}\frac{I_{nII\,0}}{I''_{1\,0}}x_M; \\ x_{IIT0} &= \frac{x_0}{2} + \frac{q^2}{2}\frac{I_{mII\,0}}{I'_{1\,0}}x_M + \frac{1-q^2}{2}\frac{I_{nII\,0}}{I''_{1\,0}}x_M; \\ Y_{T0} &= jb_0 l. \end{aligned}\right\} \qquad (9)$$

In the case of a short-circuit outside a double circuit line, i.e. when $q = 1$ or $q = 0$, and when

$$\frac{I_{mII\,0}}{I'_{1\,0}} = \frac{I_{nII\,0}}{I''_{1\,0}} = 1,$$

then

$$x_{IT0} = x_{IIT0} = \frac{x_0 + x_M}{2}. \qquad (10)$$

Thus, for short-circuits outside the double circuit line Fig. 4a each chain can be considered as a line, having a symmetrical equivalent T-circuit; for short-circuits on one of the chains, however, the undamaged chain can be, in a general case, represented with respect to the zero sequence currents by an asymmetrical equivalent T-circuit. Parameters X_{IT_0} and X_{IIT_0} of this equivalent circuit depend both on the location of the short-circuit and on the ratios of currents in the faulty and undamaged circuits.

In the first section of this article it was shown that for a uniform and a non-uniform line, which can be represented by a symmetrical and asymmetrical equivalent T-circuit respectively, the compensation admittances have different values. Since for a uniform line it is necessary to assume that

$$Y_{0km} = Y_{0kn} = j\frac{b_0 l}{2},$$

the exact compensation of capacitive currents of the zero sequence will be realized only for short-circuits outside the parallel circuits, but, for a fault on one of the circuits, the compensation will be realized with a certain error, which will depend on parameters X_{IT_0} and X_{IIT_0} of the circuit shown in Fig. 4c. For example, for $X_{IIT_0} = 0$, which will occur when

$$\frac{\dot{I}_{mII\,0}}{\dot{I}''_{10}} x_M = -\frac{1}{1-q^2}\left(x_0 + q^2 \frac{\dot{I}_{mII\,0}}{\dot{I}'_{10}} x_M\right),$$

the coefficient D of the equivalent four-pole of the line is equal to unity, and an exact compensation will take place for $Y_{okm} = 0$ and $Y_{okn} = j b_0 l$. When the admittances Y_{okm} and Y_{okn} are both equal to half of the capacitive susceptance of the line zero sequence, the under-compensated capacitive current ΔI_{ok}, according to Fig. 4c for $X_{IIT_0} = 0$, will be determined by the voltage drop across the reactance X_{IT_0} and will be equal to:

$$\Delta \dot{I}_{0k} = \dot{I}_{1\,0m} j x_{1T0} j \frac{b_0 l}{2} = -\dot{I}_{1\,0m} x_{1T0} \frac{b_0 l}{2}. \qquad (11)$$

In the limit, when $I_{Iom}\, X_{IT_0} \gg (\dot{I}_{Iom} + \dot{I}_{IIom})\, X_{om\Sigma}$, where $X_{om\Sigma}$ is the resultant reactance of the system zero sequence at the side of the substation busbars m, the current ΔI_{ok} will be nearly equal to 50 per cent of the line capacitive current.

In spite of the error, the compensation device improves the conditions of operation of the current starting device of the zero sequence, because in the presence of this device currents flowing at the ends of the line in the half-sets of the differential phase protective gear will in all cases differ less from one another, than currents in the primary circuit. Because of this the compensation device of the zero sequence currents can be recommended for very long double circuit lines.

However, taking into account that the influence of the error will be less for heavy operational currents of the starting device, it is necessary, as far as possible, to increase the operational current of the starting device from the zero sequence components at the expense of sensitivity to the components of the negative sequence currents. In the protective gears DFZ–400 M and DFZ–2 the realization of the latter condition is facilitated by the fact that for asymmetrical earth faults, both these current symmetrical components are added in the relay windings of the starting device.

For example, in the protective gear type DFZ–400 M of the 400 kV transmission line Kuibyshev HEPS–Moscow it was possible to dispense with a compensation device of the zero sequence capacitive currents because it was possible to allow the operational currents of the starting device from this sequence

to be much larger than the capacitive current of the protected line.

Design of the compensation device

In Fig.5, a block circuit diagram of the compensation device for capacitive currents in the manipulator of the high-frequency transmitter is shown; this arrangement is used in the protective gear type DFZ–400 M on the 400 kV lines. From 1956 this device is used in the protective gear type DFZ–2 on one of the 220 kV lines 250 km long for the compensation of the phase shift between the currents at the line ends, when the line operates on two phases in the single phase automatic, reclosure cycle.

The method of compensation adopted consists in applying e.m.f. $\dot{E}_{1S}$ and $\dot{E}_{2S}$ from the active-capacitive filters of the positive and negative sequence voltages to the manipulator; voltages

$$\dot{E}_{1S} \text{ and } \dot{E}_{2S}$$

are respectively equal to the corresponding components of the e.m.f.

$$\dot{E}_{1T} \text{ and } \dot{E}_{2T}$$

of the combined filter

$$\dot{I}_1 + k\,\dot{I}_2\,,$$

these components being reduced to the secondary winding of the intermediate transformer TM (Fig. 5).

When the voltage filters are connected as shown in Fig. 5 e.m.f.

$$\dot{E}_{1S}\,,\ \dot{E}_{2S}$$

are determined by the expressions [5]:

$$\left.\begin{aligned}\dot{E}_{1S} &= 1.5\sqrt{3}\dot{U}_{1b}e^{j30^\circ}n_{ky1};\\ \dot{E}_{2S} &= 1.5\sqrt{3}\dot{U}_{2c}e^{j30^\circ}n_{ky2},\end{aligned}\right\} \qquad (12)$$

where $\dot{U}_{1b}$ and $\dot{U}_{2c}$ are secondary voltages of the positive and negative sequences of phases B and C;

n_{ky1} and n_{ky2} are transformation ratios of the compensation device transformers TKY_1 and TKY_2 respectively.

Since in the combined filters of the protective gear of the DFZ–400 M and DFZ–2 types symmetrical components of phase a currents are separated, we can write [6]:

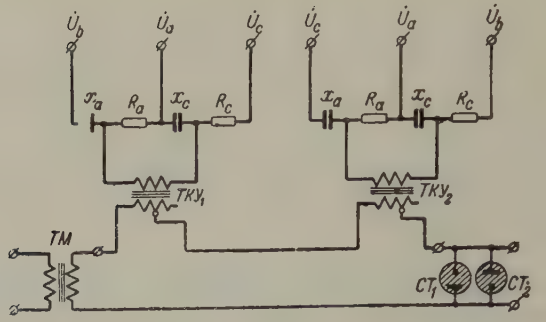

FIG. 5. Circuit showing the arrangement for compensation of the line capacitive currents for the manipulator of the carrier transmitter with the combined current filter

$$\dot{I}_1 + k\,\dot{I}_2.$$

$$\dot{E}_{1T} = \frac{2R\dot{I}_{1ka}}{k+1}\,n_{TM}; \quad E_{2T} = \frac{2kRI_{2ka}}{k+1}\,n_{TM}, \tag{13}$$

where $\dot{I}_{1ka}$ and $\dot{I}_{2ka}$ are secondary compensation currents of the positive and negative sequences;

k is the factor of the filter $\dot{I}_1 + k\dot{I}_2$;

R is the resistance of the filter $\dot{I}_1 + k\dot{I}_2$;

n_{TM} is the transformation ratio of the intermediate transformer TM.

By using these formulae it is not difficult to show that $\dot{E}_{1S}$ and $\dot{E}_{1T}$ as well as

$$\dot{E}_{2S} \text{ and } \dot{E}_{2T}$$

are respectively in phase opposition.

The unknown transformation ratios n_{ky_1} and n_{ky_2} can be determined from equalities

$$\dot{E}_{1S} = \dot{E}_{1T} \text{ and } \dot{E}_{2S} = \dot{E}_{2T},$$

if we take into account that

$$\left|\frac{\dot{I}_{1ka}}{\dot{U}_{1b}e^{j30°}}\right| = \left|\frac{\dot{I}_{2ka}}{\dot{U}_{2c}e^{j30°}}\right| = y_k,$$

where y_k – admittance factor of the compensation of the positive and negative sequences, which is reduced to the secondary side of the current and voltage instrument transformers.

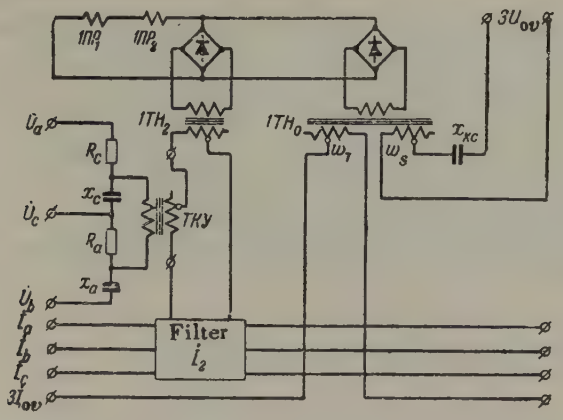

FIG. 6. Principal circuit of a starting device for negative and zero sequence current of the protective gear DFZ–2 with compensation devices for line capacitive currents.

Fig. 6 shows the principal circuit of the starting device of the negative and zero sequences of the protective gear type DFZ–2 with the arrangements for compensation of capacitive currents. The use of these arrangements, as was stated earlier, can prove necessary when the protective gear is used on 220 kV lines more than 300 km long.

The arrangement for compensation of the negative sequence capacitive current in the starting device of the DFZ–2 gear is similar to the device for compensation of the current of the same sequence in the manipulator of the high-frequency transmitter. The connexion of the voltage circuits to the filter of the compensation device according to Fig. 6, is made, however, in such a way, that the voltage vector at the output has the same direction as the vector

$$\dot{U}_{2b}\, e^{j30^0}.$$

Such a connexion is made because the negative sequence filter of the starting device of the DFZ–2 gear, unlike the filter of the manipulator of the carrier transmitter, separates the phase *c* current.

A distinguishing feature of the compensation of the negative sequence current in the starting device is the connexion of the secondary winding of the intermediate transformer to the primary winding of the saturation transformer $1TH_2$. This connexion allows the elimination of the influence of impedance of the magnetizing branch of the transformer $1TH_2$ on the correctness of the compensation. This

follows from the equivalent circuit of the starting device if we take into account that the impedance of the magnetizing branch of the transformer $1TH_2$, even before its saturation, is quite commensurable with the load impedance.

The compensation of the zero sequence capacitive currents in the starting device of the DFZ–2 gear can be realized by means of a winding w_s shown in Fig. 6 which should be added to the transformer $1TH_0$.

This winding is connected through a capacitor to the zero sequence voltage.

The ratio of the number of turns of the windings W_T and W_s of the transformer ITH_0 is chosen on the basis of the condition that the m.m.f. of the winding W_T, induced by the compensated component of the line capacitive current is equal in magnitude to the m.m.f. of the winding W_s and opposite in phase, i.e. the following equality holds good:

$$3\dot{I}_{0\kappa s} w_T = j \frac{3\dot{U}_{0v}}{x_{KC}} w_s,$$

where $\dot{I}_{0kv}$ and $\dot{U}_{0v}$ is the secondary compensation current and the zero sequence voltage;

X_{KC} is the capacitor reactance in the winding circuit.

Taking into consideration that

$$\left| \frac{\dot{I}_{0v}}{j\dot{U}_{0s}} \right| = y_{0k},$$

where Y_{0k} is the susceptance factor of the zero sequence compensation, reduced to the secondary side of the instrument current and voltage transformer; we get an expression for W_s :

$$w_s = y_{0k} x_{KC} w_T. \tag{14}$$

Conclusions

1. By using special devices for compensating capacitive currents in differential phase carrier protective gear, we can eliminate the influence of these currents on the correct working of the gear.

2. Due to the influence of mutual induction the compensation of the zero sequence capacitive currents during a fault on one of the parallel circuit of the line can be realized only with a substantial error. Nevertheless, the use of compensation devices for currents of this sequence is expedient on double circuit lines, since the presence of these devices improves conditions for the working of protective gear in all cases.

3. When compensation devices are used at both ends of the line they are connected only to the voltage of that phase sequence, the capacitive current of which they have to compensate; this ensures sufficient simplicity for the circuits of the devices used.

4. When the compensation of the total line capacitive current takes place at only one end of the line, the compensation device should be connected to both the voltage and current of the corresponding phase sequence. However, in the manipulator in the carrier transmitter, in this case, as a rule, the device could be connected only to the voltage.

5. Experience in the working of compensation devices for line capacitive currents shows that their application satisfactorily solves the problem of the use of differential phase carrier protective gear on 220 and 400 kV lines of very great length.

Translated by S. Szymanski

REFERENCES

1. E.D. Sapir, *Elektrichestvo* No. 3 (1956).
2. V.M. Yermolenko and S.Ia. Petrov, *Kompensatsia vliianiia yemkostnoi provodimosti linii elektroperedachi. (Compensation of the influence of the capacitive susceptance of transmission lines).* Biulletin' Teploelektroproyekta, No. 2 (1955).
3. S.A. Ulianov, *Korotkiye zamykaniia v elektricheskikh sistemakh. (Short-circuits in electrical systems),* Gosenergoizdat (1952).
4. K.F. Wagner and R.D. Evans, *Metod simmetricheskikh sostavhiaiushchikh. (Method of symmetrical components).* ONTI (1936).
5. A.M. Fedoseyev, *Releinaia zashchita elektricheskikh sistem. (Relay protection of electrical systems).* Gosenergoizdat (1952).
6. *Rukovodiashchiye ukazaniia po naladke, proverke i ekspluatatsii releinoi chasti differentsialno – faznoi vysokochastotnoi zashchity* tipa DFZ–2. *(Instructions for adjusting, verifying* and *operating the relay part of the differential phase carrier protective gear of the DFZ–2 type).* Gosenergoizdat (1957).

THE PROBLEM OF A CIRCUIT FOR A RECTIFYING SEMICONDUCTOR SET ON ELECTRIC ROLLING STOCK OF A.C. SINGLE-PHASE – D.C. TRACTION*

V.A. GOLOVANOV

Moscow

(Received 25 April 1958)

The progress in constructing powerful semiconductor rectifiers (germanium, silicon) made during recent years, permits their use on electric rolling stock for a single-phase a.c.–d.c. traction; this problem can be considered now as a practical problem. Besides many well known advantages [1] the use of semiconductor rectifiers on rolling stock opens up the possibility of choosing a more rational circuit for the rectifying set, which enables the weight of the main transformer and the power losses to be reduced. In this article, problems connected with this property of rolling stock equipped with a semiconductor rectifying set are discussed. The importance of making these problems clear is due to the fact that the choice of this or that solution leads to substantially different technical requirements for the performance of a semiconductor rectifier, and the choice determines the construction of the electrical equipment of the rolling stock and its power indices.

The choice of the rectifying circuit on rolling stock with static rectifiers is determined in the final result by the value of the efficiency and the possibility of effective cooling of the rectifiers.

We shall discuss in detail the problem of efficiency and consider the efficiency of a rectifying set neglecting transformer losses and power expenditure for its own needs. We shall first consider the well known circuits of a single-phase rectifying set with a centre tap in the transformer secondary circuit, and the bridge circuit.

It is known that the total number of rectifiers in a rectifying set for an m-phase network, when each arm contains a parallel branches, each branch having s series connected rectifiers, is given by the expression

* *Elektrichestvo* No. 10, 53-57, 1958.

$$N = masq,$$

where $q = 1$, or $q = 2$ depending upon whether a starpoint or a bridge circuit are used respectively.

The efficiency of any rectifying set can be expressed by the following approximate expression:

$$\eta = \frac{U_d I_d}{U_a I_d + N U_a \frac{I_d}{ma}} = \frac{1}{1 + sq \frac{U_a}{U_d}},$$

where U_d is the rectified voltage; and U_a the direct voltage drop in a rectifying element.

This expression shows that in each rectifying set connected by a bridge-circuit or the star point method, the efficiency drops with decreasing U_d. Such a drop in efficiency occurs, for example, when an electric locomotive or an electric multiple-unit is moving at lower step speeds at a voltage $U_d < U_{dr}$. Only at higher step speeds when $U_d = U_{dr}$ does the efficiency of the set reach its possible maximum value for a given circuit. The above is valid both for circuits with semiconductor and mercury rectifiers.

If we compare circuits with a star point and a bridge circuit we find that with mercury rectifiers the efficiency is higher in the first case. This is due to the fact that a mercury rectifier can withstand a sufficiently high reverse voltage U_o. In practice, in mercury rectifying circuits for any arbitrary value of U_{dr}, only one rectifier is connected into an arm, ($s = 1$).

The situation is different in the case of a semiconductor rectifying set. Due to a relatively low value of U_o of an element, it is necessary to connect into an arm as many elements as are required in accordance with the reverse arm voltage.

In the case of a bridge circuit, this voltage value is half as large as that with a star point circuit, but the number of arms is double. As a result, for a semiconductor set, the value of sq remains constant when we pass from one circuit to another and, consequently, the efficiency of a semiconductor rectifying set does not depend on the type of circuit used. Therefore, the only expedient circuit for semiconductor rectifiers is the bridge circuit.

The method of connecting of germanium and silicon rectifiers in the widely known circuits has two other specific disadvantages.

The series connexion in an arm of several rectifiers requires a parallel connexion of an ohmic resistance to every rectifier, or, as an alternative, it leads to the increase in the number of the elements in the arm by one or two rectifiers, thus increasing the reserve of strength of the set. Both measures lower the efficiency of the set. Moreover, the failure of a certain number of elements in

such a set leads to the breakdown of the whole set.

The above disadvantages can be excluded by using rectifying set circuits designed on new principles, compared with those used for circuits devised previously. Here, use is made of the specific properties of semiconductor rectifiers and the special operational conditions of a rectifying set on rolling stock. Fig.1 shows this principle circuit, [2].

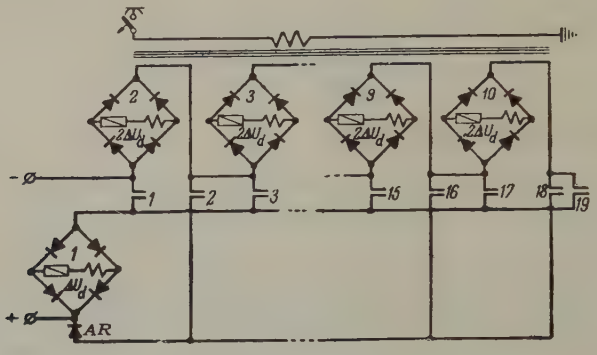

FIG.1 Circuit of a semiconductor rectifying set based on the principle of dividing it into separate sections.

The circuit is obtained by dividing the main transformer secondary winding into a number of independent main sections with a comparatively low voltage $2\Delta U$, and one auxiliary section with a voltage † ΔU. The magnitude of ΔU is determined by the voltage jump which is admissible when speed is changed from one step to another. A bridge circuit is connected to every transformer section, and into each arm of the bridge circuit one element is inserted. Every transformer section together with the bridge connected to it forms a rectifying section with a rectified voltage $2\Delta U_d$.

Collecting the number of such rectifying sections into a successive circuit we can increase or decrease by steps the voltage applied to the traction motors. The transition from one step to another is done by means of a special change-over switch, which consists of an additional rectifier AR and an additional rectifying section with a voltage of the order ΔU_d. The closing of each contactor shown in the circuit, Fig. 1, corresponds to a definite speed step. Nineteen contactors ensure nineteen speed steps. On transition from one step to another the two adjacent contactors are always closed: 1 and 2, or 2 and 3 or 3 and 4 and so on.

† The number of main sections can be arbitrary and is determined by the number of speed steps necessary for the rolling stock.

The circuit shown in Fig. 1 has several valuable advantages by which it differs favourably from the known rectifying circuits. This circuit does not require the connexion of shunting ohmic resistances since the reverse voltage of every rectifier is fixed. During the process of starting, the efficiency of the rectifying set remains approximately constant for all steps. Thus, all speed steps in this circuit can be used for continuous running. The circuit allows the same rectifying set to feed the auxiliary circuits with practically any arbitrary direct voltage, independent of the voltage applied to the traction motors. The reliability is increased since the failure of a certain number of elements causes the blowing of a fuze in the corresponding sections, and the total rectified voltage drops by a small amount equal to the section voltage. This circuit uses a method of rectified voltage regulation which basically differs from methods used in the known circuits; due to this, the circuit has no intermediate reactors and facilitates the operation of the switchgear.

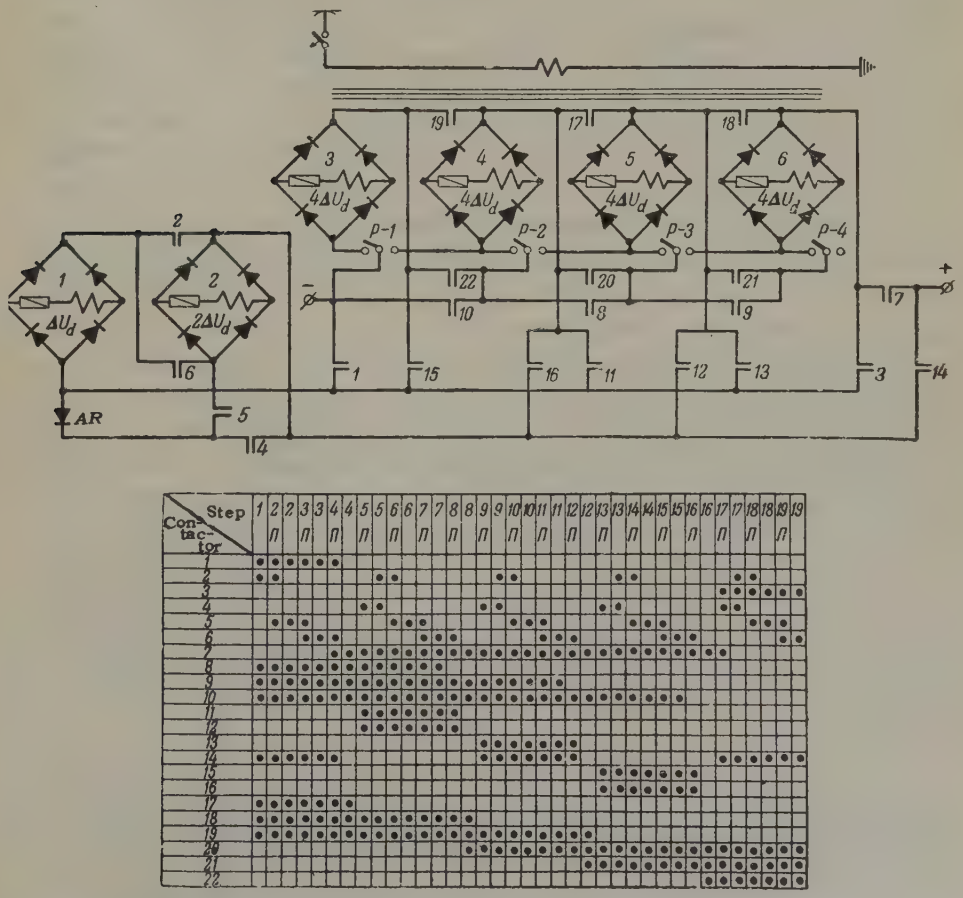

FIG.2 Circuit of a semiconductor rectifying set which allows a parallel-series switching-over of sections during the process of the rectified voltage regulation.

However, the use of semiconductor rectifiers gives us the possibility of devising a still better circuit for a rectifying set (Fig. 2), based on the method † proposed by the author; this method consists in the parallel-series switching-over of the rectifying set sections during the process of voltage regulation [3].

As in the circuit in Fig. 1, in this method of voltage regulation, the transformer secondary winding is subdivided into several main sections with the voltage $4\Delta U$. But, instead of one we have two auxiliary sections: one with a voltage $2\Delta U$ and another with a voltage ΔU. The number of main sections depends on the number of speed steps required.

The circuit operates in the following way. The first three steps are obtained by a combined connexion of the auxiliary sections 1 and 2 by means of contactors 1, 14, 2, 4, 5 and 6. By closing contactors 1, 14 and 2 we get the first step with a rectified voltage ΔU_d. By connecting contactor 5 of section 1 in parallel, section 2 is supplied with a voltage greater than ΔU_d, and the load from section 1 is transferred to section 2. Thus, the circuit of stage 2 is obtained with the rectified voltage $2\Delta U_d$. Then sections 1 and 2 are connected in series by closing contactor 6, and the circuit of stage 3 is formed with the voltage $3\Delta U_d$. For switching over to stage 4, the whole set of the parallel connected main sections 3-6 is switched to the parallel series connected sections 1 and 2; this is done by closing contactor 7, and sections 3-6 take over the total load. In this way the fourth stage circuit is connected up and the rectified voltage is $4\Delta U_d$. The switching over to stage 5 begins with connecting the rectifier AR in parallel to contactor 17 by means of contactors 4, 11 and 12; after this it is possible to switch off contactor 17.

By analogy with the procedure for the first three steps, contactors 2, 5 and 6 are operated. As a result, circuits for steps five, six and seven are connected up with the rectified voltages $5\Delta U_d$, $6\Delta U_d$, $7\Delta U_d$; in this case sections 5-6 are left idle, and the whole load is borne by sections 3-4 connected in parallel. Further switching over is performed in a similar way to that already described.

The throw-over single pole disconnectors P_1 to P_4 normally remain in the position shown on the diagram. If it is required for any reason whatsoever to switch off one of the main sections, then the disconnector of the corresponding section is set in a position opposite to that shown on the diagram, and the circuit continues its operation without change. True, in this case the total rectified voltage decreases by $4\Delta U_d$.

The circuit, in which series-parallel switching over of sections is used, has, — in comparison with circuits used up to this time, — all the advantages already enumerated for the circuit in Fig. 1. Moreover, it offers certain additional advantages.

† Author's certificate No. 108782 of 13 April 1957.

Semiconductor rectifiers are characterized by their small over-load capacity. This property contrasts with the conditions of electric rolling stock operation, which is characterized by considerable abrupt load changes, which last 0.5-15 min; these load variations occur frequently on electric multiple-units.

Considerable difficulties arise in this respect in the case of rolling stock fitted with semiconductor rectifiers, ordinary rectifying circuits, and to some extent the circuits shown in Fig. 1.

Due to the parallel connexion of the sections, the circuit proposed by the author eases the operating conditions for the semiconductor rectifying set at the time when they are most difficult; namely, during the starting period.

The drop in the value of the rectifier current, in comparison with the rated current, which is due to the parallel connexion of sections, results in a smaller voltage drop in the rectifier, and consequently reduces losses. This means that in a set designed according to the circuit shown in Fig. 2, the efficiency for the lower voltage steps will be even slightly greater than that for the higher steps. This property of the circuit makes it particularly suitable for electric rolling stock multiple-units and for electric shunting locomotives. Finally, the circuit ensures a fuller use of a rectifying set since for all speed steps the greater part of its equipment is utilized.

The choice of a circuit for a rectifying set is closely connected with the choice and parameters of semiconductor rectifiers. In the case of silicon rectifiers, which can withstand a comparatively high admissible reverse voltage, the use of the circuit shown in Fig. 3 is recommended. If we choose germanium rectifiers with a low value of reverse voltage, we have to alter somewhat the circuit in Fig. 2 in such a way that, instead of each of the main sections, two permanently series connected sections are used with a rectified voltage of the order $2\Delta U_d$. The properties of the circuits described show that on electric rolling stock, rectifying elements with a rather small admissible reverse voltage can be used. At the same time it is necessary to bear in mind that, in order to keep the efficiency of the set within the admissible limits, we cannot assume the value of the rectifier reverse voltage to be arbitrarily small.

Thus, the problem of constructing a reliable and economic semiconductor rectifying element for traction purposes is closely connected with the choice of circuit for the rectifying set.

Conclusions

1. The use of semiconductor rectifying sets offers an effective means for improvement of rolling stock for a.c. single-phase – d.c. traction systems.

2. The most rational circuit from the point of view of design and economy is a circuit, which allows parallel-series switching over of sections during the

process of rectified voltage regulation.

3. This circuit enables us to lower the requirements formulated for semiconductor rectifiers designed for operation on electric rolling stock.

Appendix

Let us consider a possible example of the use of the circuit proposed. For comparison, we take a circuit of an English electric multiple-unit with germanium rectifiers (Fig. 3), [4]. In this circuit $m = 2$, $a = 6$; $s = 50$; $q = 1$; $U_{dr} = 1500$ V; $I_{dr} = 500$ A. The circuit allows 21 speed steps, of which 1, 5, 9, 13, 17, 21 are steps which can be used for continuous running due to the symmetrical connexion of intermediate reactors in these steps. Assuming that the change-over from one step to another occurs when the rectified voltage varies by equal jumps of ΔU_d, let us consider the variation of efficiency in steps for a constant value of the rectified current I_{dr} in accordance with the expression:

$$\eta_n = \frac{1}{1 + sq \dfrac{U_a}{U_{dr}} \cdot \dfrac{21}{n}},$$

where n is the number of the steps.

In accordance with a typical volt-ampere characteristic of a germanium rectifying element [1] we assume for the rated conditions that $U_a = 0.6$ V. The results of calculations of the efficiency are given in Fig. 4.

If we assume that during the period of starting the electric coach, the current consumed by the traction motors is double their steady-state current, and the start itself lasts about 25 sec, then in the circuit in Fig. 3 each element of the rectifying set has to withstand a double load for this interval of time.

If we adjust our circuit shown in Fig. 2 to the operating conditions for the English electric multiple-unit, this will bring about the following results. Circuit on Fig. 2 should ensure under-rated conditions for higher speed steps, the voltage $U_{dr} = 1500$ V, and, consequently, the rated rectified voltage in every one of the main sections will be 316 V, and in the two auxiliary sections 158 and 78 V. Obviously, the reverse voltages per single element should be equal in both circuits 3 and 2. Let us find the order of magnitude of this value. It is quite reasonable to assume that in the circuit Fig. 3 the no-load voltage on the phase of the transformer secondary winding is approximately 2000 V. Therefore, the reverse voltage supplied to the rectifying element in the circuit is approximately 120 V. Consequently, we have to connect into the arm of the main section bridge (Fig. 2) five elements in series, and into the arms of the auxiliary sections three and two elements respectively. The number of parallel branches in each arm of all the sections is six, as in the circuit in Fig. 3.

The efficiency of the rectifying set, designed according to the circuit in Fig. 2, was calculated by the formula:

$$\eta_n = \frac{1}{1 + \frac{q}{U_{dn}} \sum U_{ai} s_i},$$

where U_{dn} is the rectified voltage of the n^{th} step; i the number of sections in the rectifying set.

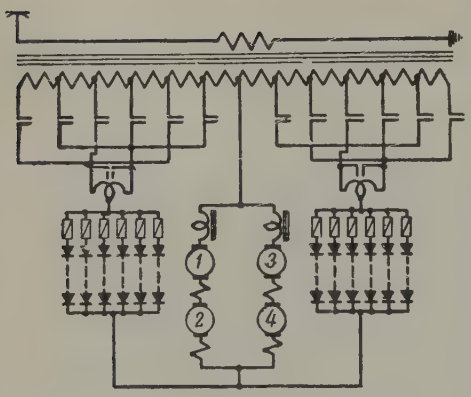

FIG.3 The principal power circuit of an English rolling stock multiple-unit with germanium rectifiers.

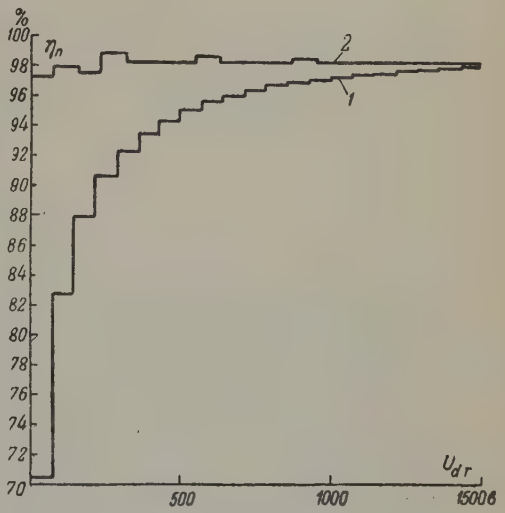

FIG.4 Efficiency of a rectifying set as a function of the rectified voltage. 1 - diagram of an English electric rolling stock multiple-unit with germanium rectifiers, 2 - diagram of parallel series switching-over of sections of a rectifying set.

For the calculation, it was taken into account that U_a for elements of parallel connected sections decreases according to the volt-ampere characteristic, [1]. The results of the calculations are shown in Fig. 4.

By examining the variations of the current throwing in the separate sections of the circuit of Fig. 2 on starting, we arrive at its values shown in the table. From this we see that the current is twice the rated value in section 5 – starting from step nine, in section 6 – starting from step twelve, in section 3 – starting from step thirteen and in section 4 – starting from step sixteen. The current throwing lasts for a much shorter time, and, consequently, starting conditions are made

easier for the whole set.

TABLE 1. Ratio of the section load of a rectifying set at the start I_{start}/I_{dn}

Sections	Steps																		
	1	2	3	4	5	6	7	8	9	10	11	12	13	14	15	16	17	18	19
1	2	—	2	—	2	—	2	—	2	—	2	—	2	—	2	—	2	—	2
2	—	2	2	—	—	2	2	—	—	2	2	—	—	2	2	—	—	2	2
3	—	—	—	0,5	1	1	1	1	1	1	1	1	2	2	2	2	2	2	2
4	—	—	—	0,5	1	1	1	1	1	1	1	1	—	—	—	2	2	2	2
5	—	—	—	0,5	—	—	—	1	2	2	2	2	2	2	2	2	2	2	2
6	—	—	—	0,5	—	—	—	1	—	—	—	2	2	2	2	2	2	2	2

Translated by S. Szymanski

REFERENCES

1. V.A. Golovanov; Primeneniye poluprovodnikovykh vypriamite-lei v ustroistvakh elektrichskoi tiagi (Use of semiconductor rectifiers in electric traction installations). *Biulleten tekhniko-ekonomicheskoi informatsii*, No. 4, Transzheldorizdat (1957).
2. V.E. Rozenfel'd and E.V. Chebotarev; Ustroistvo dlia Bezreostatnogo regulirovaniia napria-zheniia pitaniia tiagovykh dvigatelei (Device for voltage regulation without a rheostat for feeding traction motors). *Biulleten izobretenii*, No. 5 (1954).
3. V.A. Golovanov; Sposob pere-kliucheniia sektsii poluprovodnikovogo vypriamitelnogo agregata na elektropodvizhnom sostave odnofazno-postoiannogo toka (The method of switching-over of sections of a semiconductor rectifying set on electric rolling stock of an a.c. single-phase – d.c. traction system). *Biulleten izobretenii*, No. 10 (1957).
4. J.D. Watt; Redresseurs au germanium pour le service de la traction. Nouveau mode de conversion de l'energie nis au point par la BTH a l'usage des chemin de fer electrifies. *Bull. de l'Association Internationale du Congres des Chemins de fer. La traction Electrique dans les chemins de fer*, IX, No. 2 (1958).

PROBLEMS OF LIQUID COOLING IN ELECTRICAL EQUIPMENT*

O.B. BRON and D.S. ITENBERG

Leningrad

(Received 30 January 1958)

Fundamental considerations

Nowadays one cannot imagine an electrical machine without artificial cooling. In most machines this is an air ventilation system. Large turbogenerators are, however, water-cooled, the water being passed through the hollow conductors of the windings.

Electrical switchgear is a different matter. As a rule forced cooling is not applied here, the method being limited to the natural air cooling of the conductors. This can be explained by the complex design of the apparatus, by the large dimensions of the distribution gear and also by the fact that the loss of power in the equipment most commonly used is relatively small, and it is possible to make reliable and simple apparatus of acceptable size with natural air cooling. However, in recent years, a demand has grown for special apparatus which required us to use water cooling for the conductors.

First, it is necessary to mention high-frequency contactors. The development of high-frequency tempering of machine elements and the melting of metal needed the automation of processes; this can be achieved by using contactor devices.

Electromagnetic contactors were needed in systems for currents up to 1000 A, for voltages up to 1600 V, and for frequencies up to 10 kc/s. The commonly used contactors cannot satisfy these conditions.

It was necessary to work out a new, special series of high-frequency contactors. The question of cooling the live parts presented the major difficulty during the design. With natural cooling the presence of the surface effect in case of large currents and frequencies up to 10 kc/s made it necessary to build the apparatus with very large dimensions.

The application of water cooling resulted in a remarkable reduction in size and in the amount of non-ferrous metals used in high-frequency contactors, as well as making possible the replacement of a whole series of contactors designed for

* *Elektrichestvo* No.10. 65-70 1958.

current ratings of from 100 to 1000 A by a single piece of apparatus. We found that the dimensions of a water-cooled high-frequency contactor for currents up to 1000 A are smaller than for a contactor with natural air cooling for 100 A.

Water cooling was first used for small circuit-breakers with current ratings from 6 to 25 kA for ship equipment., for the chemical industry, and in several other fields.

The use of water cooling enabled the current ratings to be increased 4 to 5 times compared with naturally air-cooled equipment.

Very small alterations were required here in the design of the existing systems.

Finally, water cooling was used for making high-speed automatic mechanisms. This permitted a considerable decrease in the mass of the moving conductors, and consequently shortened the duration of the tripping processes, which essentially improves the characteristics of these devices.

The application of water cooling makes it possible to build high-speed automatic machines for currents of 5 to 10 kΩ, which was difficult and sometimes impossible by using natural air cooling.

The results of the work carried out in the factory "Elektrosila" in connexion with the water cooling of electrical equipment are published in this article.

Water and air cooling

Different views have been expressed on the artificial cooling of electrical equipment. Those who oppose water cooling consider that:

1. Water cooling results in considerable design and operating difficulties;

2. In the tripped position of the equipment there is imperfect insulation between the live conductors, since the open contacts are inter-connected by a column of cooling water;

3. The live conductors are connected to earth by the cooling water;

4. In the case of direct current, leakage through the cooling water causes an electrolytic transfer of metal from one part to another, which can put the apparatus out of order.

5. Condensation might appear when cold water is passed to the conductors. The falling drops of water can cause sparking between the conductors.

6. The water pipes can block up and then the water cooling system fails.

The opponents of liquid-cooled equipment draw the conclusion from these considerations that water cooling should not be used.

Undoubtedly, the application of liquid cooling makes the design and operation of equipment more complicated, and it should be employed only where it promises considerable advantages. In a number of cases examined below these

advantages are so great that they compensate both for the complication in operation and for necessary alterations in design.

The considerations of leakage of current through water, the electrolytic corrosion of parts of the equipment, and the imperfect insulation of the devices when water-cooling is used are greatly minimized to-day. There are simple and reliable methods of increasing the specific resistance of the water so that it can be considered practically as a dielectric (for details see below).

The application of a closed water-cooling water system, similar to that used in mercury rectifiers, removes all objections in connexion with the sweating and blocking of the pipes.

When artificial cooling of electrical equipment is chosen, a comparison should be made between water and air cooling [2].

Air at speed of 50 m/sec can remove 140 cal of heat from a surface of 1 m^2 during one hour if the temperature difference is $\Delta\tau = 1$ °C. Water at a speed of 2 m/sec subjected to the same conditions can remove 20 times more heat, i.e. 2800 cal.

Through an opening 1 cm^2 during one hour at a temperature difference of $\Delta\tau = 1$ °C it is possible to remove:

With air at a speed of v = 50 m/sec – 5 cal

With water at a speed of v = 2 m/sec – 700 cal

The heat capacity of water is 3500 times larger than the heat capacity of a monatomic gas atmospheric pressure.

Comparing water and oil cooling, it is necessary to mention the following:

The heat capacity of water is 2.5 times larger than the heat capacity of transformer oil. In the case of water cooling as opposed to oil cooling there is no danger of fire.

The viscosity of oil in the range up to 50 °C is greater than the viscosity of water a few dozens of times. The circulation of oil coolant therefore requires larger diameter tubes and a higher pressure head than water circulation.

All the previous points suggest the application of water cooling. A disadvantage of this method is the low specific resistance of tap water. This suggested the use of distilled water in a closed cooling cycle, so that the distilled water could be cooled by the tap water in a special heat exchanger.

The specific resistance of freshly distilled water is almost 40 times greater than the resistance of natural (ground) water. However, the resistance of distilled water decreases in service conditions. The water is contaminated by substances set free by the rubberized hoses, greasy bearings, stuffing boxes, pumps and so on. In given service conditions[3] after three months, the specific resistance of distilled water falls from 60 to 10 kΩ cm. But even with this decrease in specific resistance, distilled water enables us to obtain reliable

operation of cooling systems for electrical equipment.

Let us determine the magnitude of the leakage currents through the water, if specific resistance is $\rho = 10$ kΩcm. When the contacts of the apparatus are open, and at a voltage of 500 V, the diameter of the water column is 10 mm, its length is 250 mm and the leakage current will be 1.6 mA. Such a leakage does not have practical importance, and is not a danger to life. According to the rules for accident prevention, the permissible leakage current through insulations is from 20 to 50 mA; i.e. dozens of times greater than that obtained by us.

A leakage current to earth through a column of water in a pipe 10 mm in diameter and 1500 mm long is 0.27 mA; that is it is negligibly small.

Water as dielectric

The above considerations and calculations provided every reason for relying on water cooling, after taking into account the objections mentioned. However, the situation improved due to the fact that we turned to processes developed by the chemical industry for the refining of water.

The conduction of all electrolytes, including water, is dependant on the existence of ions in them. At present, there are filters capable of absorbing the ions [5]. In the simplest cases they are a device schematically shown in Fig. 1, actually used for our experiments. Insulator tube (1) is a catión filter filled with active sulphocarbon capable of holding the positive ions. Tube (2) filled with phenolformaldehide, an amino-resin, or mark EDZ-10P resin, is an anion filter which holds back the negative ions.

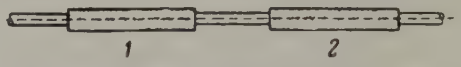

Fig. 1. Schematic diagram of the filter equipment for the chemical refining of water.

1. Cationite (filled with sulfocarbon).
2. Anionite (filled with resin).

After passing the water of the Leningrad water system through the anion and cation filters, its specific resistance was increased 100 times, and reached 10^6 Ω cm. According to the technical literature, it can be increased to 2.5×10^6 Ω cm. For comparison, we show the values of the usual specific resistance of water from different sources in kΩcm.

Tap water from Moscow	3.8
Tap water from Leningrad	10
Distilled water from distillery (freshly prepared)	60
Distilled water after three months use	10
Tap water from Leningrad after chemical refining.	1000

Ion filters in the flow system of water cooling virtually make the water a

dielectric, and eliminate all problems of leakage of the current through the water, of electrolysis of the conductors, of the reduction of the resistance of the insulation and so on.

The application of chemically-cleaned water makes it possible to decrease a hundredfold the leakage current in the water, considered above, and to bring it down to a negligible value of 16μ A.

The resistance of the water column in this case reaches 31 MΩ.

High-frequency contactors

With development of high-frequency melting and tempering of metals even before the war, the problem of manufacturing contactors capable of operating at frequencies of up to 3 kc/s, with voltages of 500 to 1500 V and currents of 100 to 1000 A. It was possible to satisfy these requirements only by developing a new series of high-frequency contactors.

Considerable difficulties were caused by the dimensions of the conductors of the contactors which were greatly heated owing to surface effect. It was possible to use several relays connected in parallel and to greatly increase the dimensions of the conductors in this way. This led to a general increase in the size of the contactors and to the irrational use of non-ferrous metals, since copper was practically not used in the contacts and busbars. It was possible to achieve a notable decrease in the dimensions of the equipment and in the quantity of non-ferrous metals by water-cooled hollow conductors and contacts.

Fig. 2 shows a photograph and a schematic diagram of a contactor of a disconnector (without arc extinction equipment).

Here the inmovable contacts 1, and the moving contact 2 are made of hollow bus-bars of rectangular cross-section. The pulling magnet system 3 can close and open the contacts. The water flows along the pipes 4, 5, 6 and 7, passes through the contacts, cools them, and leaves the system. In the whole mechanism only pipes 5 and 6 which supply the water to the moving contact have to be flexible.

The dimensions of the contactor described are suitable for 100 A. However, using water cooling, they can operate reliably at currents of over 1000 A, and a frequency of 10 kc/s. The impedance of the contacts together with the resistance of all the live parts is 36×10^{-4} Ω. In case of a current of 1000 A, the power loss is 360 W. In order to dissipate this energy on overheaters 20 °C it is necessary to use 15 l/hr of water.

The contactor described has no arc extinction equipment, and it can therefore only be operated as a disconnector. In normal operations, when the contactor has to switch off currents at a high frequency, it is equipped with an arc extinction system as shown in Fig. 3. In this system the brass plates of the arc extinction grid (1) are mounted in the narrow slot of an asbestos-cement chamber (2). In the form of a nozzle the chamber is closed on all sides, except for the narrow slot,

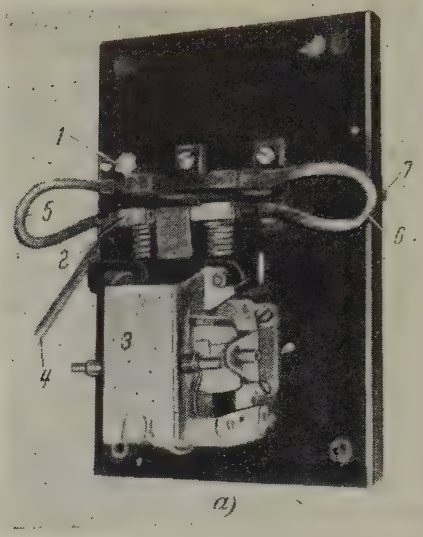

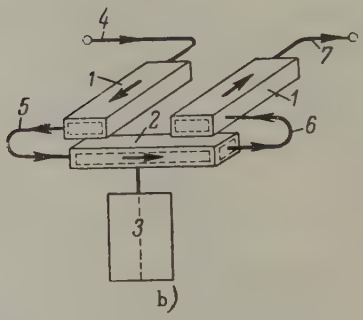

Fig. 2. High-frequency relay switch with water cooled contacts.
(a) general layout,
(b) the schematic diagram of the equipment.

into which the grid plates are inserted.

When the moving arc extinction contact (6) parts from the non-moving contact (3), the arc rises between them. The magnetic field of the coil (4) forces the arc to move to the sides of the grid, and conducts it to the internal edge of the plates. Arriving at the edge of the plates, the arc closes the outlet for the hot gases from the chamber. Pressure rises in the chamber which drives the arc into the grid. After entering the grid, the arc is extinguished at the very first passage of the current through zero.

In case of high frequency, this process is accompanied with generation of a small amount of heat [5].

The high-frequency contactor developed with water-cooled contacts, with the arc extinction equipment described has overall dimension of 360 x 250 mm. It can be operated with currents up to 1000 A, with voltages up to 15000 V and with

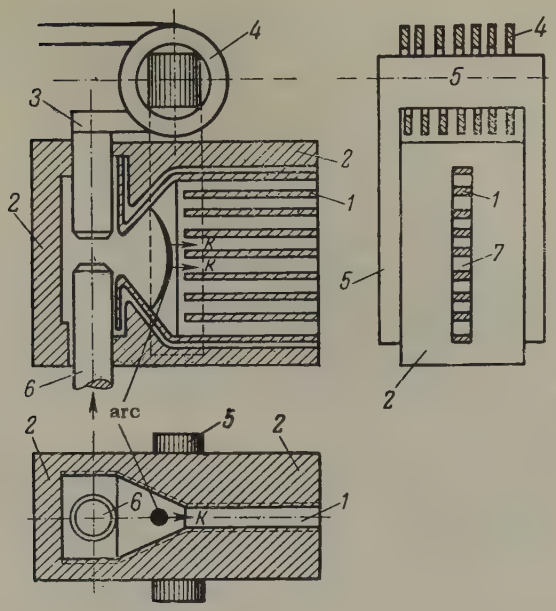

Fig. 3. Arc extinction equipment combined with high-frequency contactor.

1. the plate of the arc extinction grid; 2. extinction chamber; 3. non-moving contacts; 4. arc extinction coil; 5. magnet; 6. moving arc extinction contact; 7. the slot of the arc extinction chamber;

frequencies up to 10 kc/s. Only the main contacts are cooled by the water in the contactor. In the case of currents up to 150 A, liquid cooling is unnecessary; for currents between 150 and 750 A, it is necessary to water cool only the non-moving contacts; in case of currents higher than 750 A, the non-moving contacts as well as the bridge connecting them must be water-cooled.

The water flows to the contactors through hollow bus-bars made of copper tubes.

For comparison, we show the dimensions of the "K" series high-frequency contactors with natural air cooling. In case of a current of 100 A the dimensions are 330 x 38 mm; at 200 A 330 x 410 mm; at 400 A 330 x 600 mm; at 750 A 330 x 815 mm. Thus, dimensions of the water cooling contacter described are smaller than the 100 A contactor of the K series, and its current rating is higher than the rating of the largest in the series.

Automatic circuit breakers

In automatic circuit-breakers, water cooling of the contacts and bus-bars was introduced during the development of a class of this equipment for current ratings up to 25 kA. Such equipment was necessary for the chemical industry and for ship

equipment. The basis of development was the AS class of circuit-breakers of the "Elektrosila" factory. They are produced in standard design with the following ratings;

AS- 5	...	800 A
AS-15	...	1500 A
AS-25	...	2500 A

To increase the current ratings of this apparatus, their main non-moving contacts were water-cooled. The main contact system of such a circuit-breaker is shown in Fig. 4. The water through pipes (1) enters into the slots (2) and from here into the non-moving contact (3). It floods the body of the contact by pipe (4), goes into the insulator pipe (5) and from it enters the other non-moving contact (6). There it flows through pipe (7) and comes out into the hollow bus-bars (8) which carry off the water.

The application of water cooling permitted an increase in current rating, of circuit-breakers by a factor of 4. The current ratings, at which the automatic circuit-breakers of the AS series operate reliably, are shown in Table 1.

TABLE 1

Type	Current rating kA	
	Natural air cooling	Water cooling
AS-15	1.5	6.0
AS-25	2.5	10.0

Using four water-cooled circuit-breakers type AS-15, or two of the type AS-25 connected in parallel, we can get an automatic circuit-breaker for 20-24 kA. It has roughly the same dimensions as a three-phase circuit-breaker for 1500 A, but without water cooling.

The essential feature of the system described is that both circuit-breaker feeder bus-bars are water-cooled. This is convenient strictly from assembly considerations; there is no need for special water passing pipes, as the bus-bars act as such and the whole water-cooling system is concealed in the distributive equipment. Furthermore, this makes it possible, in some cases, to decrease the cross-section of the bus-bars, and to achieve a certain amount of economy in use of copper.

However, where there is no need to reduce the cross-section of the bus-bars for higher efficiency conditions there is an economy in reducing their temperature and consequently the power losses.

A further advantage of the system described is that it does not require the manufacture of new mechanisms but greatly increases the field of application of those already in existence (after equipping with water-cooling). The conversion of of natural air cooled into water-cooled apparatus does not cause big modifications

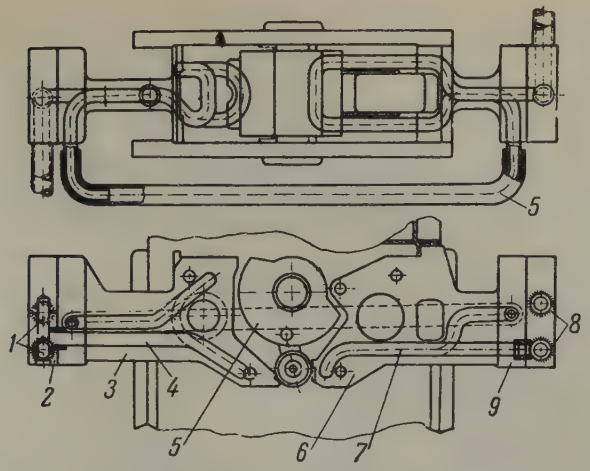

Fig. 4. The contact system of the water cooled AS series of automatic circuit-breaker.

in the design of the gear. The copper contact of an AS-25 circuit-breaker is shown in Fig. 5. On casting, holes are left in it; copper tubes are placed in them in which the water will flow.

In the circuit-breaker AS-15 apparatus at a current rating of 6 kA, the losses per pole amount to 720 W, and the water-flow through it with a temperature rise of 5° C is equal to 125 l/hr. If the pipe has a diameter of 10 mm and a cross-section of 0.8 cm², the speed of the cooling water will be 0.43/m/sec. Under these conditions the pressure drop on one pole of the equipment is 0.15 atm.

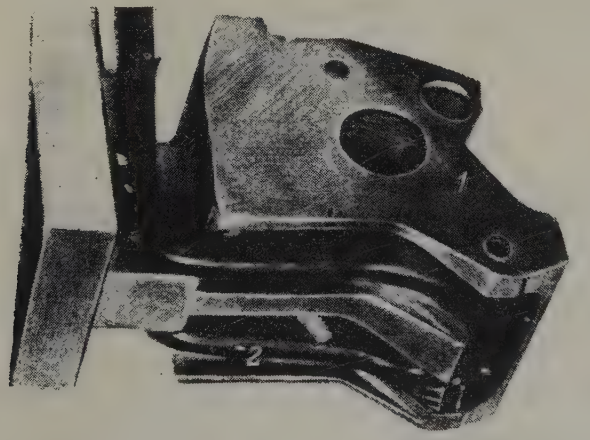

Fig. 5. Copper casting of contact (1) including the copper tube (2) for water cooling.

The maximium permissible current for the equipment in the described system is determined by the overheating of the moving main contacts, which are made in the form of rollers without water-cooling. These rollers, with a current of 6 kA

and water-cooled non-moving contacts, reach maximum permissible temperatures of 85° C.

If the design of the apparatus permitted the water-cooling of the moving contacts, the current ratings of the circuit-breaker could be increased to a much higher value. The overall dimensions of the two-pole water-cooled automatic circuit breaker for a current rating of 20 kA at 440 V are 640 x 558 x 354 mm. When we talk about water cooling, we have in mind a more or less complete project consisting of a number of such pieces of equipment, and in such cases the effect is especially great.

Long term application

Besides equipment with high current ratings and high-frequency contactors, water-cooling is expeditiously used in high-speed automatic circuit-breakers.

In the latter case, it is necessary to remember that there already exists a closed water cooling system in mercury rectifiers protected by high-speed circuit-breakers.

Therefore, the integration of high-speed circuit-breakers into this system does not involve technical difficulties and heavy expenditure.

In modern turbo-generators with a power of 200-300 MW and over, water cooling of the stator will be used. In such a case, it is obviously worth while continuing this system, and including water cooling of the bus-bars and the generator circuit-breakers.

This results both in a decrease of the dimensions of the circuit-breakers and bus-bars and in an increase in efficiency, owing to decreased copper losses, since the temperature of the live parts is decreased.

REFERENCES

1. R.S. Kuznetsov; *Elektricheskie apparaty raspredelitelnykh ustroistv nizkogo napryazhenie (Electrical equipment of low voltage distribution plant).* Gosenergoizda (1956).
2. E. Wiedemann; *Grenzleistungs - Turbogeneratoren, (Maximum voltage turbogenerators).* ETZ-A: 20, p.744 (1955).
3. P.A. Ostryakov; and I.V. Zaryanov. *Teploctvodyashchie ustanovki moshchnykh radiostantsii. (Heat dissipation equipment of large radio stations).* Svyazizdat, (1954).
4. M.S. Shkrob; *Vodopodgotovka (Water preparation).* Moscow (1952).
5. O.B. Bron and A.P. Makhonin; *Gashenie vysokochastotnoi v kontaktorakh (High-frequency arc extinction in contactors).* Symposium "Elektrosila" No.13, (1955).

ABSTRACTS FROM PAPERS PUBLISHED IN ELEKTRICHESTVO NO.10, 1958

Calculation of transient processes in linear systems: P.A. Jenkin. (pp 1-6).

The author expounds two approximate methods of calculating transient processes based on the use of integrals with a variable upper limit of a formula of right angles or of a formula of trapezoids. A table of results shows that integration based on the trapezoid formula gives practically the same result as the usual analytical method, whereas integration based on the right angle formula results in error. Such error is not considered to disturb the general character of the transient process curves and in any case can be considerably reduced by reducing the interval τ. The magnitude of τ is not known when beginning the calculations and the author recommends a preliminary approximate calculation by the method of successive ordinates using the right angle formula and then, after choosing τ, to make the calculation more precisely by the same method using the trapezoid formula. Certain values of τ may be assumed for the purpose of the calculations. The method can be used to investigate transient processes described by differential equations of high orders and also to calculate circuits with non-linear elements.

Galvanic effect of a.c. electrified railways, on single-conductor circuits: M.I. Mikhailov and L.D. Razumov. (pp 20-25)

A practical method is proposed for calculating the interference currents arising, for instance, in telegraph or distance feed circuits due to the difference in the potentials of the earth points. The maximum difference in the potentials depends on the position of the earth connexion in relation to the permanent way and several typical examples are considered. He argues that the conditions for setting single-conductor lines of communication close to the track involves consideration of the magnetic as well as the galvanic effects. The formula introduced were verified experimentally on a section of the electrified line from Ozherel to Pavelets. Considerable discrepancies were found between the calculated and measured results, but the calculations are approximately right.

Permanent magnets of the oxide anisothrope type: S.A. Medvedev. (pp 25-30)

The reduction in weight and size of electrical equipment has become very

desirable. The physics of magnetic phenomena, in particular the investigation of the processes of magnetization and magnetic polarity reversal cannot only now explain the majority of observed phenomena but investigations are also directed to the creation of new materials for permanent magnets. Success has been achieved in applying the theory to the development of pressed finely dispersed powders of different magnetic materials. The author briefly expounds this theory and considers the technology of production of oxide permanent magnets, their properties and their field of application.

Constructing the characteristics of a d.c. drive with reactor control: P.B. Resenbauli and I.N. Selivokhin. (pp 31 - 33)

The recent development of small crystals power rectifier has made it possible to produce a d.c.motor with reactor control ensuring sufficiently firm mechanical characteristics and a wide range of speed control. The author proposes a graphical-analytical method of plotting the mechanical characteristics of a d.c. motor which has been developed for a scheme of reactor feedback control. The method is based upon the determination of the relationship between the current and voltage on the armature of the motor by joint graphical-analytical solution of the feedback equations and of the characteristics of the simultaneous magnetization of the reactor material. The method is illustrated by diagrams and an example of the mathematical calculations is given.

How the armature reaction influences the operation of d.c. motors with permanent magnets: Iu. S. Zakharov. (pp 34 - 35)

The development of quality magneto-hard metals has paved the way for the use of permanent magnets as the excitation of electrical machines. In the case of d.c. motors, temperature stability and efficiency have been raised thereby and in some instances weight and size have been reduced. Difficulties have been encountered, however, in their technology of production and mathematical calculation. The author qualitatively describes the phenomena arising on the reversal of a d.c. motor with a permanent magnet. Here the de-magnetization of the machine is considered in the usual three sections. He argues that the usual methods of ageing permanent magnets do not give the desired results. For excitation, magnets are necessary which not only have a high coercive force but also a high residual inductance and a high covexity factor of the de-magnetization curve.

Equivalence of dynamic braking and starting an induction motor: V.R. Shippillo. (pp 36 - 37)

He states the equations to determine the slip of the induction motor on starting and during dynamic braking and demonstrates the analogy of braking and starting

conditions and the similarity of the characteristics if the currents are equivalent. He supports this by showing the results of tests on an R55 S 12 induction motor. He then establishes a qualitative and quantitative connexion between the dynamic braking conditions and the motor conditions of an induction machine. A simple method of calculating the characteristics of an induction motor in dynamic braking conditions is then given and illustrated graphically.

A high-speed magnetic amplifier for telemechanics: V.R. Kulikov. (pp 38-42)

High-speed magnetic amplifiers may be used in place of relay-contactor units in systems of telecontrol, (line, distribution, etc.). There are good prospects for the use of magnetic elements in tele-control equipment on sinusoidal current where there is no generator unit and the distributor is set in motion directly by a.c. impulses with a frequency of 50 c/s or 25 switch-covers per second. A simple approximate method is considered for designing a magnetic amplifier in the presence of considerable load inductance. Appendix I deals with the action of a magnetic amplifier as an impulse voltage amplifier. Here it is demonstrated that load inductance does not affect the method of operation of the amplifier. Appendix II deals with the determination of the fundamental relationships and Appendix III considers the relationship between the volume of copper and ferromagnetic material in the core.

Synchronous condensers for long-distance transmission systems: A.I. Vazhnov, E.V. Tolvinskaia, I.A. Gordon, D.A. Zavalishin and I.A. Glebov. (pp 43-47)

The method of installing synchronous condensers at intermediate points of a transmission line to increase stability is illustrated diagramatically. Increased effectiveness can be achieved by automatic control of excitation and compensation of the inductive resistance of the condensers with the aid of the capacitance which is connected in series in the circuit of the stator of the machine. Modified damping windings have been developed to overcome the difficulty of self-excitation by the machine. The calculations show that non-compensated synchronous condensers for prolonged service in normal conditions with lagging current can be based on the largest machines in current production, (75 MVA). In the case of leading current the condenser should operate with negative excitation currents. In the case of capacitive compensation it is necessary to develop certain rotor units, especially for the special damping windings of the visible (phaner) pole condenser. The insulation of the damping cores also needs to be investigated in order to prevent the possible burning of the pole terminal steel. Compensated condensers may also be made with non-visible poles. Compensated condensers operate with both leading and lagging current. Forced excitation of non-compensated synchronous condensers requires the ceiling excitation voltages to be raised.

Transients when rocking the wheels of an electric train: B.P. Petrov. (pp 48-52)

The phenomena of skidding of wheels often arise when operating electrical rolling stock and trains. The driver reduces the skidding by braking or pouring sand under the wheels. It is expedient to automate these processes. The author considers the transient processes arising in the presence of skiddings and curtailment of skidding by braking in the case of d.c. motors with series excitation. For this purpose he compares and solves initial equations which differ from those of Bader, (El. Bahnen; 11, 12, 1939), Minova and Trakhtman. The initial equations for graphical-analytical solution are compared on the usual assumptions. Here the equations are non-linear and in some cases Bashkirov's method of secants can be employed. Introducing a few additional assumptions he proceeds to analyse the processes arising on skidding and then when braking.

Protecting a.c. machines from internal faults in the stator windings; M.F. Shishkin. (pp 57-58)

Owing to the complexity of conventional differential protection this equipment is not usually installed on low output machines, for example, on generators for rural power stations. The author considers a simple and reliable protection against internal short circuits in the stator windings which can be used instead of differential protection. The method of operation of this protection is illustrated diagramatically and is based on the use of a magnetic coupling between the end connexions of the stator winding and a special protective coil. Tests have shown that such protection operates selectively in the presence of all types of internal and external short circuits except when the fault of an equal number of turns occurs in different phases of the stator winding.

Use of a method for testing the individual arc-extinguishing elements in high-voltage circuit-breakers: V.V. Kaplan and V.M. Nashatyr'. (pp 59-64)

The author discusses the theoretical and experimental basis for the widespread use of the method of testing the individual arc-extinguishing elements of high-voltage circuit-breakers in spite of the considerable development of synthetic schemes. He considers the effect of the static character of the arc-extinction process and the distribution of the recovery voltage on the operation of the circuit breaker. The results of experiments are then given, which partly corroborate his analysis of the operation of circuit-breakers with the enlistment of the theory of probabilities. He concludes that the breaking capacity of a circuit-breaker with several arc-extinguishing elements can be satisfactorily determined by summing the minimum values which have been determined for it with the same values of current for the individual elements provided that: (1) the elements of the circuit-breaker are identical in construction and have no noticeable direct effect on each

other in the sense of interaction on the intensity of the oil or gas blowing and so on; (2) the individual elements of the circuit-breaker are not connected up with low-ohmic shunting resistances or large capacitances.

Moving-coil oscillographs with frame type galvanometers: L.A. Biber and Iu. E'l'kind. (pp 70-71)

Moving-coil oscillographs have now been developed with frequencies of natural oscillations from 1.25 to 10,000 c/s and correspondingly with a current constant 8×10^{-9} - 9×10^{-3} Am/mm. Low frequency multi-channel frame-type galvonometers (up to 300-600 c/s) have magnetic damping; in the case of higher frequencies, liquid damping is employed. This apparatus is then described and their advantages are discussed: high sensitivity, simultaneous oscillographing of electrical and non-electrical magnitudes and their value in over damping conditions.

Where and why it is expedient to use 330 kV: N.N. Krachkovskii. (pp 72-76)

In connexion with the introduction of 500 kV in place of 400 kV for long distance transmission there is a large gap between the carrying capacities of 220 and 500 kV lines. The author supposes that there is a sufficiently wide range of distances and transmitted powers within which 330 kV could make considerable savings. He compares transmission of 220, 330 and 500 kV over 100, 200, 400, 600, 800 and 1000 km and determines the relationship of capital and operating costs to the power transmitted. The results are tabulated. He concludes that there are good reasons for adopting 330 kV transmission.

Measuring the torque of induction motors: E.A. Ivanov. (pp 77-79)

A method is proposed for determining the relationship M = f (s) in transient states. An inductive coil with a straight core of electrical sheet steel is used as activator. The amplitude values of the current induced in the coil-activator are proportional to the torque of the motor and the periodicity of this curve determines the value of the slip corresponding to the ordinates of the current. The method has been verified by comparison with two methods of measurement: (1) with the aid of a tensometric and (2) a capacitive coil-activator.

Studying the sparking of traction motors by means of photo-electric indicators: A.M. Trushkov. (pp 80-82)

The results of tests are given for switching experiments on traction motors carried out recently by the Novocherkask electric traction works on the Belovo-Novokyznets Tomsk section of the line with the aid of a photo-electric indicator of the variable sparking type, Mark II-1, produced by the Railway Scientific Research Institute. This indicator has a different averaging and amplifying system and a special

system of guidance to the source of the sparks. The author considers the scaling of the apparatus and takes the line density of sparking per unit length of the brush as the standard for evaluating the sparking intensity. The method of "sparkless zones" was employed to tune and regulate the additional poles of the traction machines. Typical oscillograms are shown of the mean magnitudes of the intensity of sparking of the brushes.

The increase of sparking at the beginning and its decrease at the end of the tests is attributed to temperature. The indicator has also been set up on an actual electric train and a part of the oscillogram shows how the intensity of sparking varied with the different operating conditions of the motor. The use of the photo-electric indicator is considered to be an improved method of evaluating the degree of sparking.

SHORT-CIRCUITS, ASYNCHRONOUS DRIVE AND TURBOGENERATOR RESYNCHRONIZATION*†

N.A. POLIAK

Teploe'lektroproekt

(Received 18 June 1958)

The decelerating action of a sudden short-circuit on the rotor of a synchronous generator has already long been known, [4]. The decelerating action is connected on the one hand with considerable power losses from short-circuit currents in the resistances in the stator circuit, and on the other hand with both the alternating electromagnetic torque on the generator shaft and with the power losses in the rotor circuits caused by the aperiodic component of the stator current, [3].

Until recently this decelerating action was not considered when rating the dynamic stability of parallel synchronous generators. Only a few years ago, in connexion with studies on long distance transmission line systems [1] and experiments carried out on electrodynamic models, the conclusion was reached that consideration of the decelerating action of a sudden short-circuit can make a substantial difference to the results of calculations in certain conditions.

In spite of the decelerating action of a sudden short-circuit, in the majority of cases a power surplus (torque) exists on the turbogenerator shaft until the short-circuit is tripped. This results in the fact that after the short-circuit is tripped, the rotor speed is greater than the speed appropriate to the line frequency. Under such conditions an asynchronous electromagnetic torque develops on the generator shaft, the force of which depends on the characteristics of the synchronous machine and on the parameters of the external circuit. The asynchronous torque acts favourably on the transient electromechanical process: the amplitude of the first rotor oscillation is somewhat decreased and the following are dampened.

Due to the change in speed, the turbine speed-control comes into action

* *Elektrichestvo* No. 11, 18-24, 1958.

From works by the author in the relay protection and stability department of the Teploe'lektroproekt.

altering the torque developed by the turbine. Certain conditions, for example during cascade tripping of the short-circuit, this can also have a favourable effect.

The sudden short-circuit abruptly increases the current in the excitation winding of the generator, and results in an increase in the electromagnetic decelerating torque on the exciter shaft. Rapid excitation forcing strengthens this effect somewhat. If the exciter is on the main shaft of the generator, the shaft is decelerated additionally, which also acts favourably on the transient process.

The greater the short-circuit current, the power losses connected with it (particularly in the rotor circuits), and the greater the asynchronous torque of the generator in the presence of slight slipping, the more favourable is the effect of these circumstances on the transient electromagnetic process during short-circuits in the network.

In this connexion, turbogenerators have extremely favourable characteristics which explains why in present-day electrical systems, where large thermal power stations are not connected to hydroelectric stations by particularly long transmission lines, cases of disturbance to the dynamic stability in parallel operation are exceptionally rare.

Large thermal power stations are usually connected to power-consuming centres by several transmission lines of relatively short length (100-200 km), but reasonably high voltage, (110-220 kV). This provides: (a) stable electrical connexion, i.e. a sufficiently large synchronizing torque between stations, (b) comparativily large short-circuit currents, and (c) considerable asynchronous torque on the turbogenerator shaft in transient conditions. Furthermore, modern high-speed relays and automatic devices, excitation forcing during short-circuits and high-speed and sufficiently powerful circuit-breakers are also of great value.

A theoretical-calculation study, the initial data and results of which are presented as follows, was made to determine the quantitative effect of the aforementioned conditions, and to explain those of them which are essential for the rating of dynamic stability in parallel turbogenerator operation, and also for rating the conditions of turbogenerator asynchronous drive and resynchronization. *

Rating circuit and initial data

The simplest system was considered with three parallel lines of 220 kV connected to a receiving system having a total turbogenerator and synchronous equalizer power of about 4000 MVA, (Fig. 1). Transmission distance was 200 km.

* The calculations were made by A.F. Tsukerman, a colleague at the Teploe'lektroproekt.

The voltage after reactance of the receiving system was taken as constant in magnitude and phase. This meant that the mechanical inertia constant of the rotors of the synchronous machines in the receiving system was considered to be infinitely great.

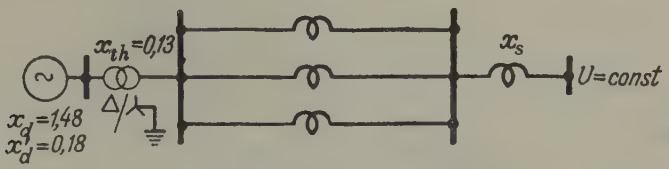

FIG. 1. Transmission circuit

The total power of the turbogenerators in the thermal station was examined within the limits of 150-600 MVA, (Table 1). In all cases, it was assumed that in normal operation prior to short-circuiting, the voltage at the outputs and the active and reactive loads of all the turbogenerators were as rated. Local demands, the station's own consumption and the power losses in the step-up transformers were not taken into consideration.

TABLE 1

Transmission parameters

Total turbogenerator power of station in MVA	x_s	In normal operation with three circuits			In post-fault operation with two circuits			
		x_l	Σx	θ, el.grad	x_l	Σx	θ, el. grad	k'_{st}
150	0.050	0.075	0.255	53	0.112	0.292	55	2.40
250	0.033	0.125	0.338	58	0.187	0.400	61	1.89
400	0.133	0.200	0.463	66	0.300	0.563	74	1.45
450	0.150	0.225	0.505	69	0.337	0.617	78	1.35
500	0.166	0.250	0.546	71	0.375	0.671	—	1.26
600	0.200	0.300	0.630	77	0.450	0.780	—	1.11

The parameters 150 MVA, $\cos\phi = 0.9$, of the bipolar turbogenerator made by the S.M. Kirov'Elektrosila' factory were taken as the ratings. This selection was made because experimental data was available for this machine concerning rotor circuit parameters for different slidings which permitted a sufficiently accurate determination of the torques in the presence of short-circuits.

The exciters in the turbogenerators made by the electric machine building factories of the Soviet Union ensure sufficiently rapid double forcing of excitation voltage during short-circuits in the network. With such forcing and short-circuits immediately after the step-up transformer or in the line the constancy of the longitudinal component of the e.m.f. is almost guaranteed after the transient reactance of the generator. The introduction of this condition made possible a considerable

simplification and speeding-up of the calculations; with the same objects in mind line capacitance and resistance before and after short-circuiting were not considered.

The greater the power transmitted in normal operation, the greater the reactances of lines and receiving system in fractions of units relative to the total rated apparent power of the turbogenerators, and the greater the angle of displacement between the vector of the rotor e.m.f. and the vector of the receiving system voltage (Table 1). The size of the static limit of transmission power K'_{st} from the condition of the equality of values for E'_d in normal and fault conditions is extremely great. Thus, the electrical transmission under consideration, even with extremely heavy circuit loads, has good static characteristics. In addition, it is apparent that in order to avoid passage into the artificial stability zone, the load on the circuit during post-fault operation should not exceed 225 MVA.

Short-circuits and dynamic stability of parallel operation

All types of short-circuit were considered, both at the beginning and at the end of one of the three circuits. It was decided that the fault line would be cut off from the high-speed series differential line protection at both ends at once in 0.20 sec, or in cascade in 0.20 sec at the fault end, and 0.80 sec at the opposite end of the line.

The rating of the dynamic stability was made for maximum power transmitted on the three lines under normal conditions of operation whereby the turbogenerators in the first half-cycle after the short-circuit is broken do not drop out of synchronization. The band of powers, limited by "stable" and "unstable" results, the "rating fork", was 25 MVA.

Two series of calculations were made: one according to the universally used (standard) method [6], i.e. without calculating the aperiodic component of the stator current, the power loss in the stator winding during short-circuiting, the asynchronous torque after the short-circuit is tripped and the action of the turbine speed control, and the other with the calculation of all these factors, (precision calculation).

For the calculation of the decelerating action of a sudden short circuit in rating the dynamic stability of synchronous machines operating in parallel, we adopted the method using the "equivalent load of the synchronous machine" during a three-phase short-circuit. Since it is applied to the turbogenerator shaft throughout the duration of the three-phase short-circuit, the equivalent load is practically speaking a sufficiently accurate reflection of the results of the decelerating action up to the moment when the short-circuit is tripped. The value of the equivalent load depends on the distance of the short-circuit from the turbogenerator outlets and on its duration, (Fig. 2). In the presence of a three-phase short-circuit near the station busbars, the equivalent load is considerable.

For example, in the presence of a three-phase short-circuit after a step-up transformer with a reactance of $X_{tr} = 0.13$, and with a short-circuit duration of 0.20 sec, the equivalent load amounts to approximately 60 MVA relative to a turbogenerator of 150 MVA, cos $\phi = 0.90$. Thus, as opposed to the widely held idea that a sudden three-phase short-circuit of short duration near the station busbars results in complete generator unloading, in the given case the equivalent load of the turbine is 40 per cent of the rated load before the short-circuit is broken. If a three-phase short-circuit should occur immediately at the turbogenerator outlets, the equivalent load for a duration of 0.20 sec could not be 60 but 300 MVA, i.e. the rated power of the turbine would be doubled, and the machine would begin to decelerate.

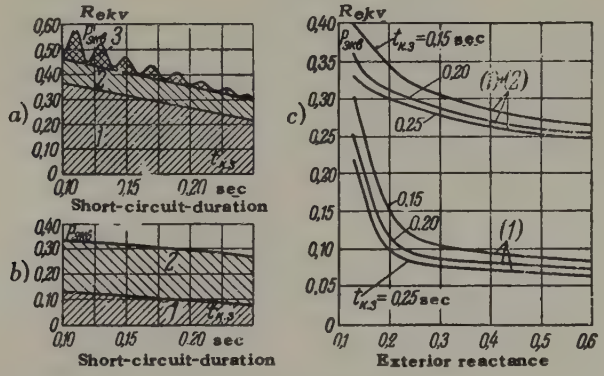

FIG. 2. Equivalent turbogenerator load with three-phase short-circuit dependant on duration of short-circuit and exterior reactance.

a – short-circuit immediately after step-up transformer; *lb* – short-circuit on 220 kV line (exterior reactance $x_{tr} + x_1 = 0.30$); *c* – short-circuits at different points on the 220 kV line. 1 – component due to power losses in rotor circuits; 2. component due to power losses in the stator circuit, (including the step-up transformers and transmission line); 3 – component due to the alternating electromagnetic torque.

In the case of distant and also of asymmetrical short-circuits, the equivalent load is considerably less. In order to simplify the calculations for asymmetrical short-circuits, we included in the equivalent load only the losses in the rotor circuits caused by the aperiodic component of the positive sequence current, and by the losses from the periodic component of the negative sequence current.

In all cases precision calculations result in greater values for permissible transmission loads, (Table 2). The more powerful the type of short-circuit under consideration is, the greater the difference. With simultaneous tripping of the fault line at both ends in 0.20 sec the difference amounts to: approximately

5 per cent in the presence of a single-phase earthing fault, with two-phase short-circuiting approximately 10 per cent, in the presence of a two-phase earth fault approximately 20 per cent smaller value, but in the presence of a three-phase short-circuit approximately 100 per cent when the fault is at the beginning of the line, and approximately 80 per cent when the fault is at the end. Thus, it is impossible to consider a three-phase short-circuit close to the stator outlets without a calculation of the equivalent load. In all cases, short-circuits at the beginning of the line are essentially less powerful than the same type of short-circuits at the end of the line.

As is known, transmission capacity is determined by the conditions of normal and post-fault operation, by dynamic stability and by the multiple of the static limit of transmitted power in post-fault operation. In order to avoid transmission passage to the artificial stability zone in post-fault operation, the load for the three lines in normal operation according to Table 1 should not exceed 450 MVA. Under such conditions transmission is dynamically stable even with three-phase short-circuiting at the beginning of the line (450 MVA), and is almost stable with short-circuiting at the end of the line (400 MVA). The necessary conditions are: tripping of the fault line at both ends at once in 0.20 sec, automatic control and sufficiently effective turbogenerator excitation forcing which in all calculations were considered as constant values for the series component of the turbogenerator e.m.f. after transient reactance. The static power limit multiple in post fault operation also remains reasonably high. In this it is seen that the transmission load in post-fault operation is the same as in normal operation. When the short-circuit is tripped more slowly and also in cascade, conditions are less favourable.

In precision calculations the equivalent load during short-circuit conditions plays an extremely important role. The calculation of the asynchronous turbogenerator torque after the short-circuit has been tripped and the remaining circumstances, including the action of the turbine speed control, are of secondary importance.

If it is not required that the transmission load in post-fault operation remain the same as in normal operation, then when the fault line is tripped simultaneously, part of the turbogenerators can be tripped, and this makes possible transmission in normal operation of 450 MVA on three circuits (Fig. 1) and when the short-circuit is tripped less rapidly.

Precision calculations, particularly the rating of the equivalent load during short-circuiting in more complex transmission systems and lines than the system shown in Fig. 1, would complicate calculations considerably and increase the volume of calculating operations. On the other hand, initial rated data are usually not so accurate as to make such complications expedient.

However, in those cases where it is a question of calculating the dynamic stability for a specific transmission system, for example, calculations made before tests or calculations necessary for detailed analysis of abnormal conditions

occurring in an electrical system, particularly if it is a question of three-phase short-circuits, the complete calculation of the equivalent load of turbogenerators and of other factors becomes necessary.

Loss of synchronization, asynchronous drive, resynchronization and synchronous swings

When the short-circuit is tripped with insufficient rapidity, the turbogenerators in the thermal station fall out of synchronization and change to an asynchronous mode of operation in relation to the generators in the receiving system. In this the turbogenerators continue to operate with full excitation as opposed to asynchronous operation caused by excitation losses [5]. After a certain time turbogenerators can be drawn back into synchronization once again.

The whole process whereby turbogenerators fall out of synchronization and are subsequently drawn back into synchronization can be conventionally divided into three stages according to time: (1) loss of synchronization and acceleration of the turbogenerator rotors, (2) rotor deceleration and (3) resynchronization and synchronous operation (Fig. 3).

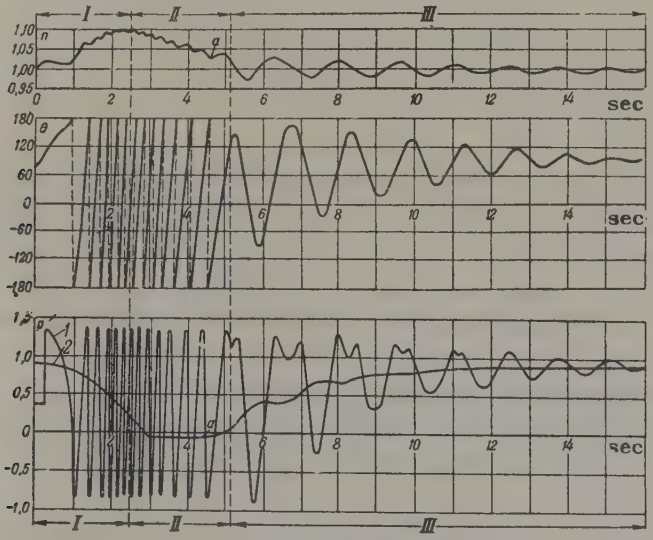

FIG. 3. Relative speed n of a turbogenerator, angular displacement of rotor θ electromagnetic power of turbogenerator (1), and power developed by turbine (2) during asynchronous drive.
a – resumption, of steam inflow into turbine; I – loss of synchronization and rotor acceleration; II – rotor deceleration; III – resynchronization and synchronous swings.

The first stage begins with the dynamic disturbance of the normal mode of operation. The electromagnetic power (load) of the turbogenerator, after

momentarily rising to the maximum value, rapidly diminishes, passes through zero and then fluctuates within considerable limits. In the conditions under consideration the average load for each cycle of asynchronous drive is small, the equilibrium of torques on the shaft of the turbogenerators is disrupted, the rotor speed increases and the turbine speed control comes into action beginning to shut off the steam inflow. The difference between the average turbogenerator electromagnetic power and the power developed by the turbine gradually decreases and disappears after a certain time. The rotor speed at this moment is at a maximum. With this the first stage ends, its duration being basically determined by the rate at which steam inflow into the turbine is decreased.

When a turbogenerator which is operating at the rated load is cut off from the system, 1—3 sec is required from the moment when it is cut off until the steam inflow into the turbine has been completely stopped. These values are smaller for steam condensation turbines of the usual type, and larger for turbines with intermediate steam superheating if the steam bypass into the condenser does not come into action. Since loss of synchronization is not accompanied by the instantaneous drop of the full load, slightly more time elapses before the steam inflow is completely cut off. In order to limit the duration of the first stage, and connected with this (and what is still more important) in order to decrease the duration of the second stage, it is important that the steam inflow into the turbine be decreased as quickly as possible.

During the second stage the deceleration of the turbogenerator rotors is caused by the action of the following three factors: (1) by the average power losses for each cycle of asynchronous drive in stator circuit resistances depending on the resistance of the transmission lines*, the characteristics of the system of turbogenerator automatic excitation control and the parameters of the external network; (2) by the asynchronous decelerating torque on the turbogenerator shaft, the dimensions of which depend on the generator characteristics and the parameters of the external network; (3) by turbine rotor vane friction in the steam medium after full stoppage of steam inflow, though there is a vacuum in the turbine condenser; we evaluated this decelerating torque at 5 per cent of the rated torque of the steam turbine.

If conditions are such that resynchronization can occur, it is performed at a speed approximately 2 per cent higher than synchronous speed.

In Table 3, the duration of the second stage in different conditions is shown. Since the cross-section of 110 kV lines is about half that for 220 kV lines, and the reactance per unit line length in both cases is practically the same, other

* The resistance of the transmission lines was also considered in calculations for asynchronous operation.

TABLE 2

Maximum permissible transmission loads for dynamic stability conditions with different types of short-circuit on the line.

Conditions for tripping fault circuit	Type and location of short-circuit		Permissible loads MVA		k'_{st}
			Standard method of calculation without considering resistance	Precision calculation	
Simultaneous tripping at both ends	Three-phase	At beginning of line	225	450	1.35
		At end of line	225	400	1.45
	Two-phase earth fault	At beginning of line	425	500	1.26
		At end of line	400	475	1.30
	Two-phase	At beginning of line	525	> 600	–
		At end of line	525	575	1.14
	Single-phase earth fault	At beginning of line	575	> 600	–
		At end of line	575	> 600	–
Cascade tripping	Three-phase	At beginning of line	150	325	1.65
		At end of line	< 150	200	2.11
	Two-phase earth fault	At beginning of line	375	450	1.35
		At end of line	300	350	1.56
	Two-phase	At beginning of line	475	525	1.20
		At end of line	425	450	1.35
	Single-phase earth fault	At beginning of line	550	600	%
		At end of line	525	550	1.17

before tests or calculations necessary for detailed analysis of abnormal conditions

things being equal, the power losses in 110 kV lines are greater, and this somewhat decreases the turbogenerator deceleration time.

TABLE 3

Turbogenerator rotor deceleration time

Power transmitted on line MVA	Deceleration time, sec		
	Generators have automatic excitation control		Generator field quenched
	220 kV lines	110 kV lines	220 kV lines
150	1.9	1.6	2.3
250	2.3	1.8	3.2
400	2.8	2.0	4.6
500	3.1	2.1	5.4

When applied to the conditions of the system described in Fig. 1, resynchronization for the two circuits remaining in operation is practicable even if the total power of the thermal station turbogenerators amounts to 500 MVA, i.e. almost 15 per cent of the receiving system power. This exceeds the power which can be transmitted with two circuits in long distance operation.

Retarding the action of the turbine speed control when steam inflow is resumed at the end of the second stage facilitates the conditions of resynchronization. However, the delay should not continue to the stoppage of steam inflow at the beginning of the loss of synchronization, since this lengthens the first stage and can in unfavourable conditions result in an excessive increase in the rotor speed, and the operation of the turbine automatic safety device. Partial steam inflow stoppage at the end of the first stage or too early steam inflow resumption during the second stage can make the conditions of resynchronization difficult. The less the residual statism* of the turbine speed control, other things being equal, the more favourable the resynchronization conditions; in our calculations statism* was equal to 4 per cent of the rated speed.

Artificial delaying of steam inflow into the turbine by means of secondary speed control until the rotor speed in the process of decelerating is almost reduced to the speed appropriate to the frequency of the network facilitates the conditions of resynchronization.

* "Statism" in Russian technical literature is defined as "the deviation of the controlled magnitude at rated load from its value on no load, expressed as a percentage, (of its value on no load). Editor's note.

With considerable loads on transmission lines automatic turbogenerator excitation control is a necessary condition for resynchronization in practice.

In actual conditions, where the constant mechanical inertia of the turbogenerator rotors and synchronous compensators of the receiving system has a decisive significance, the frequency in the receiving system with asynchronous turbogenerator drive in a large station does not remain constant, and resynchronization conditions are more difficult than those indicated here.

On the other hand, the consumption of power at the generator voltage, including devices requiring power for the station's own use, and also the presence of consumers feeding on the same station with separate h.v. lines result in the fact that with asynchronous operation there is not as considerable a power loss as in the case considered above. The increase in the turbogenerator rotor speed is less, the first and second stages are shorter and resynchronization takes place more rapidly.

Conditions of turbogenerator operation

In asynchronous operation the currents in the turbogenerator winding are higher than rated, and the electromagnetic power is alternately positive and negative, i.e. a torque with an alterating sign acts on the shaft of the aggregate; in the solid mass, (the "body"), of the rotor there are additional losses from slip frequency currents. Data are given in Table 4 concerning the conditions when the turbogenerator rotor speed amounts to 106 per cent of the rated speed. This value can be conventionally considered as the average rate of turbogenerator rotor speed before resynchronization.

The less the system of turbogenerator excitation is inert but the more effectively automatic excitation control operates, the greater the values for average stator and rotor currents and the amplitude of their fluctuations, (second terms in Table 4). In spite of the fact that the currents are great, it can be considered that asynchronous drive for about 10 sec does not cause an excessive increase in the temperature of conductors and their insulation in present-day turbogenerators with air or the usual (not internal) hydrogen cooling. This does not include, however, the new type of turbogenerator now being made with hydrogen or liquid internal cooling of the winding in which current densities are considerably higher than in turbogenerators of usual construction.

Additional losses in the solid mass of the rotor and excitation winding are not so great as to cause their excessive heating during the above-mentioned 10 sec on the condition that the maximum slip, i.e. the difference in the rotor speeds in the thermal station turbogenerators and the receiving system generators, does not exceed 10 per cent of the rated speed of rotation. In this, of course, it is seen that rotor steel banding (end-bells), of sufficient thickness is built on to the body to ensure safety at increased speed, thus eliminating the possibility of

TABLE 4

Stator and rotor currents and variation in turbogenerator electromagnetic power in asynchronous operation (in relative units)

Power transmitted on line, MVA	Generators have automatic excitation control			Generator field quenched
	Stator current	Excitation current	Limits of variation in electromagnetic power	Stator current
150	3.27 ± 2.00	1.66 ± 1.18	± 2.04	1.84
250	2.56 ± 1.62	1.44 ± 0.96	± 1.62	1.48
400	1.93 ± 1.26	1.21 ± 0.74	± 1.26	1.16
500	1.66 ± 1.10	1.12 ± 0.65	± 1.05	1.02

of any local heating of the solid masses, teeth and banding.

Voltage fluctuations in the electrical system

Asynchronous drive of turbogenerators in the station under consideration, depending on the synchronous machines of the receiving systems, is accompanied by active and reactive current fluctuations, and in connexion with this by voltage fluctuations at different points in the network, (Table 5).

TABLE 5

Voltages (in fractions of rated voltage) at the turbogenerator outlets and the end of line during asynchronous drive.

Power transmitted on line, MVA	Generators have automatic excitation control		Generator field quenched	
	Voltage at generator outlets	Voltage at end of line	Voltage at generator outlets	Voltage at end of line
150	0.78 ± 0.22	0.82 ± 0.11	0.39	0.90
250	0.77 ± 0.23	0.77 ± 0.15	0.33	0.87
400	0.76 ± 0.24	0.72 ± 0.18	0.26	0.83
500	0.76 ± 0.24	0.69 ± 0.20	0.22	0.81

The greater the total power of the turbogenerators in the station that have dropped out of synchronization, the lower the average voltage level during asynchronous drive both at the output from the turbogenerator and at the receiving

end of the transmission line. If in the system there are separate long distance transmission lines from hydroelectric stations operating as a rule with relatively small static stability reserves, then when the thermal station generators drop out of synchronization whose power amounts to a considerable portion of the power of the system, the voltage fluctuations at the end of the line can reflect unfavourably on the operation of long distance transmission from hydroelectric stations.

With the same values in relative units for the total exterior reactances, but with a lesser receiving system reactance than shown in Table 1, i.e. with greater power in the system, the voltage deviations from normal at the receiving end of the transmission line is proportionately smaller than shown in Table 5.

It would seem that after falling out of synchronization when the quenching device is tripped, the turbogenerators are no longer excited, (the field is quenched). This would eliminate voltage fluctuations during asynchronous drive, but in addition it would lower the voltage sharply at the output from the turbogenerator. Stator current fluctuations would for all practical purposes vanish, the average turbogenerator load for each asynchronous drive cycle would be decreased and this in its turn would lead to a slight increase in the duration of rotor deceleration. However, practically speaking, field quenching would be possible only in the case where the thermal station falling out of synchronization did not have local consumers, and the station's own consumption could be fed from another source independently of the common network. Since the actual conditions of operation of thermal stations do not allow this, field quenching of the station turbogenerators which have fallen out of synchronization cannot be applied in practice.

Conclusion

The dynamic stability of parallel turbogenerator operation during short-circuits in the network is always higher than the rated stability obtained by the usual standard method, the maximum difference occurring in the case of powerful short-circuits at points relatively close electrically to the turbogenerator outlets. The chief cause of this lies in the fact that in standard calculations allowance is not made for the electromagnetic torques on the turbogenerator shaft caused by the aperiodic stator current component which occurs at the instant of short-circuiting or of another abrupt change in conditions.

Thermal station turbogenerator resynchronization after loss of synchronization, depending on other gene. .tor stations in the system, is feasible in conditions close to those considered here even in the case where the total power of the station turbogenerators dropping out of synchronization somewhat exceeds the power which in continuous operation can be transmitted on the remaining lines.

The question of asynchronous drive and resynchronization of turbogenerators with internal hydrogen or liquid cooling is receiving further consideration.

REFERENCES

1. E. Ia. Kazovskii; Energeticheskie sovtnosheniya pri vnezapnom korothom zemykarii sinkhronnoi mashiny. (Power relationships during sudden synchronous machine short-circuit). *Elektrichestvo;* No. 7 (1954).
2. M.P. Kostenko; Issledovanie problem avtomaticheskogo upravleniya elektroenergeticheskimi sistemami s primeneniem metodon elektrostinemicheskoyo modelirovaniya, A study of the problems of automatic control of electrical power systems using electrodynamic modelling methods). Sessions of Academy of Sciences, U.S.S.R., on scientific problems of industrial automatization 15-20 Oct., 1956. Complex automatization of production processes. *Izd. Akad. Nauk U.S.S.R.* (1957).
3. R.A. Lyuter; Raschet momentov urashcheniya sinkhronnykh mashin pri korotkikh zamykaniyakh. (Calculation of the torque of synchronous machines during short-circuits). *Symposium No. 7 "Electrosila" factory.* Gosenergoizdat pp 29-40 (1950).
4. R. Riudenberg; Toki korotkogo zamykaniya v praktike eksplyatatsii krupnykh elektricheskikh stantsii. *(Short-circuit currents in the practical operation of large power stations).* Translated from the German. Gostekhizdat (1930).
5. I.A. Syromyatnikov; Rezhimy raboty sinkhronnykh generatorov. *(Conditions of synchronous generator operation).* Gosenergoizdat. (1952).
6. P.S. Zhdanov; Ustoichivost' elektricheskikh sistem. *(Stability of electrical systems).* Gosenergoizdat. (1948).

A SYNTHETIC METHOD OF TESTING HIGH-VOLTAGE CIRCUIT-BREAKERS*

V.V. KAPLAN, V.M. NASHATYR' and V.L. IVANOV

(Received 20 January 1958)

INTRODUCTION

Testing in an automatic reclosure cycle is of great value in rating the switching capacity of h.v. circuit-breakers in addition to checking the breaking and making capacity. Such tests should be made for all types of circuit-breakers designated for operation in these conditions. However, circuit-breakers are actually tested in an automatic reclosure cycle only in isolated cases directly on the line as there are no laboratory circuits permitting such tests with sufficiently great short-circuit powers. In connexion with this, the creation of a synthetic circuit for testing circuit-breakers in an automatic reclosure cycle is extremely significant.

In 1957 in the Gorev High-voltage Engineering Laboratory of the Leningrad Polytechnic Institute (TVN LPI) a circuit was developed on the basis of an oscillatory circuit and put into practice which allowed synthetic testing of high-speed circuit-breakers operating in a single automatic reclosure cycle, (breaking-making-breaking).

The conditions for setting up equivalent synthetic circuit-breaker testing in an automatic reclosure cycle can be formulated on the basis of the demands made on a synthetic method of testing making and breaking capacity, [1 and 2]. The following conditions form the basis of synthetic testing in an automatic reclosure cycle:

1. Only those circuit-breakers are tested in an automatic reclosure cycle which have previously undergone successful testing in a breaking cycle, and consequently perform arc quenching dependably in breaking a given current with recovery voltage at full value. Therefore, in testing in an automatic reclosure cycle, the first operation (breaking) can be performed at a decreased voltage, but naturally, at the given value for the breaking current. However, the same time must

* *Elektrichestvo* No. 11, 29-35, 1958.

be allowed for arc burning in the circuit-breaker as for breaking at full voltage. Generally, the arc burning time in the circuit-breaker must be artificially extended if it is prematurely quenched in the decreased voltage circuit.

2. The second operation of the automatic reclosure cycle (making) must be performed synthetically with the provision of complete equivalent testing conditions. The approach of the circuit-breaker contacts must occur with a voltage value corresponding to the rated line voltage. During the spark-over between the circuit-breaker contacts a making current must cross the arc gap which is of the same amplitude and curve form as in the line; an accordance must also be reached between the current derivatives in the initial instants of its flow. In addition, with the spark-over between the contacts a current impulse must cross the circuit-breaker corresponding to the capacitive discharge of the dropout lines in the system.

3. In actual conditions of circuit-breaker operation in a high-speed automatic reclosure cycle, a short-circuit current passes through the metal short-circuit contacts of the circuit-breaker for approximately 0.05 - 0.06 sec or slightly longer, from the moment of short-circuit contact to the moment when the contacts again diverge. Separate checking of circuit-breaker contact system stability with large currents (with lowered voltage), and also full preliminary testing of making capacity (at high voltage) make it unnecessary for the short-circuit current to flow while testing the switching capacity of a circuit-breaker with metal closed contacts. This results in a notable simplification in testing, since with the use of an oscillatory circuit, a great number of capacitors are required to ensure the prolonged passage of the undamped short-circuit current.

Essentially the same condition is used in the standard method of testing breaking capacity. In these tests, the duration of the "metal short-circuit", (namely, the interval of time during which the breaking current flows in the test circuit, but there is a metal contact between circuit-breaker contacts), must be reduced to zero since in actual conditions it amounts to 0.05-0.06 sec.

4. The third operation of the automatic reclosure cycle (breaking) must also be made synthetically providing for the equivalent reproduction of circuit-breaker operation on a real line. For this, from the instant preceeding current zero passage for approximately 300 - 600 μsec until zero current value, exactly to the instant when the formation of an arc quenching cycle is possible, the circuit-breaker must be in circuit where the voltage, inductance and capacitance, and the determined voltage recovery rate have the same values as in the line. With these conditions the same current to zero approach rate is ensured as in the actual line, and also voltage recovery conditions in the circuit-breaker are fully reproduced.

5. The current amplitude with each successive operation must differ little from its value in the preceeding operation, reproducing the corresponding

conditions in the actual line where the short-circuit current is little damped during the automatic reclosure cycle in the circuit-breaker.

6. Circuit-breakers on the line can operate both in a single-phase and in a three-phase automatic reclosure system with different types of short-circuit, and therefore different correlations are generally possible between the values for the voltages applied to one terminal of the circuit-breaker when making and breaking.

It is highly desirable that the test circuit in which tests are made on one circuit-breaker terminal, also makes it possible to obtain different correlations between making voltage and recovery voltage. It is at least necessary that the recovery voltage (line frequency component) should not be notably lower than the making voltage.

Principal circuit of test apparatus (Fig. 1)

Two oscillatory circuits were used in the apparatus adjusted to line frequency, one $C_0 - I_0 - L_0$ provides for the first operation of the automatic reclosure cycle (breaking), and the second $C_1 - L_1$ functions as the circuit source of the making and the breaking current for the last two operations of the automatic reclosure cycle (making, breaking).

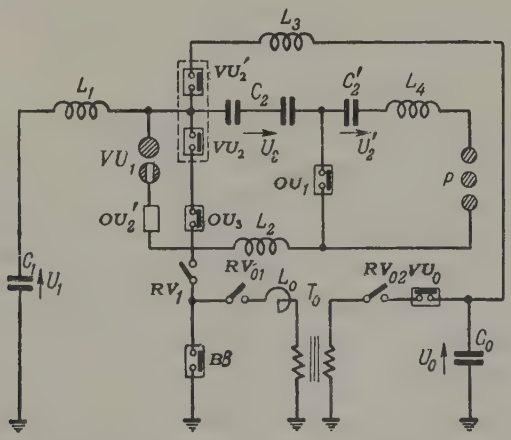

FIG. 1. Principal circuit of apparatus for the synthetic testing of circuit-breakers in an automatic reclosure cycle.

One oscillatory circuit $C_2 - L_2$ is used as the h.v. circuit in the last two operations adjusted to an increased frequency, somewhat higher than line frequency.

The circuit operates in the following manner. Initially switch RV_1 is open, and switches RV_{01} and RV_{02} are closed. The experiment begins with the closing of

switching device VU_0. The breaking current i_0 passes through the circuit-breaker being tested B. Immediately the contacts of B, operating in the automatic reclosure cycle, diverge. After one half-cycle of current flow, the arc is quenched by the test circuit-breaker. Thus, the first operation (breaking) of the cycle (breaking-making-breaking) is carried out. As was indicated above, this operation is performed at a decreased voltage, and it is expedient to use a step-down transformer I_0 in the first oscillatory circuit which makes it possible to obtain the given current i_0 with a smaller reactive power of battery C_0.

After arc quenching in B, switches RV_{01} and RV_{02} are first opened, and then RV_1 is closed which connects the test circuit-breaker to the circuit providing for the second part of the cycle (making-breaking).

Corresponding to the characteristics of the test circuit-breaker, the B contacts begin to draw together a certain time after arc quenching (making operation). The voltage $U_C = U_1 + U_2$ is applied to the B contacts in the series circuit $C_1 - L_1 - C_2 - L_2$ which is selected as equal to the making voltage for the circuit-breaker under study, (Fig. 2). At a certain position of the B contacts a spark-over passes between them, (connexion of circuit-breaker to short-circuit). An increased frequency current i_1' flows in this circuit (Fig. 2) which is conditioned by the parameters of both circuits. The parameters are selected by calculation so that the derivative of the making current is in the initial moments of flow equal to its value for the line frequency making current at a given short-circuit power.

A short time (300 - 500 μsec) after the beginning of the flow of current i_1' (Fig. 2), switching device VU_1 comes into operation. It closes the line frequency oscillatory circuit $C_1 - L_1$, and a line frequency making current i_1 of a given amplitude passes through B.* With a corresponding selection of circuit parameters and times for the operation of VU_1, passage from the series connexion of the oscillatory circuits to their parallel connexion does not result in a complete break in the making current curve at that moment, (the current derivative does not vary more than 10 - 15 per cent).

After the first zero passage the increased frequency current is broken by device OU_1, and after the first zero passage the line frequency current is broken by OU_2. Metal shorting of the contacts of test circuit-breaker B occurs during making current i_1 flow and right up to the instant of its first zero passage.

In such a manner the second operation of the test cycle (making) takes place. In the developed circuit of the testing apparatus special capacitances are provided reproducing the discharge through the test circuit-breaker of the dropout line capacitances in the system. As is seen from what has been said,

* After operation of VU_1 in the circuit C_2-L, the current continues at a higher frequency i_1.

circuit-breaker testing for a given operation is accomplished in complete equivalent conditions since circuit-breaker making at full voltage is ensured and making current curve form and amplitude are reproduced, including the current derivative in the first instants of its flow. To correspond with these conditions provision is made in the circuit for the short-circuit current not to flow through the contacts for a large part of the time t_1 of metal short-circuiting. (Fig. 2).

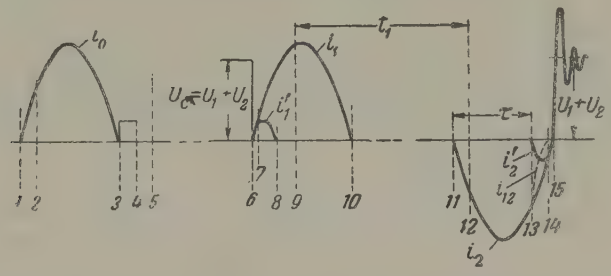

FIG. 2. Curves for currents and voltages with synthetic circuit-breaker testing in an automatic reclosure cycle.
1 – close VU_0; 2 – B contacts divergence; 3 – arc quenching in B; 4 – open RV_{01} and RV_{02}; 5 – close RV_1; 6 – spark-over between B contacts; 7 – close VU_1; 8 – open OU_1; 9 – metal shorting of B contacts; 10 – open OU_2; 11 – close VU_2; 12 – B contacts diverge; 13 – operation of P; 14 – open OU_3; 15 – tripping of B.

In the short interval before the B contact divergence in the third operation (repeated breaking) of the automatic reclosure cycle short-circuiting of the switching devices VU_2 and VU_2' occurs. Two oscillatory circuits adjusted to line frequency are connected in parallel to the test circuit-breaker and breaking device OU_3: $C_1 - L_1$ and $C_0 - L_3$. As a result the current in B and OU_3 will be equal to the sum of the currents in the two circuits, and the total current with an appropriate selection of parameters of test circuit $C_0 - L_3$ will have the same value as the making current in the preceeding operation.

After the divergence of B contacts, breaking current i_2 of a given amplitude flows through the arc formed. Almost simultaneously with B, the contacts of breaking device OU_3 break, and through it current $i_{12} = i_2$ flows for the first time.

An interval τ after current i_2 began to flow (Fig. 2) shift circuit P (Fig. 1) comes into operation, and an increased frequency current i_2' begins to flow in h.v. circuit $C_2 - C_2 - L_4 - L_2$ and the current difference through breaking device OU_3 is $i_{12} = i_2 - i_2'$. Current i_{12} passes through zero in 300-600 μsec before the current B does so, and the arc in OU_3 is quenched. The increased frequency current shorted through B flows in the series circuit formed from the two circuits $C_1 - L_1$ and $C_2 - C_2' - L_4 - L_2$ so that its derivative is the same as the line frequency current After arc quenching in B, the voltage $U_0' = U_1 + U_2 + U_2'$ recovers at its contacts.

The inductance L_4 and the voltage U_2' are selected according to the condition

of equality of making and breaking current derivatives:

$$\frac{U_c}{L_c} = \frac{U_1 + U_2}{L_1 + L_2} = \frac{U_0'}{L_0} = \frac{U_1 + U_2 + U_2'}{L_1 + L_2 + L_4},$$

where U_c, U_0' are respectively the making and recovery voltages;

L_c, L_0 are respectively the making and breaking circuit inductances.

It is obvious that the voltage U_2' can be selected at such a rating as to compensate for the damping of voltage U_2 in the making operation. If, for example, the making voltage must be equal to the recovery voltage, inductance L_4 is not connected and battery C_2' is contacted only to compensate for the damping of the charging voltage from battery C_2.

Thus, the third operation (repeat breaking) is performed in complete equivalent conditions, since even in the 300-600 μsec before current zero passage the test circuit-breaker is in a circuit where the voltage $U_1 + U_2 + U_2'$, the inductance $L_1 + L_2 + L_4$ and the capacitance determining the voltage recovery rate have the same values as in the actual line.

The circuit in Fig. 1 is extremely economical, since battery C_0 is used simultaneously as current source in the first breaking operation, and to compensate for current loss in the repeat breaking operation, while batteries C_1 and C_2 are used simultaneously for the two latter operations of the automatic reclosure cycle.

As experiments have shown, in testing a circuit-breaker during arc burning for one half-cycle of line frequency full compensation for current and voltage damping in the automatic reclosure circuit requires about 1.5 times more capacitors than for synthetic circuit-breaker testing for breaking capacity.

The circuit in Fig. 1 also permits circuit-breaker testing during arc burning for more than one half-cycle. In that case the frequency of circuit $C_0 - L_3$ will differ from the line frequency. A current flows through B in the latter breaking operation which, in the absence of losses, has the character of an oscillation beat, but with losses and appropriate selection of the test contour $C_0 - L_3$ parameters, it is practically undamped for several half-cycles, [3]. The shift circuit P comes into operation immediately before the last zero passage of the current in the test circuit-breaker. If the arc in B is permanently quenched, the circuit for artificially prolonging arc burning is switched on to it in parallel [3].

The breaking current in the first operation (breaking) can also be undamped when a test circuit has been connected in parallel to B in the same way as is done in the last operation, (circuit $C_0 - L_3$). However, in many cases the damping character of this current appears to be permissible, and in order to reproduce its effect on circuit-breaker operation in an automatic reclosure cycle the current amplitude must be slightly raised.

In testing circuit-breakers during arc burning of more than one half-cycle,

contact divergence in breaking device OU_3 is performed only after the beginning of the last breaking current half-cycle in order to avoid premature quenching.

Developed circuit (Fig. 3)

The circuit includes additional synchronizing apparatus for carrying out synthetic tests in the last two operations of the automatic reclosure cycle. Before the experiment is begun, switch RK is closed,* and ignition capacitances C_{i4} and C_{i3} are discharged through resistor R_2 ($R_2 \gg R_1$) to voltage $U_1 + U_2$.

With a spark-over between the contacts, capacitance C_{i4} is discharged through B (making operation) in the circuit C_{i4}, r, C_{i5}, R_1, IV, reproducing the capacitive discharge of the dropout lines to the circuit-breaker when it is connected to the short-circuit. The discharge circuit of this capacitance corresponds to an impulse generator circuit, and with the selection of the necessary parameters a given current impulse wave form can be produced.

Simultaneously with capacitance C_{i4} discharge, the voltage in resistor R_1 is increased leading to the operation of tri-electrode discharger P_5. Battery C_{i3} is discharged to resistor R_3, and its voltage is applied to the central electrode and sphere of switching device VU_1, (discharger of VEI construction). Discharge occurs between electrode and sphere. Arc formation is accompanied by considerable gas generation from the tube of gas-generating material set into the sphere. The gas ejected shortens the gap between the spheres, and switching device VU_1 closes. The duration of this process is 300-500 μsec from the instant of spark-over between the B contacts. The operation of discharger P_5 spheres does not result in a change in the impulse form of the current through the circuit-breaker, as the capacitance C_{i6} is substantially smaller than C_{i5}.

In the repeat breaking operation, the displacement of the instant when the increased and frequency current begins to flow relative to the beginning of line frequency current flow is controlled with the aid of a shift circuit consisting of a voltage transformer TN (Fig. 3) or a shunt-inductor connected to the B circuit, a synchronization circuit, an ignition circuit and dischargers P_3 and P_4 with devices for their operation.

The four electrode construction of discharger P_3 is due to its unusual mode of operation. The discharger must not function in the making operation during transient voltage recovery in breaking device OU_1 when the limit of this voltage is $2U_2$. Together with this in the repeat breaking operation the discharger on receiving the corresponding command to function must be in a circuit where capacitor battery C_2 voltage U_2 acts.* Finally, it must be seen that in the making operation when OU_1 contacts are closed the discharger is subject to the same voltage $U_1 + U_2$, relative to ground as is IV.

* To avoid premature operation discharger P_5 during charging of capacitance C_{i4}

† More accurately, voltage $U_2 + U_2'$; however voltage U_2' is applied to discharger P_3 even before the circuit begins to operate.

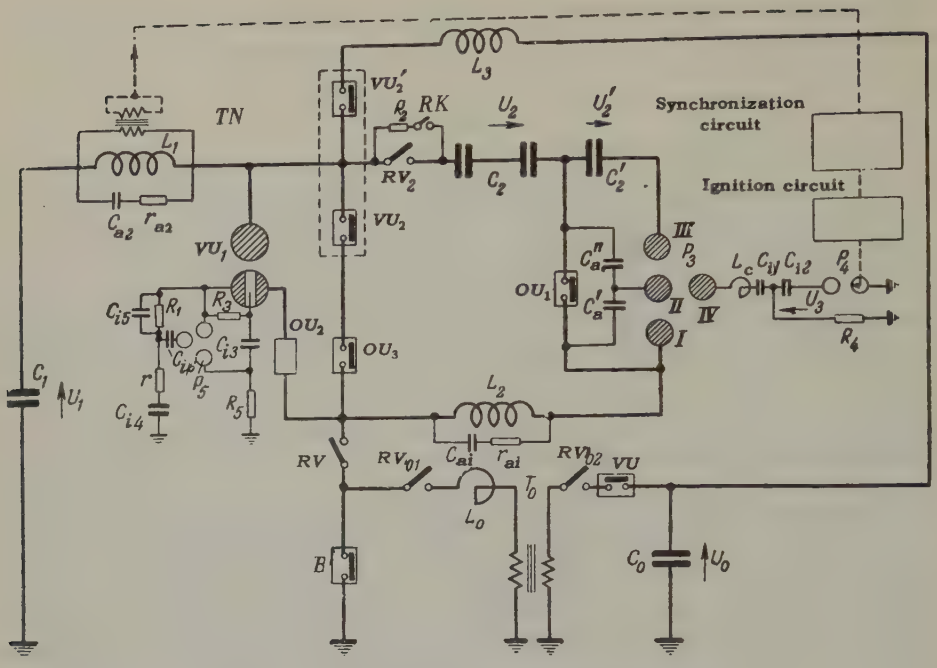

FIG. 3. Developed circuit of the testing apparatus.

This circuit for discharger P_3 makes it possible to satisfy the requirements previously indicated. The voltage recovered at OU_1 is distributed between two equal capacitances C_b' and C_b'', and therefore at each of them it does not exceed U_2. The discharge gaps *I-II* and *II-III* are selected by calculation so that they cannot operate at this voltage. When the impulse from the synchronization circuit is later received three-electrode discharger P_4 operates, and a voltage $[(\frac{U_2}{2} + U_2') + U_3]$ is applied between spheres *II-IV*, where U_3 is the charging voltage of capacitor C_{i_2}. With this a discharge takes place between spheres *II* and *IV*.

It must be noted that the arrangement of a small inductance coil L_c makes it possible to reduce the voltage U_3 somewhat, since after the operation of P_4 the voltage on spheres *II-IV* is in oscillatory operation. As a consequence, gap *II-III* is crossed since capacitance C_b' begins to be charged by capacitor battery C_{i_2} through capacitance C_{i_1} and inductance L_c. After this gap *I-II* also comes into operation after being subjected to the intense excitation of discharge gaps *II-IV* and *II-III*. Operation between spheres I-II is facilitated also by the circumstance that capacitance C_b' is charged during oscillatory operation, and the voltage on it can exceed $U_2 + U_2'$. The use of the fourth sphere makes it possible to withdraw it from the remaining spheres to such a distance as to prevent the operation of discharger P_3 on the voltage applied to *IV* in the making operation.

Controlled capacitances and resistances C_{b1} - C_{b4} and r_{b1} - r_{b4} are connected in parallel to reactors L_1, L_2, L_3 and L_4 in order to control the voltage recovery rate.

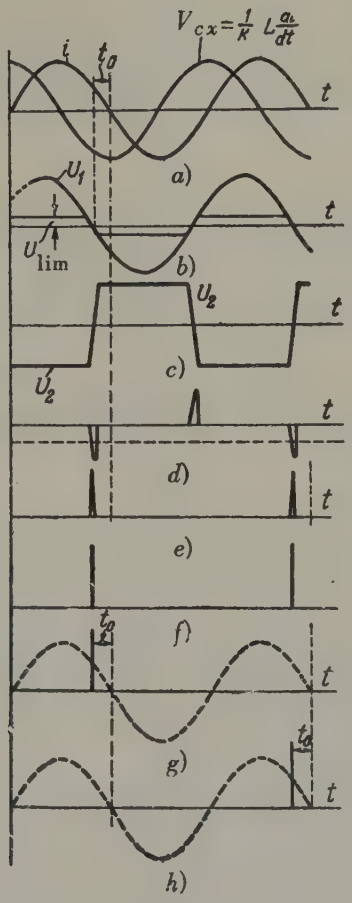

FIG. 4. Curves showing the method of operation of the synchronizing device.

The methods of operation of the synchronization circuit are explained graphically in Fig. 4. A voltage U_{cx} is supplied to the input of the circuit which is proportional to the breaking current i derivative (Fig. 4a). With the use of a phase bridge this voltage is shifted to a given angle after which the output bridge voltage U_1 is limited to the value U_{lim} (Fig. 4b). The voltage obtained is then boosted to U_2 and is supplied to a differentiating circuit, (Fig. 4c). As a result of the last two operations a voltage is obtained which is close in form to square pulses.

Therefore, in the instants after differentiation preceeding i current zero

passage for a given interval t_0 impulses of sufficiently short duration are developed (Fig. 4d) and amplified (Fig. 4e). The pulses are then supplied to a trigger mechanism developing powerful positive pulses of great steepness (Fig. 4f) which are transmitted through a special meter to the ignition circuit input (Fig. 3) immediately before one of the uneven zero passages of current i, (Fig. 4g and h). In order to produce a pulse before one of the even current zero passages, it is sufficient to vary the polarity of the input voltage U_{cx} of the synchronization circuit.

The circuit provides for great accuracy in synchronization, since its input voltage in the final analysis repeats the breaking current curve form, and the instant when the impulse is produced changes together with the variation in the i current curve form.

Results of tests

The synthetic circuit for testing circuit-breakers in an automatic reclosure cycle was put into practice in the laboratory of the TVN LPI where an air-blast circuit-breaker was tested.

Oscillograph characteristics are shown in Fig. 5 and 6 which were obtained by the use of vibrator and electron oscillographs, (Figs. 5b and 6b). In Fig. 5 an experiment is recorded for the testing of a circuit-breaker in the circuit shown in Fig. 3 without compensation for current and voltage losses, (circuit C_0-L_3 and battery C_2'); Fig. 6 records a circuit-breaker test using the complete circuit. The dotted curve on the oscillograph in Fig. 6 shows the current which in actual conditions flows through the metal shorted contacts of the circuit-breaker between the making and repeat breaking operations.

As is seen from the oscillograph (Fig. 5), without compensation for current and voltage damping the breaking current amplitude by the third operation of the automatic reclosure cycle is close to 25 per cent less than the making current amplitude. The recovery voltage is lowered by approximately the same percentage in comparison to the making voltage. As is known, damping of this order occurs with circuit-breaker testing in an automatic reclosure cycle in breaking capacity laboratories with impact generators in a full power circuit.

In circuit-breaker testing according to the circuit in Fig. 3 with the use of compensating circuits, current and voltage damping is completely eliminated, (Fig. 6); the amplitudes of all three currents and also the making and recovery voltages have similar values.

Electron-beam oscillographs show that the synchronizing devices developed make it possible to adjust the testing apparatus with great accuracy. Passage from series circuit connexion to parallel connexion in the making operation, and reverse passage in the repeat breaking operation occur without any substantial

change in the making and breaking current derivative, and the passage instants are within the limits mentioned above (t' and t'' in Figs. 5b and 6b).

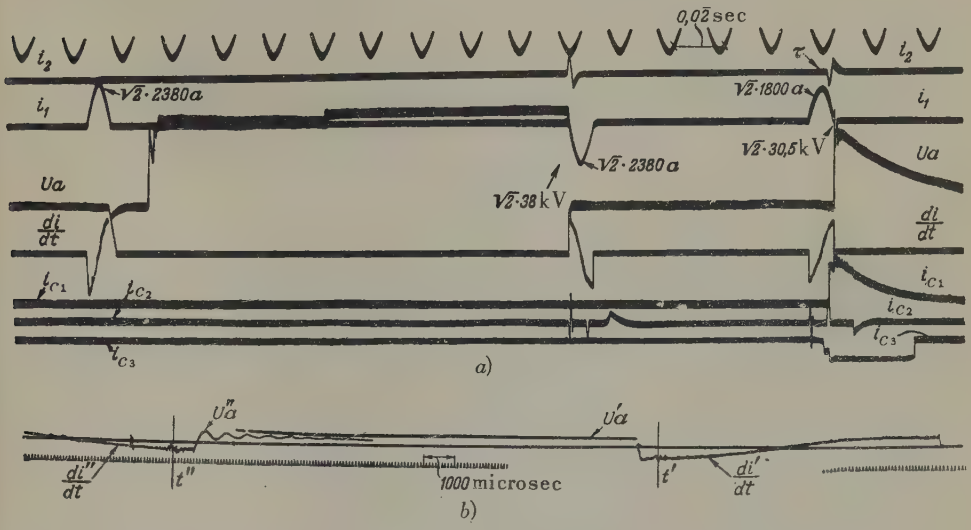

FIG. 5. Electromagnetic (*a*) and electronic (*b*) oscillograms of air-blast circuit-breaker tests in an automatic reclosure cycle in a circuit without compensation for current and voltage damping.

di/dt is the making current (*i*) derivative or breaking current (*i''*); i_2 is the h.v. circuit current; i_{c1}, i_{c2} and i_{c3} are secondary curves; i_{c1} indicates the instant of discharger P_4 operation (Fig. 3), i_{c2} the impulses developed by the synchronization circuit (Fig. 4d), and i_{c3} indicates the instants of impulse-meter and ignition circuit operation, (Figs. 3 and 4).

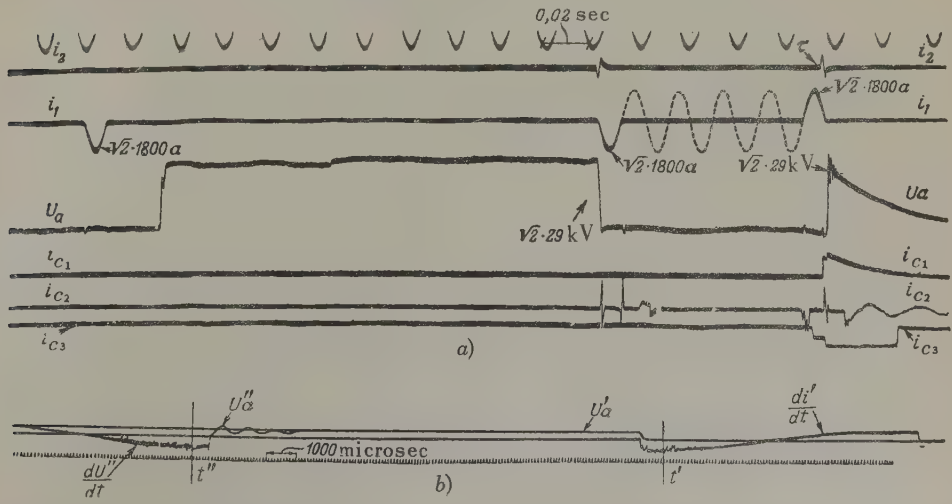

FIG. 6. Electromagnetic (*a*) and electronic (*b*) oscillograms of air-blast circuit-breaker tests in an automatic reclosure cycle. Letter designations are the same as in Fig. 5.

Conclusions

The circuit developed makes possible the solution of the extremely complex problem of a synthetic method of testing: equivalent condition testing of circuit-breakers operating in an automatic reclosure cycle. The circuit makes it possible to reproduce any correlation between making and recovery voltage.

Translated by F.J.C. Griffiths

REFERENCES

1. A.A. Gorev, V.V. Kaplan and V.M. Nashatyr'; Doukhchastotnyi kolebatel'nyi kontur dyla ispytaniya sverkhmoshchnykh vysokovol'tnykh vyklyuchetelei na otklyuchayushcohuyu sposobnost'. (Dual-frequency oscillatory circuit for testing high-power h.v. circuit-breakers for breaking capacity). *Elektrichestvo*, No. 6, (1951).
2. V.V. Kaplan and V.M. Nashatyr'; Metod issledovaniya v klynchaynshthei sposobnosti moshchnykh oyklyuchatelei vysokogo napryazheniya. (Method of studying the making capacity of powerful h.v. circuit-breakers). VEP, No. 2, (1957).
3. V.V. Kaplan and V.M. Nashatyr'; Issledovaniya otklyuchayushchei sposobnosti i nadezhnosti vnytrennei isolyatsii (Studies on the breaking capacity and reliability of the inner insulation of the MG-110 circuit-breaker). *Elektrichestvo*, No. 7, (1957).

THE ENERGY PROPERTIES OF AN ASYNCHRONOUS MOTOR WITH A SYSTEM OF IMPULSE SPEED REGULATION*

L.L. ROTKOP

ODESSA

In the present work an analysis is made of the energy characteristics of an asynchronous motor with impulse speed regulation by the use of feed-back signals indicating speed in order to attain steady mechanical characteristics (a relay system for automatic speed regulation working on the 'on-off' principle). Fig. 1 shows in block schematic form, the circuit of such a system.

The principle of operation of the circuit is as follows, [1–7]. With the application of a voltage to the motor its speed begins to increase and at a certain value of speed n_1 the input to the relay element reaches the pick-up value of the relay x_2 (n_1). When this happens the relay operates and the voltage U_1 at the output of the amplifier is reduced to a very small quantity, (if an amplifier-contactor arrangement is used, the voltage U_1 is reduced to zero). The speed of the motor falls, and at a certain speed n_2 the input to the relay falls to the release value, x_2 (n_2). The relay restores and the voltage U_1 at the output of the amplifier increases to its maximum. The speed of the motor again begins to rise to the value n_1 and so on. In this way the speed of the motor oscillates between the values n_1 and n_2 with a mean value $n_{av} = \frac{1}{2}(n_1 + n_2)$; the value n_{av} depends on the conditions of the speed arrangements in question. In place of the amplifier and relay element, a contact or a contact-less apparatus may be used. The permissible loading on the shaft of the motor over all ranges of the regulated speed is determined by the magnitude of the losses in the motor.

Over the normal range of operation of the motor in the system shown in Fig. 1, a self-oscillating regime is set up. In this, the period of oscillation consists of the periods of acceleration and deceleration of the motor.

To determine the losses in the motor it is sufficient to find the power loss per cycle. The motor losses during the time of deceleration are zero (the motor is switched off), or if a contact-less control system is used, practically zero. The

* *Elektrichestvo* No. 11, 38-42, 1958.

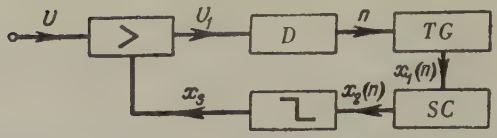

FIG. 1. Block schematic diagram of a system of control with impulse regulation of speed.
D – Asynchronous motor. TG – Tachogenerator.
SC – Speed control.

motor losses during the period of acceleration from speed n_2 to n_1 will be:-

$$\Delta A_u = \int_0^{t_p} (k + v)\, dt = kt_p + \int_0^{t_p} 3I_2'^2 (r_1 + r_2')\, dt, \tag{1}$$

Where k, v are the permanent and variable losses in the machine.

t_a is the time of acceleration of the machine.

r_1 is the resistance per phase of the stator of the motor.

I_2', r_2' is the current and resistance of the rotor applied to the stator.

From the equations of the dynamics of transmission:

$$dt = -\frac{J\omega_0\, ds}{M - M_s}, \tag{2}$$

The losses in the motor, ignoring mechanical losses are:

$$3I_2'^2 r_2' = 9.81\, M\omega_0\, s. \tag{3}$$

Substituting (2) and (3) in (1) we get the losses per cycle.

$$\Delta A_u = kt_p + \frac{J\omega_0^2}{2}\left(1 + \frac{r_1}{r_2'}\right)\frac{M}{M - M_s}(s_2^2 - s_1^2)\, 9.81. \tag{4}$$

In deducing equation (4), it is assumed that the difference between the speeds n_2 and n_1 is fairly small so that the torque of the motor, the statistical torque and the phase resistance of the rotor may all be reckoned as constant during the time of acceleration.

Moreover, in equation (4), the losses from transient current components are not taken into account. These may reach fairly high values if the rotating motor is switched on; however, inasmuch as in impulse speed regulation the motor adapts itself by increasing the nominal slip, the transient components of the current are rapidly damped.

In using a contact control system, the masses of the system must be fairly large in accordance with the conditions of stability so that the number of times the motor is switched on does not exceed 200-300/hr, [1]. In this the time of acceleration of the motor appears a little greater than the transient components of the current and consequently the losses from its action can be ignored.

In using contact-less apparatus for control, the frequency of auto-oscillation of the system may be noticeably increased. In this case the voltage applied to the machine on switching on reaches a steady value in a time equal to the delay in the amplifier and relay. In this case the transient components of the current are fairly small and may be ignored.

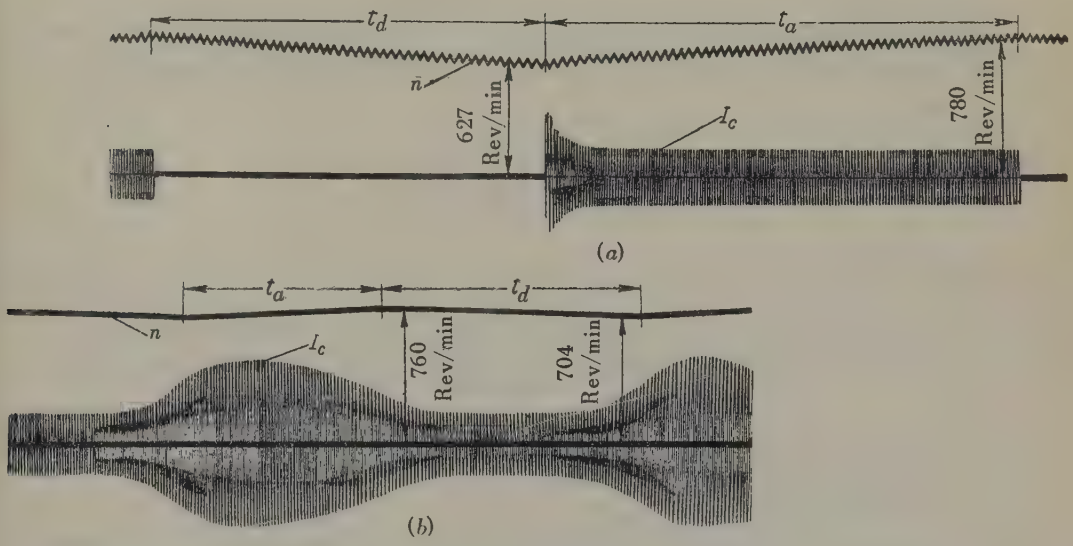

FIG. 2. Oscillograms of stator current I and speed n of an asynchronous motor AOS 51-4 in a relay system of speed regulation.

a — Using a contact apparatus for control, (contactor and relay); b — using a contact-less apparatus for control (magnetic amplifier and magnetic contact-less relay)

In Fig. 2 oscillograms of stator current and speed are shown for an asynchronous motor type AOS 51-4 in a relay system of speed regulation using contact control apparatus (contactor and relay) and also contact-less apparatus, (magnetic amplifier and magnetic contact-less relay). The oscillograms in Fig. 2 underline the validity of the assumptions made above.

The power loss per cycle will be:-

$$\Delta P_u = \frac{\Delta A_u}{t_p + t_d} = k\,\frac{M_s}{M} + M_s\omega_0\left(1+\frac{r_1}{r_2'}\right)s_{av}9{,}81, \qquad (5)$$

where:- $t_a = \frac{J\omega_0}{M - M_s}(S_2 - S_1)$ – time of acceleration

$t_d = \frac{J\omega_0}{M_s}(S_2 - S_1)$ – time of deceleration. $(M = 0)$

$S_{av} = \frac{S_2 + S_1}{2}$ – average slip.

The power loss in the normal regime is:-

$$\Delta L_{nor} = k + M_{nor}\omega_0 s_{nor}\left(1 + \frac{r_1}{r_2}_{nor}\right) 9.81. \tag{6}$$

The permissible moment of load capacity of the machine for a different mean speed may be obtained from equations (5) and (6) using the relationship $\Delta L_{nor} = \Delta L_{nor} k_m$:

$$M_{sper} = A\frac{1+\alpha}{1+\frac{A}{M}\alpha} k_m, \tag{7}$$

where

$$\alpha = \frac{k}{v}; \quad A = M_{nor}\frac{s_{nor}}{s_{av}} \cdot \frac{1+\frac{r_1}{r'_{2nor}}}{1+\frac{r_1}{r'_2}},$$

k_m – coefficient taking into account the deterioration of ventilation caused by a decrease in speed.

Comparison of equations (5) and (6) shows that with impulse speed regulation, the variable losses are increased and the constant losses are reduced in comparison with normal conditions. For a given mean speed, both the constant and the variable losses increase with increasing load. The reason for this is that during the period in the cycle the motor is switched off, the constant losses are zero, so that if the relative time of switching off is $t_a/t_a + t_d$ the load of the motor is increased or decreased by this ratio.

As a consequence of this, the characteristics of the energy properties with impulse speed regulation are different from the characteristics of other types of regulating systems in which the permanent losses are not usually dependent on the load.

Equation (7) has the form:

(*a*) For motors with normal performance, $(r'_2 = r'_{2nor} = \text{const.})$

$$M_{sper} = M_{\kappa} \frac{s_{nor}}{s_{av}} \frac{1+\alpha}{1+\frac{M_{nor}}{M} \cdot \frac{s_{nor}}{s_{av}} \alpha} k_m. \tag{8}$$

(*b*) For motors with increased slip, type AOS ($r_2' = r_{2nor}' = \text{const.}$)

$$M_{sper} = M_{nor} \frac{s_{nor}}{s_{av}} \cdot \frac{1+\alpha}{1+\frac{s_{nor}}{s_{av}} \frac{1-e^{-s_{nor}/0.2}}{1-e^{-s_{av}/0.2}} \alpha} k_m \tag{9}$$

where:

$$M = M_n (1 - e^{-s/0,2}) \text{ [Л. 4].}$$

(*c*) For motors with phase rotors, the magnitude A in equation (7) is defined by the formula:

$$A = M_{nor} \frac{S_{nor}}{S_{av}} \left(1 + \frac{r_{per}'}{r_{2nor}'}\right), \tag{10}$$

where: r_{per}' – is the additional resistance in the rotor circuit applied to the stator.

If simultaneously with the change in condition of the given system of speed control the rotor resistance is changed in accordance with the relationship

$$r_{per} = r_2 \left(\frac{S_{av}}{S_{nor}} - 1\right),$$

then:

$$M_{s\,nor} = M_{nor} k_m. \tag{11}$$

(*d*) For motors with Shenfer rotors, with longitudinal slots and copper rings:-

$$M_{sper} = M_{nor\,sh} \frac{s_{nor\,sh}}{s_{av}}^{*} B \frac{1+\alpha}{1+\frac{M_{nor\,sh} B \alpha s_{nor\,sh}}{M_n (1 - e^{-s_{av}/0,4})\, s_{av}}}$$

in which

$$M = M_n (1 - e^{-s/0,4}) \text{ [Л. 4];}$$

$$r_2' = k_1 r_{2nor}' \sqrt{s} \text{ [Л. 5]; } r_{2nor}' \approx r_1,$$

* Sh has been used for Shenfer

where, $s_{\text{nor sh}}$, $M_{\text{nor sh}}$, and M are nominal slip, nominal and permissible moments after changing the factory rotor.

$$B = \frac{(k_1\sqrt{0{,}2}+1)\sqrt{s_{\text{av}}}}{(r_1\sqrt{s_{\text{av}}}+1)\sqrt{0{,}2}}.$$

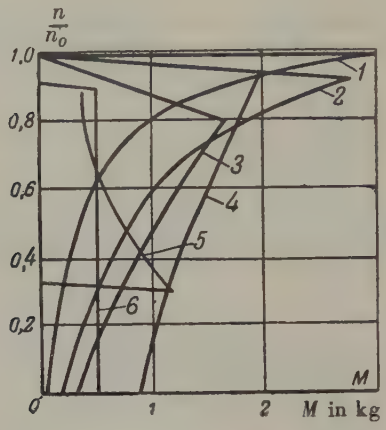

FIG. 3. Relationships between permissible moment and motor speed for motors of various performance. 1. Motor AO 51-4 2. Motor AOS 51-4 3. Motor AO 51-4 with Shenfer rotor. 4. Motor AK 51-4 5. D.C. motor, output 0.55 kW, speed 450-1450 rev/min 6. Motor PNZ 17.5. Output 0.8 kW, 1450 rev/min.

In Fig. 3, curves are plotted from equations (8), (9), (11) and (12) showing the relationship $M_{\text{s per}} = f(n_{\text{av}}/n_0)$ for motors of different design but of identical dimensions and weight, (80-84 kg). The values of the coefficient k_m for motors AO and AOS were taken from [6].

For the purpose of comparison, curves of the relationship $M_{\text{s per}} = f(n/n_0)$ for d.c. motors are also shown. The speed of the motors was changed by varying the supply voltage and the excitation current.

In both cases, motors were chosen with similar dimensions and weight, (80 kg).

In Fig. 4 are shown the mechanical characteristics $n_{\text{av}} = f(M)$ obtained experimentally and the relationships $M_{\text{s per}} = f(n_{\text{av}})$ plotted in accordance with experimental results and with equation (12) for an unventilated motor of 3 kW output, $n_a = 750$ rev/min, enclosed design ($(k_m = 1)$, with a Shenfer rotor using a system of speed control similar to Fig. 1, with a contact-less device for control (a magnetic amplifier and a magnetic contact-less relay). In practice, the

permissible temperature of the steel rotor was assumed to be 95° C. The curves in Fig. 4 show a degree of accuracy sufficient for practical calculations of the equations given above for the calculation of the permissible load of the motor for impulse systems of speed regulation.

From a comparison of the curves in Fig. 3, the following deductions can be drawn:-

(1) Motors of normal type are little suited to impulse speed control. From the viewpoint of the most suitable system for speed regulation over the whole of the range of regulation, one should choose a motor with increased nominal slip, of the AOS type with Shenfer rotor, enclosed and with a phase rotor. For low output motors up to 20 kW it is better to use a motor of the AOS type or with a Shenfer rotor as it is simpler and more reliable. For higher output units one may recommend the use of motors with phase rotors.

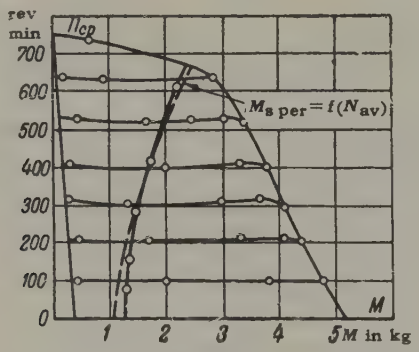

FIG. 4. — Mechanical characteristics and the relationships $M_{s\,per} = f(n_{av})$ for motors of 3kW output, $n_0 = 750$ rev/min, enclosed type, with Shenfer rotor and a speed control system similar to that in Fig. 1, with a contact-less control relay.

———— Experimental results.
---------- Calculated from Equation 12.

(2) For the regulation of speed with constant torque, the dimensions and weight of asynchronous motors with squirrel-cage rotors and of d.c. motors are approximately equal. For speed regulation in mechanisms where the torque is proportional to the speed ($M_s = N + Sn^d$) the dimensions and weight of the variable current motor are less than those for the d.c. motor.

(3) Over a sufficiently wide range of regulation when a d.c. motor-generator system is used, the dimensions of the impulse speed regulation equipment with an asynchronous motor is always less than that of the motor-generator system.

Consequently the installation costs of impulse speed regulation are considerably less than for a motor-generator system.

The coefficient of useful operation (c.u.o.) of a motor in a system of impulse speed regulation may be found from the expression:-

$$\frac{\eta_p}{\eta_{nor}} = \frac{P_p(P_{nor} + \Delta P_{nor})}{P_{nor}(P_p + \Delta P_u)}$$

or, substituting the values ΔP_{cyc}, ΔP_{nor} from equations (5) and (6) according to the formulae

$$\eta_p = \frac{n_{av}}{n_{nor}} \cdot \frac{as_{nor}\left(1 + \frac{r_1}{r'_{2nor}}\right) + \left(1 + s_\kappa \frac{r_1}{r'_{2nor}}\right)}{\frac{M_{nor}}{M} as_{nor}\left(1 + \frac{r_1}{r'_{2nor}}\right) + \left(1 + s_{av} \frac{r_1}{r'_2}\right)} \eta_{nor} \qquad (13)$$

where: η_{reg}, $P_{reg} = 9.81\, M_s\, \omega_0\, (1 - s_{av})$ – the efficiency and output on the shaft of the motor when operating on the regulated characteristic.

η_{nor}; $P_{nor} = 9.81\, M_{nor}\, \omega_0\, (1 - s_{nor})$ – the same in nominal conditions. Equation (13) may be simplified if a contactor is used as an amplifier for the drive of an AOS type metor ($r_2' = r_{2nor}' = \text{const}$; $r_{2nor}' \simeq r_1$), since the first terms of the numerator and denominator are much smaller than the second terms, and so one may ignore them.

$$\eta_p = \eta_{nor} \frac{n_{av}}{n_{nor}} \frac{1 + s_{nor}}{1 + s_{av}}; \qquad (14)$$

For a motor with a Shenfer rotor:-

$$\eta_p = \eta_{nor\,sh} \frac{n_{av}}{n_{nor}} \cdot \frac{k_1 + \sqrt{s_{nor\,sh}}}{k_1 + \sqrt{s_{av}}} \approx \eta_{nor\,sh} \frac{n_{av}}{n_{nor\,sh}}. \qquad (15)$$

If a contact-less device (magnetic amplifier) is used in the main circuit of the motor, in equation (13) the magnitude r_1 will comprise the total resistance of the stator winding and of the amplifier. In this case the value of the efficiency is slightly reduced and for an AOS type motor equation (13) may be represented in the form, ($r_2' = r_{2\,nor}' = \text{const}$): $r_{2\,nor}' \simeq r_{1d}$)

$$\eta_p = \eta_{nor} \frac{n_{av}}{n_{nor}} \cdot \frac{1 + s_{nor} \dfrac{r_{1d} + r_{amp}}{r_{1d}}}{1 + s_{av} \dfrac{r_{1d} + r_y}{r_{1d}}}, \qquad (16)$$

Where: r_{1d} – is the resistance per phase of the stator winding of the motor.

r_{amp} – is the resistance per phase of the amplifier.

Equations (13) – (15) show that the efficiency of a motor in a system of impulse speed control at any given speed is independent of the load on the shaft. This is in consequence of the particular power characteristics shown above for impulse regulation.

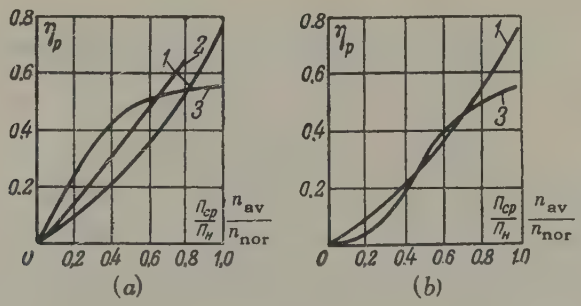

FIG. 5. Relationship between efficiency of the motor η_{reg} and speed n_{av} of the machine with (a) M_s = const. and (b) $M_s = Sn$.

1. Motor, AOS 51-4 type. 2. Motor, AO 51-4 type with Shenfer rotor. 3. Motor PNZ – 17.5 in a motor-generator system.

Fig. 5a shows the characteristics $\eta_{reg} = f(n_{av}/n_{nor})$ for an AOS 51-4 motor plotted according to equation (14), a motor AO 51-4 with a Shenfer rotor plotted according to equation (15) and a motor PNZ 17.5 with M_s = const. in a motor-generator system. The systems of impulse regulation with M_s = const. have a lower efficiency than those with direct current.

Fig. 5b shows curves of the efficiency for the same machines with speed regulation of the mechanism when $M_s = Sn$. If the torque of the transmission mechanism is proportional to the speed to a power higher than the first, the efficiency of the impulse system may show a larger value than that of the motor-generator system.

In Fig. 6 the curves are drawn showing $\eta_{reg} = f(n_{av})$ as obtained by experiment and by calculation from equation (16) for an AOS 51-4 motor with a speed control system as in Fig. 1, using a magnetic amplifier in the main circuit and a

magnetic contact-less relay in the control circuit, [7]. The curves in Fig. 6 show that the equations given above are accurate enough for demonstrative calculations of the efficiency of a system using impulse speed control.

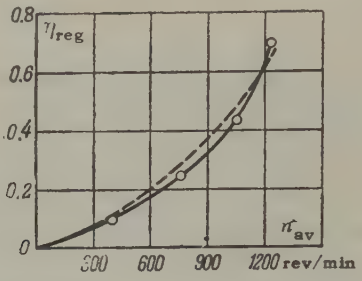

FIG. 6. Curves of the relationship between efficiency. η_{reg} and speed n_{av} of an AOS 51-4 motor in a system of speed control similar to Fig. 1.

———— Experimental results.

---------- According to equation (16).

For comparison of the power characteristics of the different systems of regulation, it is essential to make the comparison according to the integral characteristics of the regulating cycle, [3]. If, in the range of regulation D and the number of steps m, each speed step is accomplished in the same time interval, then the efficiency of the regulating cycle may be obtained from the equation, [3]:

$$\eta_{u.p} = \frac{\sum_{1}^{m} P_{pq}}{\sum_{1}^{m} (P_{pq} + \Delta P_{uq})}, \tag{17}$$

Where, P_{pq} ; ΔP_{cyc} – are the useful power and loss of power at the qth. regulating step.

Since $$P_{pq} = \frac{M_{cq} n_{cp.q}}{975} \; ; \quad P_{pq} + \Delta P_{uq} = \frac{P_{pq}}{\eta_{pq}}$$

and if the difference in speed for the two selected steps is equal when $m = 1$, $n_{av} = n_{nor}$, then for $m \to \infty$ for an AOS type motor:

$$\eta_{u.p} = \frac{\left(1 - \frac{D-1}{2D}\right)\eta_{nor}}{1 + s_{nor} + \frac{n_{nor}}{n_0} \cdot \frac{D-1}{2D}} \approx \eta_{nor} \frac{D+1}{3D-1}. \tag{18}$$

This, the equations introduced above enable us to analyse the power characteristics of a system with impulse regulation of speed approximately but quite fully.

Translated by F.P. Froom

REFERENCES

1. N.N. Krechtovich; Elektroprivod s impul'snym upravleniem skorostyu asinkhronnogo dvigatelja. Electrical transmission with impulse control of the speed of an asynchronous motor). *Elektrichestvo:* No. 3 (1956).
2. E.P. Sarkisyan; Impul'snyisposob upravlenija elektroprivodom s asinkhronnymi dvigateljami (An impulse system of control for electrical transmission with asynchronous motors) Dissertation.
3. A.T. Golovan; *Elektroprivod (Electrical Transmission).* Gosenergoizdat (1948).
4. V.V. Gorskii; Aproksimirovanie mekhanicheskoj kharakteristiki asinkhronnykh dvigatelyei. (An approximation of the mechanical characteristics of an asynchronous motor). *Elektrichestvo;* No. 3 (1957).
5. A.G. Ivakhnenko; *Avtomaticheskoye reguliravanie skorosti asinkhronnykh dvigateljei nebol'shoi moshchnosti. (Automatic regulation of speed for low-output asynchronous motors). Annals Akad. Nauk S.S.S.R.* (1953).
6. V.I. Vasin; *O regulirvanai i skorosti korotkozamknutykh asinkhronnykh dvigateljei. (On the speed regulation of squirrel-cage asynchronous motors).* VEP No. 9 (1956).
7. L.L.Rotkop; *Impul'sny metod regulirovanja skorosti asinkhronnogo dvigatelia c primeneniem beskontaktnoi apparatury upravleniya. (An impulse method of speed regulation for an asynchronous motor by the use of a contact-less control apparatus).* VEP. No. 1 (1958).

ON THE CONDITIONS OF THE FORMATION OF FLASHOVER OR ARCING ON TO THE FRAMEWORK OF TRACTION MOTORS*

A.S. KURBASOV

All-Union Scientific-Research Institute of Rail Transport

(Received 2nd August, 1957)

As a result of investigations carried out by various authors [1-4], it has been established that with d.c. high-voltage machines (among which are traction motors usually utilized on electrified railways), the principal cause of flashover or arcing on to the framework are the conducting bridges between adjacent commutator segments caused by fragments from the brushes or by formations of carbon dust. In [4] it was shown that single flashes from shortings, having a high initial resistance (the appearance of such bridges is most probable in operating conditions), easily occur when the maximum intersegmental voltage is greater than 33-34 V; this after all is the ignition voltage of a flash.

To determine the maximum current of a single flash I_m for a specific machine, the following simple expression is recommended:

$$I_m = \frac{U_m - U_d}{z},$$

where U_m is the maximum intersegmental voltage; U_d is the voltage necessary for maintaining the flash, equal to 26-28 V for copper commutator segments; and z is the total resistance of the part of the winding connected to two adjacent commutator segments.

Reference [4] is a continuation of the study of the conditions of the passage of a single flash on to adjacent commutator segments, that in the end must lead to flashover and the study of the conditions of arcing of a single flash on to the framework of a traction motor. Appropriate experiments have been conducted by the author, the results of which are presented here.

* *Elektrichestvo* No. 11, 55-58, 1958.

For conducting the experiments to investigate the conditions of the arcing of a single flash on to adjacent commutator segments, an experimental installation, described in [4], was completed with one circuit having defined parameters, (Fig.1). Vectors of the e.m.f. in circuits I and II had a similar direction that sufficiently well suits the co-ordination in time of the intersegmental voltages for two adjacent pairs of commutator segments. Owing to the presence in the circuit of a thyratron, the circuit of transformer T_1 was connected up when the value of the network voltage was zero.

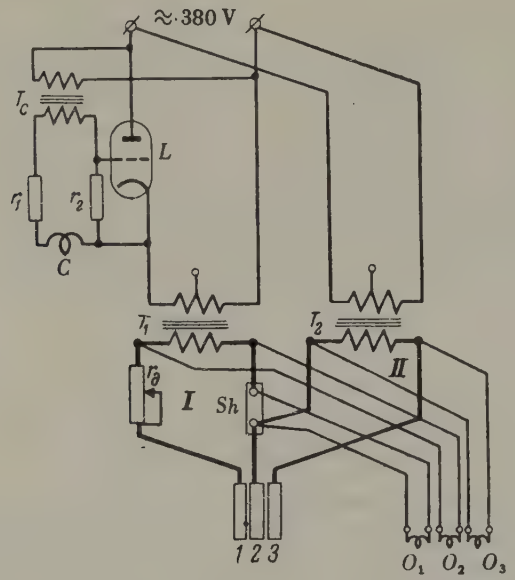

FIG. 1. Circuit of the installation for determining the conditions of the formation of flashover from flashes between two neighbouring commutator segments. T_1, T_2, T_C – transformers; L – thyratron; sh – shunt; r_1, r_2, r_d – resistors; C – choke; 1, 2, 3 – commutator segments; O_1 O_2, O_3 – oscillograph oscillators; I and II – circuits of the scheme.

On conducting the experiments a single flash was induced with the aid of shortings on to commutator segments 1 and 2 (circuit I); the current of this flash was regulated by resistor r_d and was registered by oscillator O_1 of the oscillograph. The presence of arcing on to commutator segments 2 and 3 (circuit II) was determined by oscillator O_3.

On the commutator segments of some traction motors the effect was verified of the change of the maximum voltage of circuit II in the conditions of the arcing of a single flash on to the adjacent commutator segments. It was established that

by changing the maximum voltage of circuit II from 35-60 V with one and the same commutator division (for segments of one and the same motor), for the formation of a flash to commutator segments 2 and 3 it was necessary to have one and the same current for the starting flash. Clearly, in order to obtain the arcing of a flash it is necessary that its flame links adjacent commutator segments. Conditions for the breakdown of the gap in the conditions under examination are probably lightened at a voltage on the commutator segments (2 and 3), which considerably exceeds what is possible on usual d.c. machines.

Thus, it was discovered that the maximum current of a flash in circuit I, inducing a flash to the adjacent pair of commutator segments, is solely dependent on the magnitude of the commutator division [$I_m = f(\beta_{com})$]. This dependence reflects the conditions of the transition of a single flash into a flashover which is ultimately an electric arc shorting either a considerable part of the commutator segments or all the commutator segments situated between brushes of unlike polarity. Experiments were conducted with a voltage on circuit II equal to 37-39 V; the speed of the air being blown past the commutator segments amounted to 15 m/sec. Below is established the effect of a change of this speed on the magnitude of the current I_m inducing arcing on to an adjacent pair of commutator segments.

In Fig. 2 are represented the characteristic oscillograms of the experiments connected with the investigation of the conditions of the passage of a single flash on to a neighbouring pair of commutator segments.

On the right-hand oscillogram (Fig. 2b) is registered by oscillator O_3 a flash on to commutator segments 2 and 3, indicated by a characteristic change of voltage on these segments. With the corresponding experiment for the left-hand oscillograms, there was no arcing of a flash on to the adjacent commutator segments.

Fig. 3 shows the experimental dependence $I_m = f(\beta_{com})$; Fig. 4 shows a curve making it possible to judge how the current I_m required for the formation of a flash on to segments 2 and 3, varies depending on the speed of the air v blowing on the commutator segments. From this curve it follows that in the zone of speeds exceeding 12 m/sec, I_m varies insignificantly, (these speeds are typical for the ordinary duties of traction motors). From the above relationship $I_m = f(\beta_{com})$, one may conclude that for railway traction motors in which there may arise powerful single flashes with a maximum current of up to 2000 A, the passage of these flashes on to adjacent commutator segments is inevitable; for auxiliary machines, in which the maximum current of a flash amounts to 40-100 A, the subsequent development of a single flash is difficult. These conclusions are well confirmed by experiments in the operation of the machines referred to.

A single flash – apart from the flashover, the electrodes of which are the commutator segments – may lead to a breakdown of the gap between the commutator

and the framework; that is, it may lead to "arcing". Careful research into the conditions of the incidence of arcing, involves a considerable complication of the

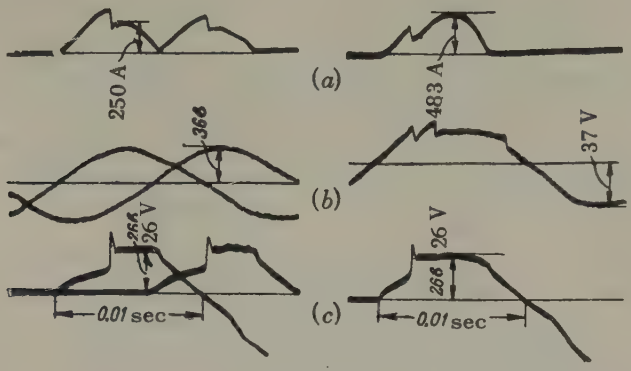

FIG. 2. Characteristic oscillograms of tests for determining the current of single flashes producing arcing on to adjacent pairs of commutator segments.
a) current of the initial single flashes; *b)* voltage on the commutator segments, to which the initial flash must pass; *c)* voltage of the initial single flash.

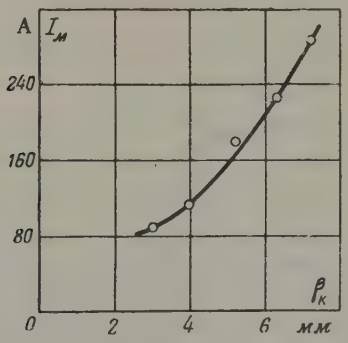

FIG. 3. The dependence of the maximum current of a flash, inducing arcing on to an adjacent pair of commutator segments, on the size of the commutator division.

original experimental plant, as in this case it is necessary to reconstruct near the commutator segments an electric field and a field of the speed of the blowing air exactly the same as in real traction motors. To produce an installation appropriate in full measure to the stated conditions was impossible even though the difficulties connected with such an accomplishment can quite be overcome. In connexion with what has been explained, experiments were carried out for investigating the conditions of arcing of single flashes on to the section of the framework situated

over the commutator and on to the bearing guard, without blowing air on the commutator segments.

The arcing of a single flash on to the part of the framework situated over the commutator is most probable, as in this direction stream powerfully ionized gases from a single flash, owing to the powerful flow of convection; arcing on to the bearing guard also seems possible in so far as it is nearer than other components of the framework, being situated near the commutator. The individual parts of the framework on to which arcing is assumed, were made of aluminium segments and coated with the varnish normally used for painting the internal walls of the traction motor frame.

The electrical circuit of the installation for investigating the conditions of arcing of single flashes on to the framework is shown in Fig. 5. This circuit makes it possible to vary the voltage U_{com} between the commutator segments and plate A from zero to 5 kV. By the matching of resistors r_1 and r_2, the inducements are eliminated in oscillator O_2 by which is registered the presence of arcing of the single flash on to the plate, which acts as a part of the framework of a traction motor.

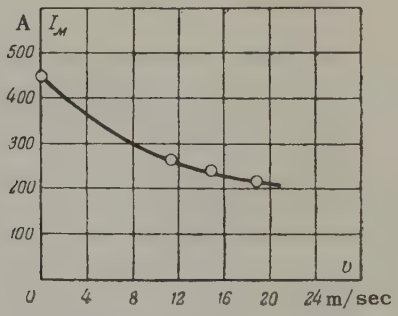

FIG. 4. The variation of the maximum current of a flash inducing arcing on to an adjacent pair of commutator segments, dependent on the speed of the air blowing on them with a constant value of commutator division.

In the experiments flashes were formed on the commutator segments by a short from a fragment of a brush with different values of voltage U_{com} (1, 2 and 3 kV) and different distances l between commutator segments and plate A. A characteristic oscillogram of a flash which produced arcing on to plate A is shown in Fig. 6.

After a large number of tests, the dependence was plotted of the maximum current of a flash – inducing a flashover on to the framework with voltages of 1, 2 and 3 kV – on the shortest distance between the commutator segments and the plate

acting as a section of the framework. This dependence is shown in Fig. 7. From an examination of Fig. 7, it follows that the variation of voltage U_{com} within the indicated limits has but small influence on the conditions of the arcing of a single flash on to the framework. Arcings were registered only when the flame of the flash touched or came very close to the plate acting as a section of the framework. It follows clearly that a breakdown from flashes with minor intensities can only be expected with voltages U_{com} measuring dozens of kV.

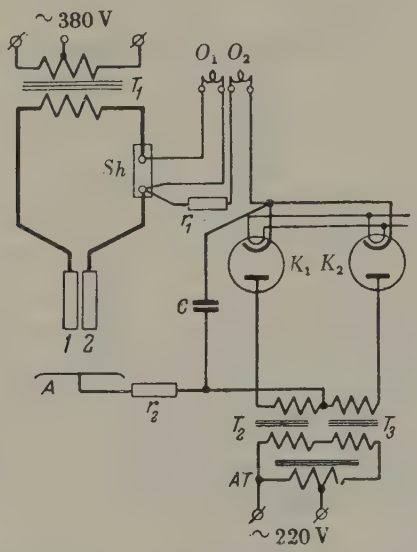

FIG. 5. Circuit of the installation for determining the conditions of the arcing of a single flash on to the framework of a traction motor.
AT – autotransformer; T_1T_2, T_3 – transformers; K_1, K_2 – kenotrons; r_1, r_2 – resistors; C – capacitor; sh – shunt; 1, 2 – commutator segments; A – screen acting as the machine frame; O_1, O_2 – oscillograph oscillators.

From the dependencies obtained, it follows that traction motors have such design dimensions and winding parameters that arcing of single flash on to the framework is fully possible. Thus, the traction motor DPE-400 I_m = 1800 A, has a minimum distance from the commutator to the part of the framework situated over the commutator of 140 mm.

A rather unexpected result was obtained when investigating the conditions of arcing of a single flash on to the bearing guard. Several dozen tests were arranged with various distances between the plate acting as the bearing guard, and the commutator segments, for flashes with different intensities, and yet arcing was not registered even with l = 35 mm, I_m = 1800 A and U_{com} = 3 kV. From these

tests it follows that the arcing of a single flash on to the bearing guard is difficult. When carrying out more careful investigations in this direction, the field of the speed of the air blowing on the commutator has to be taken into account.

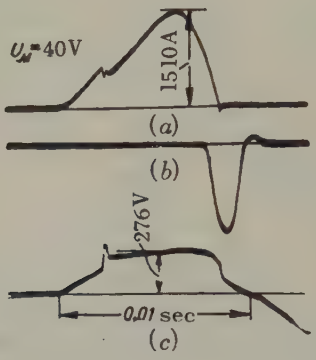

FIG. 6. Characteristic oscillograms of tests for determining the current of a single flash, inducing arcing on to the framework. a – current of a single flash; b – current of oscillator O_2, recording the arcing of a single flash on to the framework; c – voltage of a single flash.

From the results of the investigations carried out, it is possible to answer the following questions:

(1) Whether a single flash occurs in a given machine;
(2) If a single flash occurs, then what its intensity is;
(3) Whether a single flash of a given intensity will lead to flashover or arcing.

Consequently it is possible to select parameters of a d.c. machine with which flashover or arcings caused by short-circuits are impossible.

It follows from the dependencies introduced above, that the prevention of the development of a single flash into a flashover or arcing is rather difficult in the case of powerful machines having a possibly great intensity of single flashes. This would involve either an inordinate increase of the dimensions of the commutator (increase of the commutator division), or a considerable complication of the winding, (introduction into the section of the armature of an additional resistance, fitted near the risers of the commutator). For preventing flashovers and arcings it is necessary to take measures to stop the rise of the single flash. Certain possible measures as well as avenues for further investigation in this direction are set out in [4].

The basic mathematical criterion, determining the possibility of the appearance of the single flash, is necessarily considered to be the maximum permissible

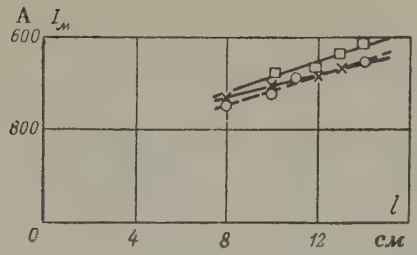

FIG. 7. Dependence of the maximum current of a single flash causing arcing on to the framework, on the shortest distance to the part of the d.c. machine frame situated over the commutator, with various values of voltage between the commutator and the framework.

$\bigcirc - U_{com} = 3\,kV$; $\square - U_{com} = 2\,kV$; $\times - U_{com} = 1\,kV$.

intersegmental voltage, equal in the case of the existing design of commutators, to 33-34 V.

Translated by David Rex-Taylor

REFERENCES

1. A.B. Ioffe; Potentsialnye usloviya na kollektore i puti ikh oblegcheniya. (Potential conditions on a commutator and the means to their alleviation). *Elektrichestvo*, No. 1 (1954).
2. M.D. Nakhodkin and V.S. Khvostov; *K voprosu o prirode krugovogo ognya na kollektore visokovol'tnykh mashin postoyannogo toka. (On the question of the nature of flashover on to commutators of high-voltage machines).* V.E.P., No. 4 (1956).
3. B.S. Sukhorukikh; *Issledovanie svoist dugi na kollektore i primenenie dugovikh kharakteristik pri analize protsessa vozniknoveniya i razvitiya krugovogo ognya v tyagovikh dvigatelyakh. (Investigation of the characteristics of arcing on a commutator and the application of arcing characteristics for the analysis of the process of the rise and development of flashover in traction motors).* Dissertatsia TsNII, MPS (1956).
4. A.S. Kurbasov; *Issledovanie uslovii vozniknoveniya i razvitiya vspyshek na kollektorakh tyagovykh elektrodvigatelei. (Investigation of the conditions of the rise and development of flashes on the commutators of electric traction motors).* Vestnik Vsesoyuznogo Nauchno-issledovatel'skogo instituta zheleznodorozhnogo transporta, No. 2, (1957).

ABSTRACTS FROM PAPERS PUBLISHED IN ELEKTRICHESTVO No. 11, 1958.

Experimental study of power system performance characteristics: S.A. Sovalov, S.I. Leznov and M.I. Smirnov. (pp 1 - 7).

The author sets out the main results of experimental investigations made in the summer of 1957 in the Inter-connected Power System Centre into the variations of frequency in a power system in the presence of control and automatic control and the character of the total load variations as well as the experimental determination of the total (frequency) statism (statism is defined as the division of the controlled magnitude on rated load from its value on no-load expressed as a percentage of its value on no-load) of the power system, the slope of the static load characteristic, the initial speed of change of the frequency in the presence of a sudden disturbance of the active power balance with an equivalent mechanical inertia constant. The results are valuable for questions of frequency regulation and for analysing normal and fault power system conditions.

Economic evaluation of energy losses by comparison of various schemes for the construction of power installations: D.S. Stepanov. (pp 7 - 10).

Only correct estimation of the power losses to be expected in planned power systems and in existing installations enables the most economic choice to be made, for instance, of conductor cross-sections, and transformer powers, distribution network voltage, transmission voltage, the position of substations and condenser stations and so on. Here he adds the recurrent cost of the power losses on full load of the system to the once and for all capital cost of erection. The article represents a strictly economic appraisal of the methods of evaluating the cost of power transmission.

Unbalanced bridge circuits for measuring corona losses: N.P. Emelianov and L.I. Tsepliaev. (pp 11 - 14).

When measuring corona losses the main difficulty is the extremely low power coefficient of the circuit to be measured. In order to improve the power coefficient the line charging current is now compensated in the U.S.S.R. by four arm bridge schemes. A calibrated high-voltage condenser is used for one arm and the corona producing line is used for another high-voltage arm. The phase displacement difference for the high-voltage arms should equal the phase displacement difference

for the low-voltage arms. Assuming there is no leakage in the calibrated condenser and the experimental line before corona, elements should be used for the low-voltage arms which give the same phase shift; i.e. capacitances or resistances. In practice, owing to the leakage of the calibrated condenser for compensation of the bridge in the pre-corona condition of the line, it is necessary additionally to introduce (1) resistances into the arms in the scheme with capacitances in the low-voltage arms and (2) capacitances into the scheme with resistances. When corona arises on the line the bridge is not compensated and becomes unbalanced. The author treats the problem mathematically. In certain conditions he recommends the connexion of a current winding of a wattmeter in the bridge diagonal and a voltage winding at a voltage proportional to line voltage.

Constructing locus diagrams for an induction motor with a saturable reactor: F.N. Zuikov and A.I. Khozhainov. (pp 14 - 18).

Saturable reactors are now used as the power elements of automatic control and regulation systems of cranes, winches, pumps and so on. Investigation of these systems is carried out by graphical-analytical methods. The author investigates the locus of an induction motor with a saturable reactor in the stator circuit when the currents and voltages are sinusoidal in all operating conditions. The author relates the inductive resistance of the reactor to the inductive resistance of the stator and then on the basis of the equivalent network shown in the text and taken from Kostenko's work 'Electrical Machines' 1949 he derives the total equivalent resistance of the main circuit. He introduces a circular diagram of an induction motor for different values of resistance when the equivalent inductive resistance of the reactor in the stator circuit is constant. Other diagrams show the curve and ellipses of simultaneous steel magnetization, the relationship between the equivalent inductive resistance of the choke and the slip for different values of magnetization current (const.), current circles for two limiting values of the equivalent inductive resistance of the reactor when the magnetization current is constant and comparative experimental and calculated relationships between the active current component and of ϕ s for different values of magnetization current (const.).

Several basic circuits for the autodyne: O.V. Benedikt. (pp 24 - 29).

The author considers certain feedback circuits for an autodyne and typical properties and fields of application of autodynes. He assumes the autodyne has a slipping stator excitation winding as this is not important in principle. After showing an example of a feed-back circuit he considers three cases when static conditions are disturbed: a change in the speed of the armature, in the voltage and in the voltage level. Unlike the motor-generator, the autodyne is a source of stabilized voltage. The relationship due to hysteresis between the voltage and the voltage level is then shown diagrammatically for test autodynes A2-B, A-3B and A-6B which have windings compensating the influence of friction on the

torque. The autodyne is considered in circuits as a power converter, and as an automatic regulator of other equipment. The different circuits are shown diagrammatically. Rotor over-excitation of the autodyne is also discussed.

Coefficient of commensurability at feeding an induction motor from the synchronous generator: Ia. B. Kadymov and M.M. Rasulov. (pp 35-38).

The operating conditions of a synchronous generator operating in an autonomous system are determined by the relationship between the power of the generator and the motor connected thereto. If the power of a short-circuited motor is commensurate with the generator power, then the power at the generator terminals can decrease to values at which the stable operation of the remaining consumers becomes impossible and the motor will not start. In order therefore to start the motor reliably, it is necessary to choose the right power relationship of the motor and generator. This relationship (the coefficient of commensurability or the relationship between the reactances of the generator and motor), is then established and the author considers the value of a system of automatic control of excitation of synchronous generators for increasing the coefficient of commensurability. The method of determining this coefficient is then examined for the case when the parameters of the machines are familiar and when different methods of regulating excitation are employed. Two examples of the calculations are given.

Inverter duty of type RMNB-500 × 6 rectifiers: L.S. Fleishman and M.V. Gel'man. (pp 43-46).

Recuperative braking on electric railways requires the conversion of one or several rectifiers to inverter duty when there are no other d.c. consumers. The unstable operation of the rectifier on inverter duty can cause a break in recuperation. Until recently the RMNB-500 × 6 rectifiers have been defective on inverter duty. The article considers the causes of instability of an inverter which have been investigated in the mercury arc rectifier laboratory of the Ural electrical apparatus works and gives the results of tests after taking special steps to improve the reliability of inverters. The author considers three inverter schemes: (1), with two reverse (inverse) stars and balancing reactor, (2), with a three phase bridge scheme and (3), with a six-phase zig-zag. The value of synthetic schemes is discussed. Shunting circuit valves and a cathode reactor were installed with an inductivity of 50-100 mH, which improved reliability considerably.

Transients in a motor drive with reactor control of the winch in a multi-scoop drag: L.F. Shkliarskii. (pp 47-50).

A previous article by the author "Automation of the Electrical Drive of a Multi-scoop Drag", Elektrichestvo, 1, 1957, considered the calculation of the static mechanical characteristics of the winch of multi-scoop dredges with an additional resistance in the rotor circuit of the induction motor and a saturable choke (reactor) connected asymmetrically in two phases of the rotor. The present article

follows on with an analysis of the transient processes arising in such drives. In view of the complexity of transient phenomena the author considers a simple and practical method of calculating these transient processes is desirable. The method is based on the use of the static characteristics which can be derived from the catalogue data of the motor and reactor. Laboratory investigations show that the error in the calculations is not over 10 per cent.

Motor-generator drive with a rotary and magnetic amplifier: A.V. Basharin. I.N. Vinogradov. A.I. Vychkov. and J.B. Byval'kevich. (pp 51-55)

To improve and develop reverse d.c. drive, rotating machine (rotary) amplifiers, semiconductor rectifiers and recently magnetic amplifiers have been employed. The quality of such systems was first measured by the degree to which the current diagram was filled. Originally the current diagram was considered to be rectangular. Then other shapes (e.g. triangular shape) were recognized to be optimum in certain cases. Later it was established that when the time of the transient processes had to be a minimum or when the system of drive had to be most productive, the "coefficient of current diagram filling" can characterize the quality factor of the control system. The present article acquaints the reader with the system of drive developed by the Faculty of Industrial Electrification of the Lenin Institute of Electrical Engineering in Leningrad. The system is based on the use of magnetic amplifiers and symmetrical semiconductor ceramic non-linear resistances. This system conforms to the best static and dynamic characteristics plotted from the maximum coefficient of current diagram filling according to the system developed by the TsKB "Elektroprivod" with matched cut-offs. The Lenin Institute system however needs to use a minimum of contact apparatus for starting, reversing and braking (without creep speeds).

Ferrites with a rectangular hysteresis loop: L.J. Robkin. B.Sh. E'pshtein and Ia. G. Koblents. (pp 59-68).

Such materials have been widely used in the memory apparatus of digital computers and "answer" computers, automatic control apparatus, magnetic amplifiers, non-linear elements for multiplying frequency, communications apparatus and so on. The paper is intended to acquaint a wide circle of engineers with the methods of production, the application and the main parameters and characteristics of certain Russian ferrites with a relative residual induction > 0.85.

Protective relaying on the basis of the "Hall effect." V.K. Sirotko. (pp 69-71).

The "e.m.f. Hall pick-up" employed in the Electromechanical Institute of the Academy of Science U.S.S.R. is shown. The design of the apparatus is considered and its method of operation. Calculations and experiments have shown that the executive relay device based on the "Hall effect" and having approximately the same sensitivity as the best inductance relays has a minimum power consumption on operation of 10^{-4} ... 10^{-5} W. To evaluate the speed of operation of the relays

and study their behaviour during transient processes in long distance transmission lines, a short-circuit was imitated both inside and outside the operating zone of the relay. No incorrect operation of the relay was recorded. The operating time of the relays in the presence of short circuits within the protected zone did not exceed 10 msec.

A telemechanical system using magnetic elements with rectangular hysteresis loops: V.A. Tutevich. (pp 72-73).

There are good prospects for the development of contactless elements especially magnetic elements with rectangular hysteresis loops which can operate from an a.c. network and thereby facilitate the construction of simple telemechanical systems. Such magnetic elements embody the cyclical and continuity principles based on the division of ducts using a distributive unit and the synchronization of the transmitting and receiving points of the telecontrol system. The system can either signal the state of eight objects, (the operating time of three of them being fixed by a scheme made from filamentless thyratrons), or, control five objects, (three signals being used here for calculating the products by filamentless thyratron counters), or finally, control only two objects, (six signals being used for operating three differential filamentless thyratron counters). Continuous registration of indications is effected. The transmitting and receiving commutators are synchronized. The system can be used for transmitting orders as well as for indication and counting.

A quick method of appraising the danger of electrical sparking: P.A. Fetisov. (pp 74-78).

There is a large number of explosive mixtures of gas and air which need to be calculated to produce appropriate spark-proof equipment. These calculations take an exceptionally large amount of time. The new quick method is based on (1) the relationship obtained between the probability of ignition when the ignition current varies, (2) the fact that each mixture has a definite point in relation to other mixtures which determines its capacity to ignite from an electric spark and, (3) the curves of the probability of explosion of mixtures investigated by the author are practically parallel. His method is explained and illustrated by diagrams and test results are tabulated. The new method is quicker and explosion-proof characteristics can be plotted in the voltage range up to 60 V and with an inductance of 1 H at one or two experimental points. The difference between the results achieved by the old method is 4-5.5 per cent. The article was written with the requirements of the chemical industry in mind.

An over-voltage recorder for 6-10 kV networks: V.D. Iurenkov and G.A. Dorf. (pp 78-82).

This recorder has been developed in the All-Union Scientific Research Institute of Electrical Engineering for measuring the atmospheric and internal over-voltages

in 6 - 10 kV networks. It comprises capacitance limiters, a three phase spherical discharger and a three phase recorder of operation, all connected in series, (see figure in the text). When a voltage wave passes to the discharger with an amplitude greater than the setting value, there is a cascade breakdown of the discharger sparkgap and of the paper of the operation recorder. A hole is left on the paper strip showing the discharge. The moment of operation of the apparatus is determined with an accuracy of up to ± 15 min on moving the strip. The measurement of voltage impulses of a few microseconds is considered in connexion with radiation. When a capacitor and resistance were connected in the apparatus, faulty operation was overcome.

THE ELECTRICAL PROPERTIES OF COMPRESSED AIR IN AN AIR-BLAST CIRCUIT-BREAKER*

E.M. TSEIROV

(Received 15 May 1958)

One of the factors which limits the working capacity of an air-blast circuit-breaker considerably is the low electrical strength of the contact gap in its quenching chamber in spite of the comparatively high pressure and, consequently, the high electrical strength of the compressed air in it.

A distinction should be made between the two forms of electrical strength of the contact gap in quenching chambers: *static and dynamic*. Static strength is described as the minimum magnitude of the discharge voltage between the open contacts of the chamber during no-load operation (without breaking the current). Dynamic strength is described as the gradually increasing minimum discharge voltage between the contacts after the current has been broken in the chamber. It can be shown that the static and on the whole the dynamic electrical strength of the contact gap of a quenching chamber depends not only on the air pressure, but also on the construction of the chamber, the arrangement of its contact system and so on. The discharge voltage gradient (electrical strength) varies substantially both along the axis of and across the contact gap. Therefore, it is necessary to differentiate between the overall *integral* electrical strength and the *local* electrical strength of the gap which is characteristic for a given point on it.

Observation of the electrical properties of air in the contact gap of a chamber result in the conclusion that the electrical strength of moving air is always less than that of still air, other conditions being equal. This is most simply seen in a jet flowing from a compressed air tank.

The results of measurements of the puncture voltage at various points in an air jet flowing through a glass nozzle are presented in the form of curves in Fig. 1. The measurements were made with the use of a probe consisting of two hemispheres 4 mm in diameter fastened to thin but sturdy electrodes; the clearance between the hemispheres was 1.0 mm. In the course of the experiment the line frequency voltage applied to the electrodes of the probe was slowly raised until

* *Elektrichestvo*, No. 12, 1-9, 1958.

a spark-over occurred. The effect of the probe on the accuracy of measurements was apparently small, since changing its position in the jet did not affect the result.

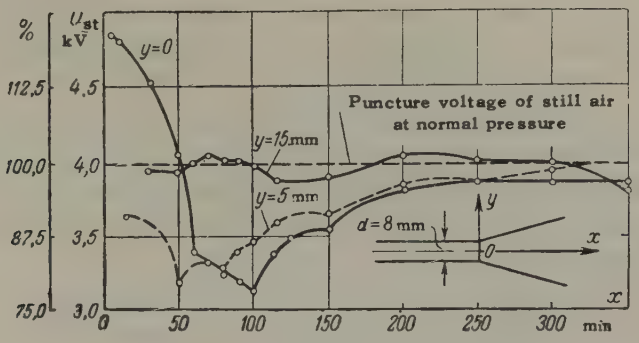

FIG. 1. Local electrical strength of a free air jet flowing through a nozzle of diameter $d = 8$ mm at a pressure $p = 3.5$ atm.

Regarding the magnitude of the discharge voltage which is determined directly by the probe and which is related, of course, to the length of the discharge gap, we have the following information: in immediate proximity to the outlet section of the nozzle ($x \approx 0$; $y \approx 0$) the puncture voltage is equal to 4.8 kV (puncture voltage gradient 48 kV/cm); along the jet stream it drops rapidly, and at a distance of approximately 50 mm from the nozzle it becomes equal to the electrical strength of still air at normal pressure which in this case was 4.0 kV. On further movement of the probe the puncture voltages continue to drop, reaching 3.14 kV at $x = 100$ mm, i.e. falling almost 1 kV below the electrical strength of air at normal pressure. After passing this minimum value the curve for the electrical strength rises slowly to approximate the electrical strength of air at normal pressure.

These results were obtained with an air pressure of 3.5 atm in the tank supplying the nozzle. Numerous similar experiments with other original pressures always led to identical results in practice. Thus, we arrive at the conclusion that in a free air jet there are areas with a substantially reduced electrical strength which is less than that of still air at normal pressure.

The curve for $y = 5$ mm shows a minimum value for the puncture voltage at approximately the same position as when $y = 0$. At a distance of 15 mm from the axis, the puncture voltages do not differ in practice from the voltages for still air at normal pressure.

There is nothing paradoxical, naturally, in the results obtained since it is well known that a gas jet flowing from a nozzle at sonic speed expands so strongly

that for a certain time the pressure within it becomes less than that of the surrounding space; this is marked in particular by a reduction in electrical strength.

The case in question is of importance to us in that it clearly demonstrates the fallacy in considering a moving gas as a homogeneous medium possessing certain mean parameters, and, consequently, corresponding mean electrical properties. In studying the operation of quenching chambers in air-blast circuit-breakers consideration must be made, evidently, of the possible presence of zones of substantially reduced electrical strength in the contact gap area. In this connexion investigations of the electrical strength of standard quenching chambers are of great interest.

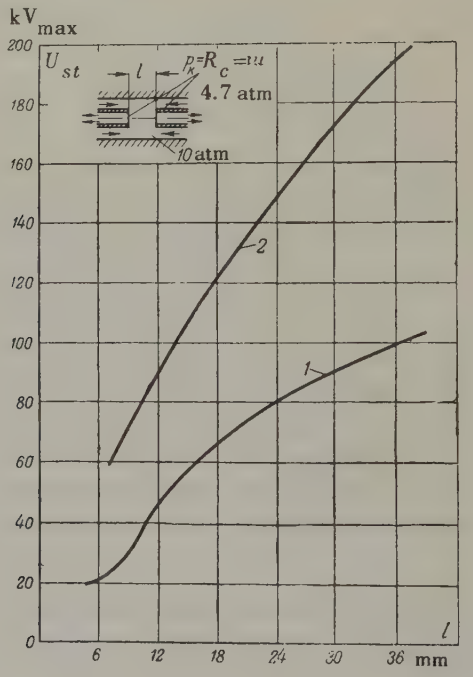

FIG. 2. Integral electrical strength of the contact gap in a standard quenching chamber.
1— usual compressed air flow, p_0 = 10 atm; 2— exhaust outlets closed, p_0 = 4.7 atm.

Curve *1* in Fig. 2 characterizes the electrical strength of the contact gap in an ordinary quenching chamber equipped with simple hollow cylindrical contacts as is shown in the diagram in the same figure. The curve for the electrical strength was made in natural conditions, i.e. on an ordinary circuit-breaker during no-load operation.

With fully opened contacts when the length of the contact gap reached 35-36 mm (internal diameter of contacts 32 mm), the minimum puncture voltage reached 100 kV max; here the air pressure directly at the contact intake was 4.7 atm, but 10-11 atm in the chamber itself, (Fig. 2).

If the flow of compressed air from the quenching chamber is prevented, keeping all other conditions the same, then in the presence of a constant pressure in the chamber equal to 4.7 atm (i.e. the same as in the preceding case at the contact intake) the rise in the electrical strength on increasing the length of the contact gap will be described by curve 2, (Fig. 2). If the total length of the contact gap is 35 mm, the minimum puncture voltage according to this curve is 185 kV max. Thus, in spite of the fact that in the first case the mean air pressure in the contact gap was certainly higher since in the chamber itself the pressure was maintained at 10 atm, its electrical strength was substantially (1.8 times) lower.

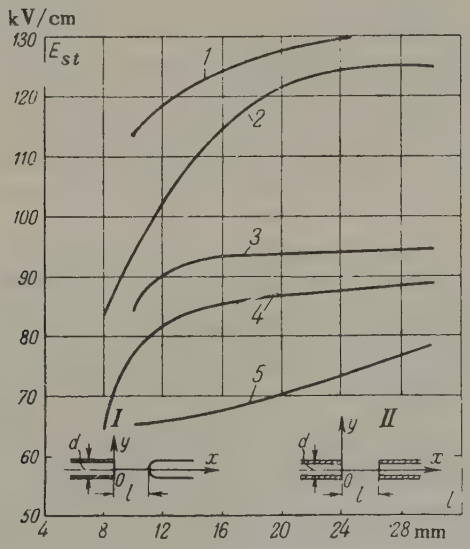

FIG. 3. Local electrical strength of contact gaps. 1 — electrical strength at point ($x = l^{-2}$; $y = 0$) with contact system *I*; 2 — same at point ($x = l/2$; $y = 0$); 3 — same at point ($x = 2$; $y = 0$); 4 — electrical strength at point ($x = l/2$; $y = 0$) with contact system *II*; 5 — same at point ($x = 2$, $y = 0$). $d = 19$ mm; $p_0 = 4.0$ atm.

Fig. 3 shows the results of measurements of the local electrical strength of contact gaps for system *I* where one of the contacts in the chamber is hollow and the other solid (unilateral blast), and for system *II* where both contacts in the chamber are hollow (bilateral blast). The measurements were made in the presence of strictly constant pressure in conditions where the effect of the walls or

other extraneous factors was eliminated in actual practice. In this series of experiments the pressure in the chamber itself was maintained at 4 atm; the internal diameter of the contacts d was in both cases 19 mm. The measurements were made on the axis of the stream (longitudinal axis of the contact system $y = 0$) half-way between the contacts ($x = l/2$) and 2 mm from the plane passing across the contact faces. The contact distance l was varied within the limits of 8 - 30 mm (0.42 - 1.58) of the internal diameter of the hollow contact).

From curve *1*, Fig. 3 it is seen that with an increase in the distance l between the contacts, the local electrical strength of the air near the face of the fixed contact rises evenly; when $l = 25$ mm it is 130 kV/cm. This curve is obviously higher than all the others, i.e. the electrical strength of the air stream in immediate proximity to the face of the fixed contact is greater than in the contact gap.

Curve *2* shows a similar dependence for the point exactly half-way between the contacts. When the length of the contact gap is small, the electrical strength of the air at this point is also comparatively small. For example, when $l = 8$ mm we have $E_{st} = 84$ kV/cm. With an increase in l the electrical strength rises with extreme rapidity, reaching 125 kV/cm when $l = 25$ mm, i.e. the maximum value for the given case. Further increase in the length of the contact gap no longer has any effect.

Curve *3* gives the same dependence for the point at the hollow contact intake. The character of the curve shows that beginning from the determined limit the electrical strength depends little on l. Actually, when $l = 10$ mm $E_{st} = 84$ kV/cm, and even when $l = 15$ mm the electrical strength in actual practice reaches its maximum value of 93 - 95 kV/cm, and from then on no longer depends on l.

If values for local electrical strength E_{st} are compared say for $l = 25$ mm, the following figures are obtained at the fixed contact, half-way between the contacts and at the hollow contact intake: 130, 125 and 94.5 kV/cm.

The lower two curves are for system *II*, i.e. bilateral blast. Curve *4* shows that at the point $x = l/2$ the electrical strength of the air depends greatly on the quantity l; when $l = 8$ mm, $E_{st} = 64$ kV/cm, and when $l = 30$ mm, $E_{st} = 89$ kV/cm. The electrical strength at the hollow contact intake (curve *5*) depends on l to a lesser degree. So, when $l = 10$ mm, $E_{st} = 65$ kV/cm, and when $l = 30$ mm, $E_{st} = 78$ kV/cm. Curve *5* for the electrical strength is substantially lower than curve *4*. Thus minimum electrical strength is observed in the zone near the intake holes of the hollow contacts.

Comparing on the one hand curves *1*, *2* and *3* and on the other hand, curves *4* and *5*, we see that the values for the electrical strength in the latter (i.e. in a bilateral blast) are considerably less than in the former (i.e. in a unilateral blast),

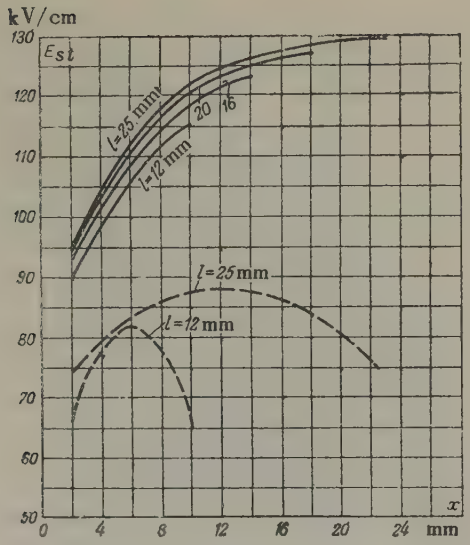

FIG. 4. Local electrical strength along the contact gap axis for various values of l

Four upper curves — unilateral blast; two lower curves — bilateral blast;
d = 19 mm; p_0 = 4.0 atm.

other conditions being equal.

The local electrical strength along the axis of the contact gap for various lengths of l is presented in Fig. 4. The four upper curves which are for a unilateral blast show very clearly that the electrical strength is distributed with extreme irregularity along the contact gap. On altering the length of the contact gap l the character of the irregularity remains unchanged, but the absolute values for the electrical strength decrease with a decrease in l.

The two lower broken curves represent the distribution of electrical strength along the axis of the contact gap with two hollow contacts (bilateral blast) in the same external conditions. The form of the curves is conditional; only those points determining the minimum and maximum values for the electrical strength are reliable. The curves show that the electrical strength is distributed with irregularity along the axis of the gap, and what with a decrease in l its absolute value falls.

The distribution of air flow speeds in the contact gaps in question which is measured with a special thermoanemometer is shown for a unilateral blast in Fig. 5 and for a bilateral blast in Fig. 6. The shape of these curves is well in keeping with the character of the variation of the electrical strength in the contact gap. According to Fig. 5 the maximum speed is observed immediately at the

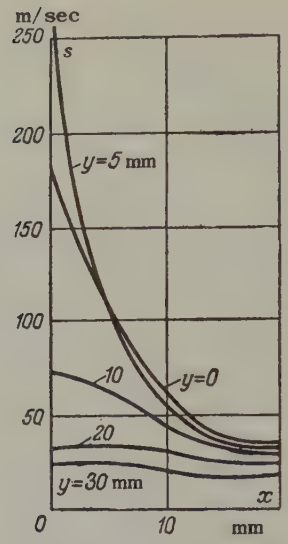

FIG. 5. Distribution of the air flow speeds s along the contact gap with a unilateral blast. Contact system I (Fig. 3).
$d = 19$ mm; $l = 25$ mm; $p_0 = 4.0$ atm.

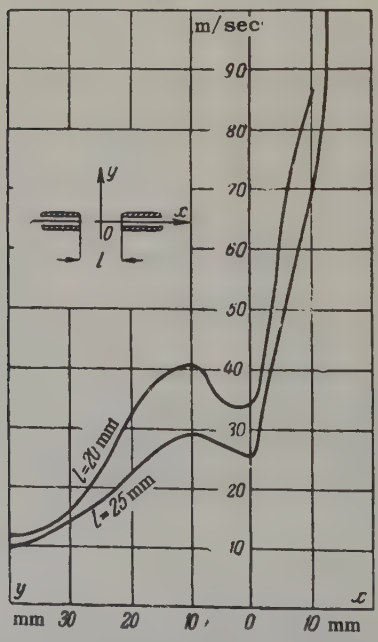

FIG. 6. Distribution of air flow speeds s along the x and y axes of the stream in the presence of a bilateral blast.
$d = 19$ mm; $p_0 = 4.0$ atm.

hollow contact intake where, of course, there is the least pressure and consequently the least electrical strength. On the other hand, in immediate proximity to the fixed contact the flow speed is small, the pressure higher and the electrical strength of the air at a maximum.

The speed distribution curves were measured, as is seen from Fig. 5, not only on the axis of the stream but also parallel to it for $y = 5$, 10, 20 and 30 mm. The further from the axis the measurements are made, the less the speed: the curves for $y = 10$, 20 and 30 are lower than for $y = 0$.

Fig. 6 represents the flow speed distribution along the transverse and longitudinal axes of the stream formed by the two hollow contacts. Along the y axis the speeds are in general relatively small. At the origin, i.e. at the centre of the stream, the flow speed barely reaches 25-33 m/sec.

Along the x axis, moving towards the intake section of the contacts, the speed increases quite rapidly, reaching 88-100 m/sec. In Table 1 data are presented allowing a comparison to be made between the values for the flow speeds and electrical strength on the longitudinal axis of the stream in both contact arrangements, ($d = 19$ mm). In the given conditions the contact arrangement with two hollow contacts has lower values for the air flow speeds and electrical strength.

TABLE 1

Type of blast	l, mm	Point with minimum speed		Point with maximum speed	
		Speed, m/sec	Electrical strength, kV/cm	Speed, m/sec	Electrical strength, kV/cm
Unilateral	20	22	127.5	190	94.0
	25	34	130.0	190	94.5
Bilateral	20	33	87.0	87	70.0
	25	25	88.0	100	74.0

Both the presence of high flow speeds in the contact gap of the chamber and as high as possible an electrical strength of the air in the chamber are important for successful quenching of an electrical arc. Therefore, the arrangement with two hollow contacts must yield, apparently, to the arrangement with one hollow contact.

However, the known positive qualities of the bilateral blast compelled us to

study this system more closely.

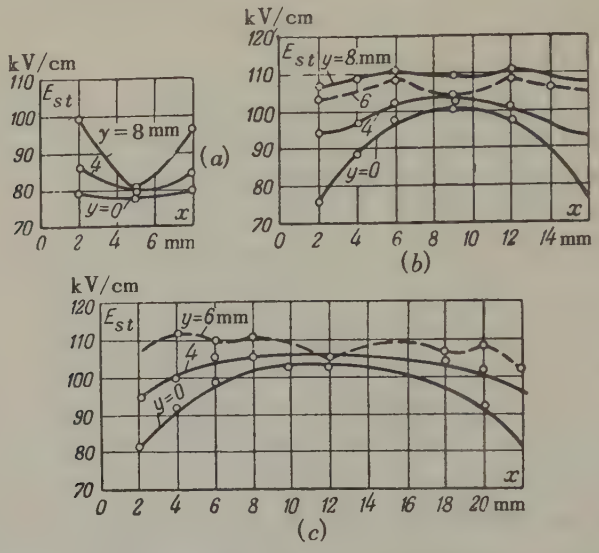

FIG. 7. Local electrical strength of the contact gap with bilateral blast. Contact system II, (Fig. 3).
d = 19 mm; p_0 = 4.0 atm.
(*a*) — l = 10 mm; (*b*) — l = 19 mm; (*c*) — l = 25 mm.

It has been pointed out that the state of the local electrical strength at various points on the contact gap is substantially affected by the length of the gap itself. The curves in Fig. 7 are of interest in this connexion. Here are shown three families of curves characterizing the local electrical strength of the contact gap measured both along the longitudinal axis of the stream x, and also at various other points. When l = 10 mm, the values for the local electrical strength on the axis of symmetry (y = 0) depend little on the point of measurement: the curve for the electrical strength is deflected downwards only slightly. With a rise in y the dependence of the electrical strength on x increases. All three curves are deflected downwards, i.e. the electrical strength at the mid-point of the gap is less than it is close to the contacts themselves.

With an increase in the length of the contact gap l to 19 mm, the character of the curves alters sharply. The curve for the electrical strength on the x axis becomes convex; now at the mid-point of the contact gap E_{st} = 90 kV/cm, and at the contact faces E_{st} = 74 kV/cm. In immediate proximity to the x axis when y = 4 mm, the character of the curve remains as before but the absolute values for the electrical strength rise. The curves for the electrical strength when y = 6 mm and y = 8 mm have an unusual form. It is characteristic that at certain points the electrical strength on the line y = 6 mm drops even lower than on the line y = 0.

Further increase in l gives a smoother curve and raises the local electrical strength noticeably, particularly at points distant from the contacts. For example, when $l = 25$ mm, on the x axis ($y = 0$) we get $E_{st} = 81$ kV/cm at points when $x = 2$ mm or $x = (l - 2)$ mm, but when $x = l/2$ we get $E_{st} = 103$ kV/cm. It is easily seen that the lowest electrical strength is as a rule observed on the x axis of the stream ($y = 0$) throughout its length, the minimum values being found in immediate proximity to the contacts.

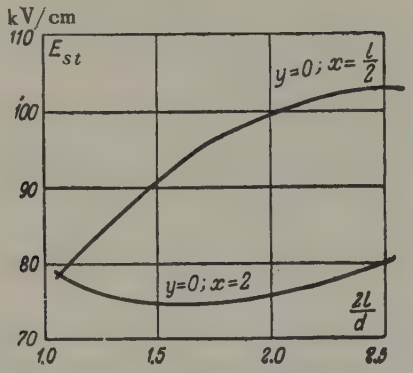

FIG. 8. Dependence of the local electrical strength of the contact gap on the value of the dimensionless parameter $2l/d$.

The area of the cross-section of the openings through which the air flows from the contact gap is equal to $2\pi d^2/4$; the lateral surface of the cylinder through which the air passes to these openings is πdl. Consequently, if it is required that a given lateral surface does not limit the air flow to the contact openings the relation $l = d/2$ must at least be maintained between them. Taking this contact gap length per unit, we plot the dependence of the local electrical strength of the latter on the dimensionless parameter $2l/d$, (Fig. 8). The electrical strength at the contact intake has little dependence on the parameter $2l/d$ within the limits of the given data. But when $2l/d = 1$ and when $2l/d = 2.5$ it remains almost unchanged. However, the electrical strength at the point $x = l/2$ shows quite a strong dependence on this parameter.

Thus, an increase in the length of the contact gap should raise its integral electrical strength not only because of this factor, but also as a result of the rise in the value for the local electrical strength.

In Fig. 9 curves are shown for the rise in the electrical strength of the air at the contact intake along the radius of the latter for various contact-gap lengths l. From the curves it is apparent that with an increase in the radius R and, moving away from the centre, the electrical strength rises smoothly. When the contact gap

l = 14 mm and more ($d = 2R$ = 19 mm), the electrical strength no longer depends on its length in actual practice.

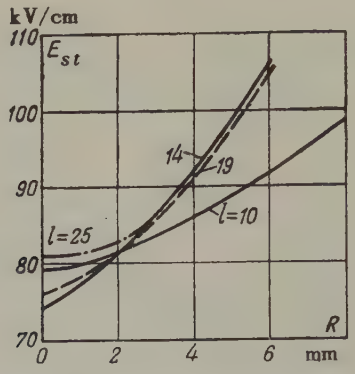

FIG. 9. Relation of the local electrical strength along the radius of contact intake.

In summarizing all this information on the distribution of local electrical strength in this type of contact gap, it is perhaps possible to conclude that the geometric path of an electrical discharge in the gap follows chiefly along the longitudinal axis, passing then to the contact walls according to radius.

Direct experiments on the contact gaps of a standard quenching chamber with a bilateral blast clearly showed that in every case the spark-over does not pass between the faces of the contacts, but between their internal surfaces. The tendency of both the integral and, naturally, the local electrical strength of the given contact gap to rise was the result of its particular construction whereby one of the hollow contacts was equipped with a diaphragm as is shown in the drawing in Fig. 10. The results of measurements of the local electrical strength in this type of arrangement are shown in the form of curves in the same figure. The measurements were made at different points on the x axis of the stream.

The comparison of these curves with the corresponding characteristics in Fig. 3 (curves *3* and *4*) show first of all that the values for the local electrical strength at the intake to the hollow (not equipped with a diaphragm) contact (curve x = 2, Fig. 3) have risen somewhat in comparison with the data given previously (curve *5*). For example then, when l = 30 mm, we get 96 kV/cm against the previous 78 kV/cm, i.e. a rise in the electrical strength of 1.2 times. The electrical strength of the air in the diaphragm-equipped contact, i.e. at the point x = 2, rose with particular strength to reach 118 kV/cm when l = 30 mm, i.e. it increased 1.5 times. A similar substantial increase in the electrical strength was noted at the point $l/2$, equalling 117 kV/cm against 94 kV/cm, i.e. it rose 1.25 times. Thus, diaphragming one of the hollow contacts raises the electrical

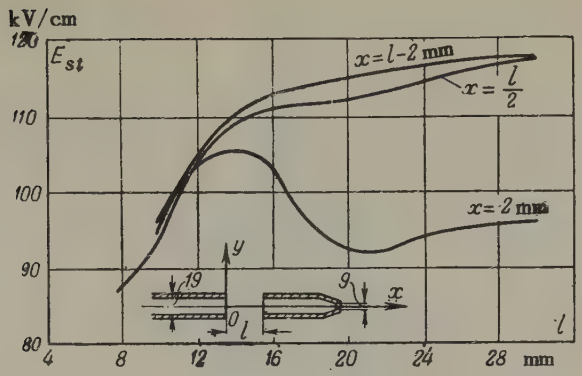

FIG. 10. Dependence of the local electrical strength of the contact gap on l for the case where one of the hollow contacts is equipped with a diaphragm.
$d = 19$ mm; $p_0 = 4.0$ atm.

strength of the contact gap substantially, approximating it to that in a unilateral blast arrangement.

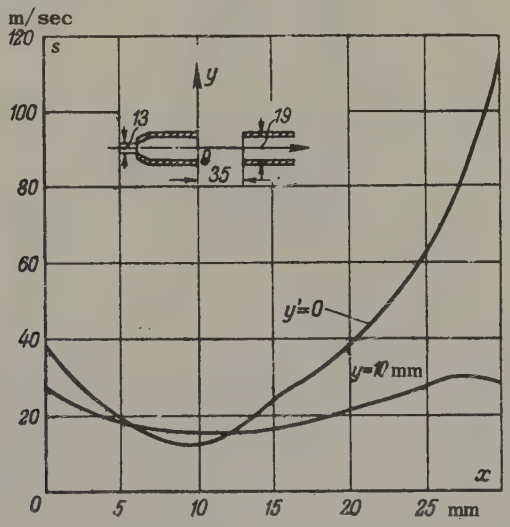

FIG. 11. Distribution of the flow speeds along the contact gap with one of the two hollow contacts equipped with a diaphragm.
$d = 19$ mm; $p_0 = 4.0$ atm.

The flow speed distribution in the gap in question is shown in Fig. 11. Here the speeds were measured exactly on the x-axis of the stream ($y = 0$) and along it at a distance of $y = 10$ mm. It is easily seen that in the given arrangement the

points with a minimum flow speed are displaced in a direction towards the diaphragm-equipped contact.

The integral electrical strength of the contact gaps should apparently be determined proceeding from the minimum values for the local electrical strength. If we consider the information in Fig. 3, when $l = 25$ mm the minimum electrical strength for a unilateral blast is equal to 94.5 kV/cm, and consequently the overall integral electrical strength amounts to approximately $94.5 \times 2.5 = 236$ kV.

In exactly the same way the minimum electrical strength for a bilateral blast amounts to 74 kV/cm, and correspondingly, the integral electrical strength is $74 \times 2.5 = 185$ kV. However, direct measurements of the integral electrical strength, as can be seen from Fig. 2, show that it is substantially smaller even in conditions of considerably higher air pressure. This unfavourable circumstance is related to the fact that in practice the electrical field is itself unevenly distributed along the contact gap. The highest gradients are found in the areas immediately adjacent to the contacts. Consequently, the gradient of the electrical field applied to the contact gap will be highest at the hollow contact, and the electrical strength will be lowest. The overall electrical strength of the contact gap is sharply reduced. Here the bilateral blast is also operating in the least favourable conditions.

Studying the electrical properties of contact gaps in quenching chambers is completely pointless if it is not accompanied by a study of their breaking capacity. Therefore, this side of the problem is considered below.

The investigations described, explaining in some degree the causes of the low overall electrical strength of a contact gap, do not permit a numerical evaluation to be made of the latter.

In order to bridge this gap an experimental determination of the static integral electrical strength of a contact gap was made on a standard quenching chamber of a 110 kV, 4000 MVA circuit-breaker equipped with a bilateral blast, (Fig. 12). It consists of two quenching elements. Its moving contacts *1* are actually simple cylindrical tubes which carry off the arcing products into the atmosphere. The fixed contacts *2*, which are also hollow, are equipped with diaphragms as is seen in the figure. In the course of the tests three types of fixed contact were used: (1) simple tubes without diaphragms, (2) diaphragms as shown in Fig. 12, and (3) with a special grid diaphragm (see below).

The measurements of the static electrical strength (minimum discharge voltage) were made entirely in natural conditions, i.e. on a standard form of circuit-breaker actuated by its pneumatic system. The air pressure in the tank was raised to 16 atm before beginning the experiment. The internal diameter of the hollow contacts was 32 mm; the airline supplying the quenching chamber was

90 mm in cross-section.

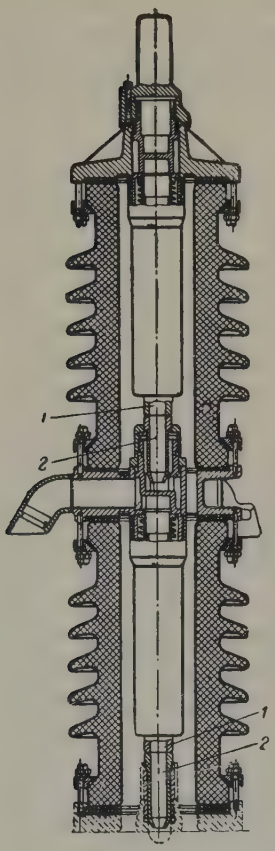

FIG. 12. Cross-section of the standard quenching chamber of a 110 kV circuit-breaker with a bilateral blast.
1 — moving contacts; 2 — fixed contacts.

Fig. 13 shows the relations of the rise in the static integral electrical strength of the contact gaps in the course of the motion of the moving contacts of the quenching chamber. They pertain to its upper element. Both the time which has passed from the beginning of contact separation and the path covered by the moving contact during this time are shown on the abcissa.

On full contact separation, equal to 32 mm, the minimum puncture voltage determined by many experiments was equal to 90 kV according to curve *1*. If consideration is made of the fact that the air pressure in the chamber during those experiments reached 12 atm, the result obtained is not encouraging.

Curve *2* shows that if the fixed contact is equipped with a diaphragm the

electrical strength of the gap rises considerably, reaching 160 kV max on full separation of the contacts. It increased even more when the fixed contact was equipped with a new grid diaphragm, i.e. when many fine choking openings were used instead of a single one (diagram and curve *3*).

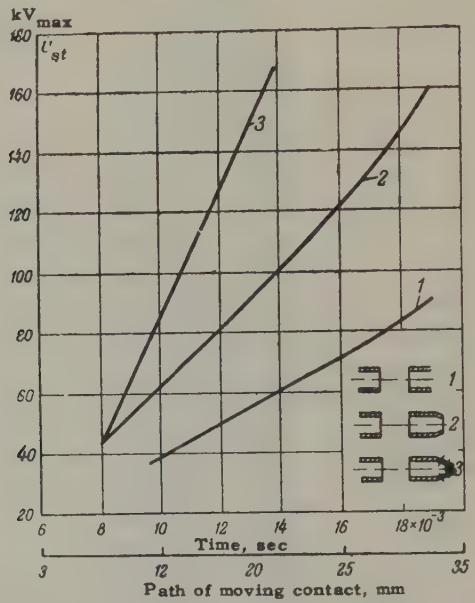

FIG. 13. Dependence of the electrical strength of the upper contact gap of a quenching chamber (Fig. 12) on time and gap length. Pressure in the circuit-breaker tank 16 atm; diameter of air supply line 90 mm.
1 — contact gap with ordinary hollow contacts in the form of smooth tubes 32 mm in diameter; 2 — same except that the fixed contact has a conical diaphragm with an outlet of 15 mm; 3 — same, except that the diaphragm has many fine openings.

Only those contact devices which to a varying degree find practical application have been described above. Generally speaking, there are other means of substantially raising electrical strength, but they fail to meet even the minimum requirements for breaking capacity.

It must be said here and now that diaphragming one of the hollow contacts in a bilateral blast system raises the capacity of the chamber to withstand the recovery voltage amplitude, but at the same time it reduces its capacity to withstand the higher frequency of this same voltage. However, the rational application of diaphragms will make it possible to obtain a more ideal combination of both these and other properties in practice.

Between those limits of recovery voltage frequency which are at the present accepted in world practice, a limited degree of the application of diaphragms to one of the contacts has a strong effect on the breaking capacity of quenching chambers in actual practice. The application of the grid diaphragm will increase its potentialities even more.

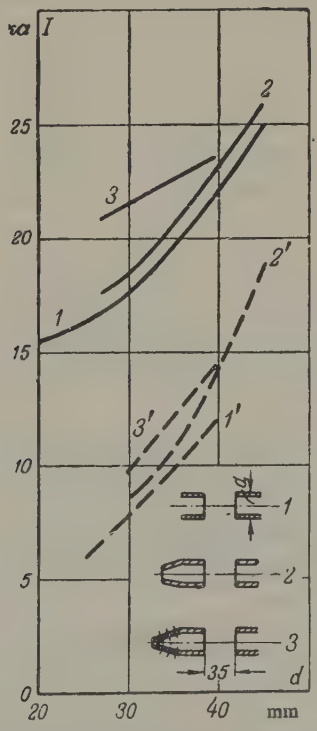

FIG. 14. Dependence of the breaking current of a 110 kV air-blast circuit-breaker on the internal diameter of the contacts. The quenching chamber has two elements. Air pressure 20 atm; total length of the contact gap $l = 35$ mm; airline diameter 90 mm. The continuous curves correspond to the amplitude of the recovery voltage $U_r = 180\ kV_{max}$ with frequency $f_0 = 800$ c/s, and the broken curves for $U_r = 220\ kV_{max}$ and $f_0 = 3000$ c/s.

For an illustration of this, Fig. 14 shows the results of an investigation of a standard industrial type of 110 kV air-blast circuit-breaker having a quenching chamber with two elements in series. The quenching chamber was equipped with three contact systems in the course of the tests: (1) ordinary hollow contacts as in system *1* (Fig. 14), (2) exactly the same contacts, one of which was equipped with a diaphragm as in system *2*, and (3) the same contacts, but with a grid diaphragm as in system *3*.

The curves represent the lower limit of the short-circuit currents which are broken in the given conditions. They were obtained by numerous and repeated experiments. The breaking current did not have an aperiodic component. In the conditions described, at least for internal diameters of the contacts up to 40 mm inclusive, the application of diaphragms somewhat increased the potentialities of the circuit-breaker. Its limiting breaking power when $d = 40$ mm was 4200 MVA with the application of contact system *1*, 4500 MVA with system *2* and 4700 with system *3*.

However unassuming this result may seem, it does show that the diaphragming of contacts, substantially raising the electrical strength of the contact gap (as has been indicated above), not only does not limit the breaking capacity but even increases it somewhat.

In the case where the diameter of the hollow contacts of the chamber in question is increased to 45 mm, its breaking power on application of system *2* was raised to 4900 MVA which could not be reached on application of system *1* due to failure to break the corresponding currents in the presence of a natural oscillation frequency of $f_0 = 3000$ c/s.

Diaphragming has a particularly favourable effect on raising the breaking capacity in the presence of relatively small breaking currents and smaller hollow contact diameters. For example, when $d = 30$ mm, changing from system *1* to system *3* makes it possible to raise the power of the circuit-breaker from 3000 to 3800 MVA, i.e. 25 per cent.

We also reach basically the same conclusions in the case of circuit-breakers of other voltage classes.

Diaphragm application made it possible to raise the breaking power of a 154 kV air-blast circuit-breakers from 4000 to 6000 MVA without actually altering the construction either of the quenching chamber or, in effect, of the contact system, and retaining the number of its elements (three) unchanged.

So that an opinion may be formed regarding the capacitive current (no-load line) breaking capacity of a quenching chamber having a diaphragm-equipped contact system, we present the results of tests of a 400 kV, 10,000 MVA air-blast circuit-breaker. Table 2 contains the basic findings from these experiments which concern us. The circuit-breaker had seven elements connected in series and the pressure of the air in its tanks was maintained at 20 atm. The internal diameter both of the moving and of the fixed contacts was 32 mm; the fixed contact was equipped with a diaphragm in the shape of a convergent cone, as has already been described, with an outlet diameter of 15 mm.

The information in Table 2 shows conclusively that the contact system is

capable of withstanding an extremely high voltage developing in the circuit-breaker on breaking no-load lines. This is perhaps its most important advantage in comparison with the usual system of two simple hollow contacts.

TABLE 2

Broken capacitive current, A	Voltage sustained by chamber 0.01 sec after the current is broken, kV	Multiple of overvoltage in relation to $U_p = \frac{420}{\sqrt{3}} = 243$ kV
470	432	1.78
550	475	1.96
620	456	1.88
570	755	3.11
560*	434*	1.78*
400	567	2.34
590	745	3.07
570	896	3.69
695	695	2.86
695	670	2.78
650	756	3.12
568	820	3.38

* In this experiment there was a repeat ignition.

Conclusions

1. The electrical strength of moving compressed air is lower than that of still air, other conditions being equal.

2. The formation in the compressed air stream of areas with substantially lowered pressure in comparison with mean gas-dynamic values is a cause of the reduction of its electrical strength.

3. The electrical strength of the compressed air in the contact gap of a quenching chamber depends essentially on the position of the point of measurement, varying both along its longitudinal axis and also in other directions.

4. This fact necessitates that a distinction be made between the local electrical strength of a gap at a given point and its overall (integral) electrical strength.

5. The integral electrical strength of contact gap, which is a deciding factor determining the working capacity of the quenching chamber, in the final analysis determines the value of its minimum local electrical strength to a considerable extent.

6. The characteristics of a contact gap should be improved not only by raising its integral electrical strength but also by raising its local electrical strength.

7. A contact system with one contact hollow and the other solid has

substantially higher values for electrical strength than a contact system with two hollow contacts, other conditions being equal.

8. The disadvantage of a contact system with two contacts hollow can to a certain degree be alleviated by diaphragming one hollow contact.

9. Diaphragm application, raising the electrical strength of a contact system with two hollow contacts, improves its capacity for breaking short-circuit currents and particularly for withstanding the high voltages applied to the circuit-breaker on breaking long distance no-load lines.

10. Study of the electrical strength of the contact gaps in quenching chambers of air-blast circuit-breakers shows that the different properties of compressed air are utilized in them to a very small degree. In this connexion unremitting and careful work is necessary to rectify this deficiency and increase the potentialities of modern air-blast circuit-breakers.

The author wishes to thank engineers Katkov and Kuligin of the Lenin high-voltage department of the VEI who have given him great assistance in this work.

Translated by F.J. Griffiths

THE OCCURRENCE OF SUB-HARMONIC RESONANCE IN UNBALANCED CONDITIONS*

M.G. PORTNOI

(Received 31 May, 1958)

In recent times several works [Ref. 1 – 4] have appeared describing experiments on sub-harmonic resonance in electrical systems. In these works its appearance was investigated on 400 kV lines with capacitative and inductive compensation, on which it was assumed that the magnetizing characteristic of the compensating reactors is approximated with sufficient accuracy by the equation:-

$$i = a\psi + \beta\psi^3. \qquad (1)$$

The sub-harmonic resonance is observed in a number of other cases, one of which is described in the present article.

When one phase of a 110 kV line 67 km long was disconnected the voltage transformers connected at each end of the disconnected phase were faulted. Investigations carried out jointly by VNIIE and 'Moldavenergokombinat'† showed that sub-harmonic resonance arose with the disconnexion of one phase of the line and the current in the voltage transformer grew to some 15 times greater in comparison with the normal magnetizing current, (Fig. 1a).

When this case was analysed it was ascertained that the magnetization curve of the voltage transformer is very far from the curve of the equation described in (1) above.

As a result the method did not permit the theme to be developed by the techniques described in [1 – 4] in the references.

It was desirable to substitute a method suitable for any given form of the magnetization curve. One of these methods was the use of a mathematical model,

* *Elektrichestvo*, 12, 18-22, 1958.

† V.M. Popov, G.T. Fomichev, N.B. Glagoleva, M.P. Savitskaia and the author took part in the investigations.

described in detail in many works, for example in the work by Korn, [5]. The investigation was undertaken with the help of this method.

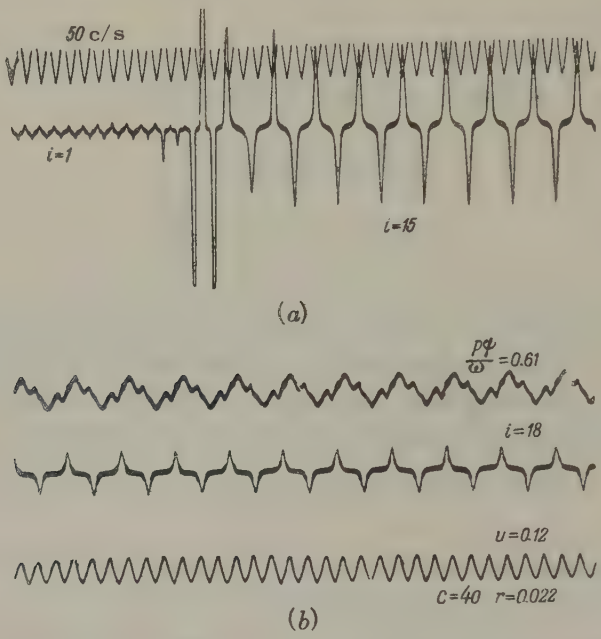

FIG. 1. Oscillograms of the sub-harmonic current in the voltage transformer on disconnexion of one phase of the line.
(*a*) Traced under actual conditions. (*b*) Traced on the mathematical model.

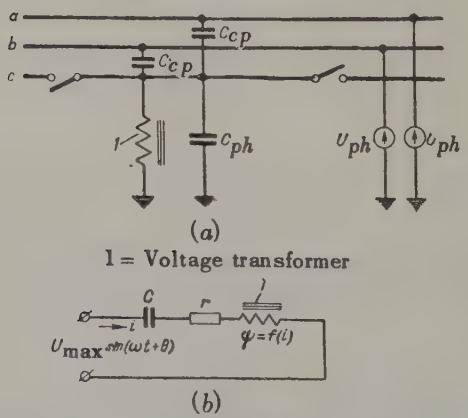

FIG. 2. Equivalent networks for a line. (*a*) With one phase disconnected. (*b*) Equivalent network.
($V_{max} = 2V_{ph} \times C_{ip}/C$; $C = 2C_{ip} + C_{ph}$).

To set up the differential equations let us examine the equivalent network for the line in unbalanced conditions.

Fig. 2a shows the equivalent circuit for the line after one phase has been disconnected. Let the two sources of e.m.f. in the diagram be replaced by one equivalent source, and the three capacitances be replaced by one equivalent capacitance, (Fig. 2b). Such a transformation is independent of frequency and so both circuits will give one and the same differential equation,

$$\frac{d\psi}{dt} + ir + \frac{1}{C}\int i\,dt = V_{\max}\sin(\omega t + \theta), \tag{2}$$

which is fundamental to the following analysis.

To set up the magnitudes entering into equation (2) on a structural model we will express them in relative units, taking the basic nominal parameters of the voltage transformer. $v_b = 98\,\text{kV}$; $i_b = 0.167\,\text{A}$; $\omega_b = 314$.

After differentiating equation (2) and solving it with regard to the higher derivatives and substituting the symbol p for d/dt we get:

$$p^2\psi = \omega\, V_{\max}\cos(\omega t + \theta) - \frac{\omega^2}{C}i - \omega r p i. \tag{3}$$

Let the non-linear relationship $i = f(\Psi)$ in Fig. 3 be assigned.

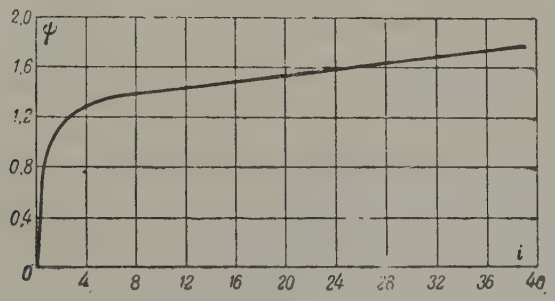

FIG. 3. Magnetizing curve of the voltage transformer.

A circuit fitting equation (3) was selected from among the elements of the mathematical model type I.P.T-5.* The model works with sufficient accuracy at frequencies not above 5 c/s, and so the input voltage had a frequency of 1 c/s and was derived from a special low frequency generator. The value of the initial interlinkage is set up at the input of the non-linear block *NB* as shown in Fig. 4.

* Y. Luginskii and Savitskaya took part in the work on the model.

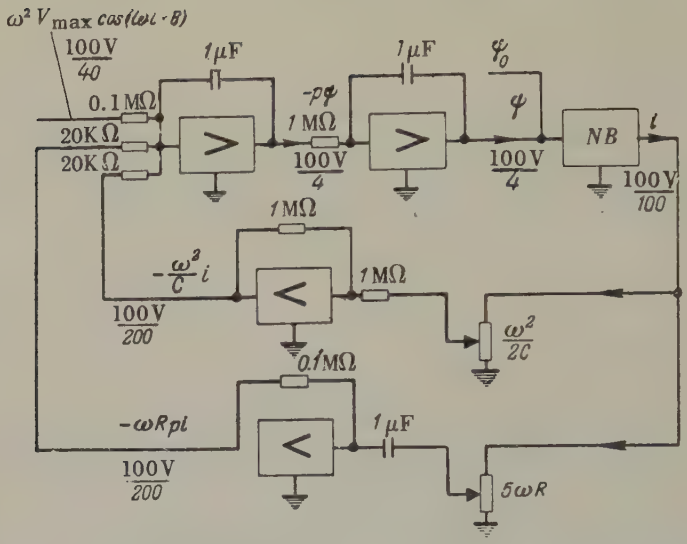

FIG. 4. Structural schematic of the mathematical model

Fig. 1 shows oscillograms of the sub-harmonic oscillations taken during tests on the power system and on a mathematical model with almost the same circuit parameters as the power system. Comparison of the oscillograms shows that the mathematical model that satisfies equation (3) gives results that coincide fairly well with the test.

The formation of sub-harmonic oscillations in the circuit in question (Fig. 2a) occurs as follows.

With the disconnexion of one of the phases, the voltage on the disconnected phase increases for a short time as a result of the cross distribution of voltage between the capacitances and the re-striking of an arc in the circuit-breaker. Subsequently, the arc in the circuit-breaker is quenched and the damped free-oscillation current appears in the circuit, the form of which is slightly distorted by the additional voltage of the circuit.

As a result of the non-linearity of the inductance, the frequency of free oscillation is reduced as the amplitude is reduced. This reduction of frequency with attenuation is clearly shown on the oscillogram reproduced in Fig. 5.

After this, the frequency of free oscillation remains at a fraction of the frequency of the additional voltage, the damping of the free oscillations may cease, so that they will be maintained by energy derived from the source of supply. In this way the free oscillations are transformed into sub-harmonic oscillations.

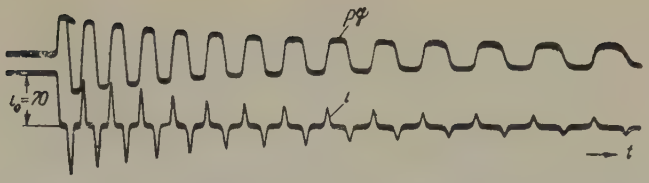

FIG. 5. Oscillogram of the open circuit damping current when:-
$C = 40$: $r = 0.0064$: $i_0 = 70$.

Let us consider the relationship between the magnitude of the sub-harmonic currents and the circuit parameters.

In the case under consideration the shape of the curve of the sub-harmonics differs insignificantly from the form of the curve of the free oscillating current. These circumstances determined by the order of the magnitudes of the circuit (a small value of applied voltage and a relatively large resistance) enables one to employ an approximate method to determine the amplitude of the sub-harmonic current.

The effect of the resistance on the magnitude of the current may be ignored, which is quite acceptable.

In the process of damping the free oscillations (Fig. 5) the frequency of the real oscillations of the system is varied from the maximum value ω_{max} of the assumed magnitude of the original current i_0 to the minimum value $\omega_{min} = \frac{1}{\sqrt{L_{Lin}\, C}}$, in which is assumed the inductance of the transformer appropriate to the linear portion of its magnetization curve. The relationship of the real frequency of the system to the amplitude of the current may be written in the following form

$$\omega = \frac{1}{\sqrt{L_{Ass}(i_m)\, C}}, \tag{4}$$

where $L_{Ass}(i_m)$ = the inductance determining the frequency of free oscillations.

On the other hand one may get the frequency of free oscillation in a system without damping [7] as a result of the solution of the differential equation:-

$$\frac{d\psi}{dt} + \frac{1}{C}\int i\, dt = 0. \tag{5}$$

After differentiation, eliminating t and integrating we get:

$$\frac{\dot{\psi}^2}{2}+\frac{1}{C}\int_0^{\psi_m} i\,d\psi=0, \tag{6}$$

Whence:-

$$\dot{\psi}=\frac{d\psi}{dt}=\sqrt{-\frac{2}{C}\int_0^{\psi_m} i\,d\psi}$$

and

$$T=\frac{2\pi}{\omega}=2\pi\sqrt{L_{Ass}C}=4\sqrt{C}\int_{\psi_m}^{0}\frac{d\psi}{\sqrt{-2\int_{\psi_m}^{\psi} i\,d\psi}}. \tag{7}$$

Furthermore, as a result of combining (4) and (7) we get:-

$$L_{Ass}=\frac{4}{\pi^2}\left[\int_{\psi_m}^{0}\frac{d\psi}{\sqrt{-2\int_{\psi_m}^{\psi} i\,d\psi}}\right]^2. \tag{8}$$

Using equation (8) and the magnetization curve it is possible to construct the curve $L_{Ass}=f(i_m)$ (see Appendix).

Equally possibly, this curve may be more easily plotted from experimental data with oscillograms of the damped free oscillations.

Using the relationship $L_{Ass}=f(i_m)$ (Fig. 6) one may determine the sub-harmonic oscillatory current for any given value of capacitance. For this, at the given sub-harmonic frequency $\omega=1/3$ and capacitance C the inductance is determined $L_{Ass}=9/C$ and from the curve $L_{Ass}=f(i_m)$, i_m is determined.

Fig. 7 shows the dependence of the amplitude of the sub-harmonic current on the capacitance (or length of line) obtained by the given method (curve 1) and with the help of the mathematical model (crosses) according to the circuit shown in Fig. 4. The two curves practically coincide.

From Curve 1, it is evident that the longer the line, the greater the amplitude of the sub-harmonic current. The inductance of the voltage transformer, taken from the linear portion of the magnetization curve determines the minimum length of line with which it is possible for sub-harmonics to arise.

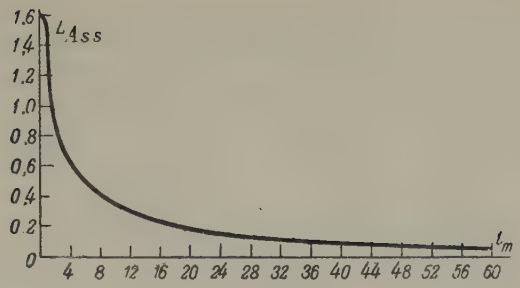

FIG. 6. Relationship of the inductance L_{Ass} to the amplitude of the current of free oscillations.

The curve $i_m = f(C)$ determined from the mathematical model (crosses) is chosen for two supply voltages: $U_m = 0.05$ and $U_m = 0.15$, but in the latter case resonance will only occur when $C > 10$, and if $C < 10$, resonance will occur at the fundamental frequency (curve 2).

With the aid of the mathematical model, the limiting values of the resistance were determined for the two values of voltage at which sub-harmonic resonance may exist, (Curves 3 and 4). The analogous relationship for resonance at the fundamental frequency is shown in curve 5.

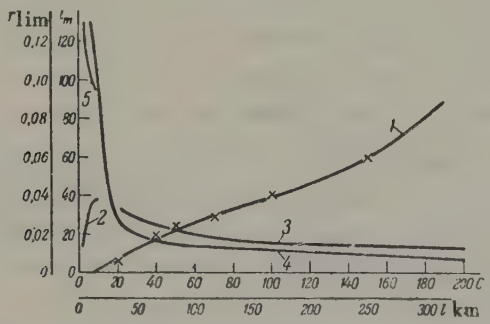

FIG. 7. Relationship of the amplitude of the sub-harmonic oscillation current and the limiting resistance to the length of line. 1. Relationship $i_m = f(l)$ for voltages 0.05 and 0.15. 2. The same with resonance at the fundamental frequency and a voltage of 0.15. 3. The relationship $r_{lim} = f(l)$ for a voltage 0.15. 4. The same for a voltage 0.05. 5. The same for resonance at the fundamental frequency.

Fig. 8 shows the relationship of the limiting value of the resistance to the supply voltage for one value of capacitance.

The resistance of a NKF-110 voltage transformer is about 6000 Ω. The equivalent voltage in the equivalent circuit for a 110 kV line is about

0.15 V*. Thus, the appearance of dangerous resonances on 110 kV lines may be observed in those cases where the line is less than 100 km long and has two voltage transformers connected to it (one at each end) or when the line is less than 50 km long and has one voltage transformer connected to it.

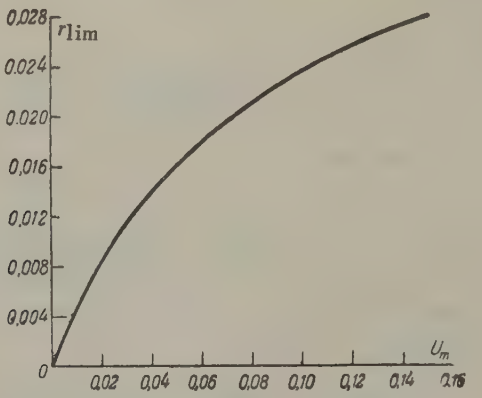

FIG. 8. Relationship between the limiting active resistance and the supply voltage when capacitance $C = 28$.

To obviate the appearance of sub-harmonic resonance on 110 kV lines when unbalanced conditions occur it is sufficient to connect a resistance of 4 Ω, calculated for a prolonged flow of current of 0.2 A to the high-voltage side of the voltage transformer. The connexion of such a resistance does not in practice lead to error in the operation of the voltage transformer.

It only remains to observe that these methods are only necessary in cases of single phase automatic reclosure with automatic transfer to unbalanced conditions. If there is no automatic transfer to unbalanced conditions it is sufficient to disconnect the voltage transformers before a phase is disconnected and to reconnect them again afterwards if they are necessary.

Appendix

Determination of the relationship between the inductance of the voltage transformer and the amplitude of the open-circuit current. Determine the inductance from equation (8). For this, divide the magnetization curve of the transformer into sections, for each of which take a linear relationship $\psi = f(i)$: for $0 < \psi < \psi_1$ and $0 < i < i_1$ $\psi = \gamma_1 i$,

* The values of phase and interphase capacitances were taken from the work by Mel'nikov, [6].

$$i = \frac{\psi}{\gamma_1};\ \text{for}\ \psi_1 < \psi < \psi_2\ \text{и}\ i_1 < i < i_2\ \ \psi = \gamma_2 i + \psi_{10},\ i =$$

$$= \frac{\psi - \psi_{10}}{\gamma_2};\ \text{for}\ \psi_2 < \psi < \psi_3\ \text{и}\ i_2 < i < i_3\ \psi = \gamma_3 i + \psi_{20},\ i =$$

$$= \frac{\psi - \psi_{20}}{\gamma_3}\ \text{and so on}$$

Determine the relationship $L_{Ass} = f(i_m)$ for $i_2 < i_m < i_3$.

The integral which enters the right-hand side of equation (7) may be calculated by means of step changes from one limit right through to the other. As as result:-

$$\sqrt{L_{Ass}} = \frac{2}{\pi}\left[\int_{\psi_m}^{\psi_2} \frac{d\psi}{\sqrt{-2\int_{\psi_m}^{\psi}\frac{\psi-\psi_{20}}{\gamma_3}\,d\psi}} + \right.$$

$$+\int_{\psi_2}^{\psi_1} \frac{d\psi}{\sqrt{-2\left(\int_{\psi_m}^{\psi_2}\frac{\psi-\psi_{20}}{\gamma_3}\,d\psi + \int_{\psi_2}^{\psi}\frac{\psi-\psi_{10}}{\gamma_2}\,d\psi\right)}} +$$

$$\left. +\int_{\psi_1}^{0} \frac{d\psi}{\sqrt{-2\left(\int_{\psi_m}^{\psi_2}\frac{\psi-\psi_{20}}{\gamma_3}\,d\psi + \int_{\psi_2}^{\psi_1}\frac{\psi-\psi_{10}}{\gamma_2}\,d\psi + \int_{\psi_1}^{\psi}\frac{\psi}{\gamma}\,d\psi\right)}}\right] =$$

$$= \frac{2}{\pi}\left[\sqrt{\gamma_3}\left(\sin^{-1}\frac{\psi_2 - 2\psi_{20}}{\psi_m - 2\psi_{20}} - \frac{\pi}{2}\right) + \right.$$

$$\left. +\sqrt{\gamma_2}\left(\sin^{-1}\frac{\psi_1 - 2\psi_{20}}{a_1} - \sin^{-1}\frac{\psi_2 - 2\psi_{10}}{a_1}\right) - \sqrt{\gamma_1}\sin^{-1}\frac{\psi_1}{a_2}\right]$$

Where:-

$$a_1 = \frac{\gamma_2}{\gamma_3}[(\psi_m - 2\psi_{20})^2 - (\psi_2 - 2\psi_{20})^2] + (\psi_2 - 2\psi_{10})^2;$$

$$a_2 = \frac{\gamma_1}{\gamma_2}[(\psi_m - 2\psi_{20})^2 - (\psi_2 - 2\psi_{20})^2] +$$

$$+ \frac{\gamma_2}{\gamma_3}[(\psi_2 - 2\psi_{10})^2 (\psi_1 - 2\psi_{10})^2] + \psi_1^2.$$

Using equation (C) and the magnetization curve one may plot the relationship

$L_{Ass} = f(i_m)$.

Translated by R.P. Froom

REFERENCES

1. S.S. Shur; *Delenie chastoty v prosteishei tsepi so stal'yu, (The division of frequency in very simple circuits with iron). Elektrichestvo,* 11 (1954).
2. L.F. Dmokhovskaya and V.I. Levitov; *Subgarmonicheskie kolebaniya v prosteishikh shkemakh i dal'nikh elektroperedachakh (Sub-harmonic oscillations in very simple circuits and in long distance transmission lines). Elektrichestvo*; 11, (1955).
3. M.S. Liebkind; *Subgarmonicheskie kolebaniya v prostoi posledovatel'noi tsepi. (Sub-harmonic oscillations in a simple sequence circuit). Izv. Akad. Nauk. SSSR,* 9 (1953).
4. A.I. Dolginov; *Rezonans v elektricheskikh tsepyakh i sistemakh. (Resonance in electrical circuits and systems).* Gosenergoizdat (1957).
5. G. and T. Korn; *Elektronnye modeliruyushchie ustroistva. (Electronic modelling devices).* Foreign Literature Publishing House), Izd. Irvostran. Literature (1955).
6. N.A. Mel'nikov; *Raschety rezhimov raboty setei elektricheskikh sistem. (Calculations of the operating conditions of networks in electrical systems).* Gosenergoizdat (1950).
7. R. Rudenberg; *Perekhodnye protsessy v elektroenergicheskikh sistemakh. (Transient processes in electrical power systems).* Izd. Inostran Literature, (Foreign Literature Publishing House), (1955).

EXPERIMENTAL INVESTIGATION OF DEFORMATIONS AND VIBRATIONS OF THE STATOR WINDINGS*

M.F. IUDOV

(Received 3 January 1958)

Introduction

The determination of electrodynamic stresses in the windings of electrical machines by an analytical method is a difficult and painstaking problem, since it is necessary in calculations to take into account the influence of the curvature of conductors of the frontal parts, of the adjacent steel parts of the stator and also of the current in the rotor winding. For a rough estimate of the electro-dynamic stresses we can use simplified formulae, [1 and 2]. However, even if we know these stresses it is practically impossible to determine with sufficient accuracy the deformations of the stator winding produced by them. This is due to the fact that, owing to the lack of sufficient knowledge of mechanical properties of the insulation, we cannot determine the value of its reaction nor the reactions of the elements holding the stator winding. Therefore, along with further studies of the mechanical stresses in the stator windings more attention is being paid in recent time to their experimental investigation, [3]. In the present article some results of the experimental investigation of deformations and vibrations of the stator windings of hydro-electric generators and high-voltage electrical motors are given; these investigations were carried out by the author in the VNIIE MES.

Methods of experimental investigations

The VNIIE has recently carried out research work to design the necessary apparatus and to establish methods of investigation of the results of the action of electrodynamic stresses on windings of generators and synchronous motors. In the first stage, the deformation of the surface layers of the insulation and displacement (vibration) of the frontal parts of the winding were measured with respect to the clamping flange of the active steel and the stator body. In the first place the bars, situated on the boundary of the phase zone (extreme bars in each phase) were

* *Elektrichestvo*, No. 12, 39-43, 1958.

examined, since the largest electrodynamic forces act on them, [1-3].

Deformations and vibrations were measured by the wire strain gauges and tensometric amplifying devices of two types: IDD-3 [4], developed by the ORGRES, and UD-3 [5], developed by the Laboratory for the investigation of stresses of the Machine Research Institute of the Academy of Sciences, U.S.S.R. To measure the winding vibrations of the electrical motor type MS-395-AV 8/28 a high-speed cine-camera was used.

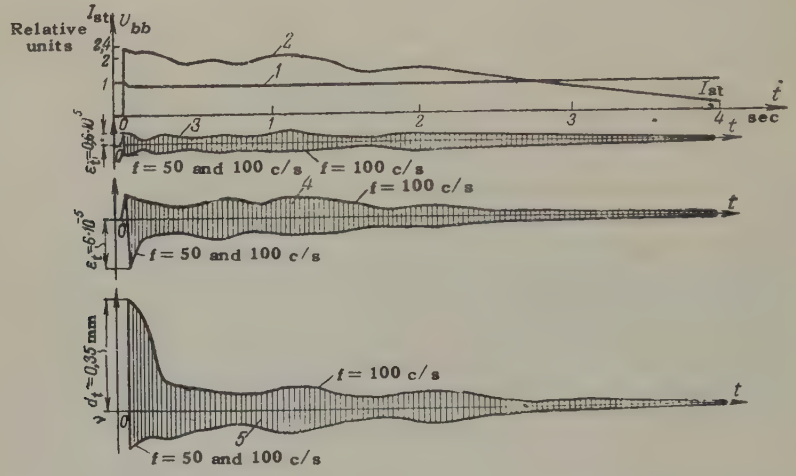

FIG. 1. Switching-in to the grid of a generator type SV (1160/180) – 72 by the method of self-synchronization

1 – busbar voltage 154 kV; 2 – stator current; 3 – relative extension of insulation of the frontal part of the stator winding at the slot outlet; 4 – the same as curve 3 but in the middle of the straight portion of the frontal connexion; 5 – mutual displacements of the head of the frontal connexion and the clamping plate of the active steel in a tangential direction, (on the stator circumference).

In the references certain data are given concerning permissible and breaking deformations of normal mica isolations and of the varnish films used for its manufacture, for loads of constant sign [6]. But, unfortunately, the necessary data on the permissible variable sign deformations of the compound insulation of the stator windings are absent. Therefore, in evaluating the experimental results, a comparison was made of deformations and vibrations of the stator windings, which were recorded under various operational conditions of generators. As permissible values of deformations such magnitudes were taken as occur under conditions to which the machine could be subjected (for instance, a sudden short-circuit on the machine terminals), or under conditions which frequently occur in machine operation and do not cause damage to the machine. In particular, the deformations and vibrations of the generator windings were compared with the deformations and

vibrations of the windings of the high-voltage electrical motors which are frequently restarted.

Results of the investigations of the generators

On the basis of an analysis of oscillograms of the operation of generators with increased values of the stator current, we can conclude that deformations and vibrations usually vary with a frequency of 100 c/s, but, due to the influence of the aperiodic component of the current, components of deformations and vibrations are observed which vary with a frequency of 50 c/s (Figs. 1 and 2).

The deformations and vibrations which arise are approximately proportional to the square of the stator current.

The increased amplitudes of the heads of the frontal parts as well as the deformation of the insulation which occurs under transient conditions, are of a short duration, and, after the decrease of current in the stator winding, they decrease sharply. No permanent deformations of the insulation and displacements of the frontal parts of the stator were recorded.

From an analysis of oscillograms obtained we can draw the conclusion that practically no substantial retardation in the value of the amplitudes of deformations and vibrations of the frontal parts of windings, due to the stator current, was recorded; and this applies to the first current half-period after the connexion of the generator to the grid and also to the whole period, when the increased current is flowing.

This indicates that the frequency of the free oscillations of the frontal parts of the windings is higher than the frequency of variations of the disturbing electrodynamic forces. Therefore, in calculating the results of the action of the electrodynamic forces on the windings, the shock value of the stator current should be taken, and we cannot neglect the supertransient component.

All the generators and motors tested had double-layer chain stator windings with continuous compound insulation. The working conditions of the generators, on which the winding deformations were measured, are given in Table 1 and their rated data in Table 2.

The results of tests of the hydro-electric generators types SV (1160/180) – 72 and AT-I-W-72 are discussed below. These generators were most thoroughly tested. Thus, to measure deformations 50 strain gauges were attached on frontal parts of each of these generators.

As can be seen from Table 1, the maximum insulation deformation was recorded during asynchronous running with excitation and was equal to 2.1×10^{-4} of relative units (the relative extension of insulation is given), when the amplitude

TABLE I

Multiples of the stator currents, amplitudes of maximum vibrations and of relative extensions of the frontal parts of the stator winding

Operating conditions	Stator current I/I rat.		Amplitude of vibrations, μ		Amplitude of relative extension $\times 10^{-5}$					
	Type of generator				Generator type AT-1-W-72			Generator type SV $\frac{1160}{180}$-72		
	AT-1-W-72	SV $\frac{1160}{180}$-72	AT-1-W-72	SV $\frac{1160}{180}$-72	Point 1 L		Point 11 L	Point 37 L		Point 41 L
					Calculated	Experimental	Experimental	Calculated	Experimental	Experimental
Normal starting	0	0	0	70	0	0	0	0	0	0
Parallel operation.	0.95	1.1	5	15	—	0	0	—	0	0
Exact synchronization.	0.36 (δ=7°)	0.9 (δ=21°)	80	200	—	0.6	—	—	—	0.5
Self-synchronization.	2.1	2.5	80	350	4 4	0.6	0.7	10.8	10	3.5
Dropping of the normal load	0.95	1.1	60	290	—	0,15	—	—	0	0
Asynchronous running with excitation.	—	4.4	—	460	—	—	—	34	21	3 3
Sudden three-phase short-circuit.	2.6	2.8	50	440	5	—	0.8	13.6	7	—
Sudden two-phase short-circuit with an earthed neutral.	1.8	2.4	170	300	3.2	—	1.5	10	6.1	—
Sudden two-phase short-circuit with a non-earthed neutral.	2.1	2	125	360	4.4	—	2.1	7	7.2	—

N.B: All short-circuits occurred behind the step-up transformer.

of the stator current beats was equal to 4.4 times its rated value. This deformation varied with a frequency of 100 c/s.

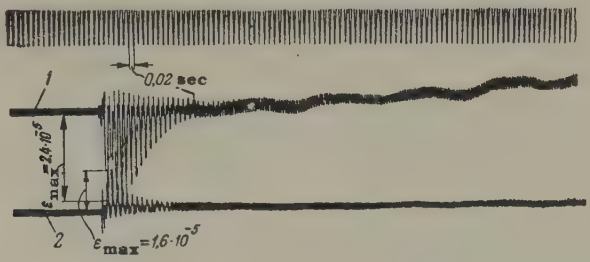

FIG. 2. Deformation of the insulation of the frontal part of the bar of a generator type SV (1030/120)—68 when switching-in to the grid by the method of self-synchronization.
1— in the middle of the frontal part; 2— on the straight portion near the bend.

Approximately equal deformations occurred in the presence of a short-circuit behind the step-up transformer for the rated value of the open-circuit current and the switching-in of the generator to the grid by the method of self-synchronization; this result is quite understandable, since the maximum current values are approximately equal under these conditions. Deformation of the insulation of the frontal parts was practically absent during normal starting, parallel operation with the grid, switching-in of the generator to the grid by the method of accurate synchronization and during a sudden decrease of the load.

If we compare the insulation deformations along the frontal part under the same conditions and with the same stator current, we find that the maximum deformation was recorded on the straight portion of the frontal connexion and at the part which projects from the slot. The relative extensions of the insulation of the frontal part of the bar, located on the slot top is greater than the relative extension of the insulation of the bar in the frontal part, situated at the slot bottom, a result which can be explained by the more rigid fastening of the lower layer of the winding.

The maximum amplitude of vibrations of the frontal part head was: during asynchronous running with excitation - 460 μ, for a sudden three-phase short-circuit behind the step-up transformer — 440 μ; for switching-in to the grid by the method of self-synchronization — 350 μ; for an exact synchronization — 200 μ; for the 100 per cent load drop — 290 μ; on starting — 70 μ and for the parallel operation with the grid — 15 μ.

Table 3 shows the results of the analysis of deformations and vibrations of the frontal parts for all cases of switching-in of a generator type SV (1160/180)— 72

Maximum electrodynamic forces, bending moments, stresses in copper and vibrations of heads of the frontal parts of the stator windings, of generators

Type and rated values	Operating conditions	$X''_{st.g} + X_t$ (relative units)*	I/I rat		Number of slots per pole and phase	Length of the frontal, parts, mm	Current on the side of the coil in or the bar for the rated load A	Total modulus of cross sections of individual wires of a coil or a bar, cm^3	Electrodynamic force kg/cm	Max. bending moment, kg/cm	Stress in copper of the frontal part of the section kg/cm²		Displacement /vibration/ of heads of frontal parts with respect to the clamping plate of active steel, μ
			Calculated	Experimental				Calculated	Calculated	Calculated	Calculated	Experimental	Experimental
SV 1160/180-72, 90.000 kVA, 3765 A, 13,8 kV, 83.3 rev/min, factory "Elektrosila". Bar winding	Short-circuit beyond the step-up transformer		2.57	2.8	$2\frac{1}{4}$	420	$1\times1887,5$	1.02	1	60	60	60	440
	Switching-in to the grid by method of self-synchronization	0.24+0.15		2.5					1	60	60	85	350
	Short-circuit on the generator terminals	0.24	4.15	—					2.8	170	165	—	—
AT-1-W-72, 90.000 kVA, 3765 A, 13.8 kV, 83.3 rev/min. Firm GEC coil winding	Short-circuit beyond the step-up transformer	0.23+0.13	2.78	2 6	$2\frac{3}{4}$	420	$\frac{4\times3\,765}{9}$	0.48	1.3	17	35	7	50
	Switching-in to the grid by method of self-synchronization	0.23+0.13		2.1					1.3	17	35	6	60
	Short-circuit on the generator terminals	0.23	4.35	—					3.3	41	86	—	—
SV (1250/170)-96; 68, 750 kVA, 2280 A, 13.8 kV, 62.5 rev/min factory "Elektrosila" coil winding.	Short-circuit beyond the step-up transformer	0.28+0.14	2 36	—	$2\frac{7}{16}$	317	3×380	0.42	0.4	5	12	—	—
	Short-circuit on the generator terminals.	0.28	3 53	—					0.93	12	26.3	—	—
SV (1030/120)-68, 50.000 kVA, 2750 A, 10 kV, 88.2 rev/min factory "Elektrosila". Bar winding.	Short-circuit beyond the step-up transformer	0.24+0.04	3.58	—	$2\frac{10}{17}$	380	$1\times1\,375$	0.3	1.8	23	78	—	—
	Switching-in to the grid by method of self-synchronization		3.58	2 5					1.8	23	78	24	—
	Short-circuit on the generator terminals	0 24	4.2	—					3	37	124	—	—
VGS (325/135)-14, 18, 750 kVA, 1030 A, 10.5 kV 428 rev/min KHETZ, coil winding.	Switching-in to the grid by method of self-synchronization.	0.21+0.07	3.3	3.4	4	370	$\frac{1\,030}{7}$	0.34	1.6	12	35	38	300

N.B: X'' st.g. — supertransient reactance of the generator;
X_t — inductance of the step-up transformer.

to the grid by the method of self-synchronization. As can be seen from Table 3 the probability of the maximum deformation and vibration of the frontal part is insignificant. This scattering of the values of deformations and vibrations is explained by the influence of the aperiodic component of the stator current.

TABLE 3

Maximum values of vibrations and deformations of the frontal parts of the stator winding when switching-in to the grid a generator type SV (1160/180)–72 by the method of self-synchronization.

Stator current, A		Amplitude of vibrations of the frontal part head, μ	Deformation of insulation of the frontal part; relative units $\times 10^{-5}$	
$i_{s.m.}$	I''		Point 41 L	Point 37 L
—	—	180	—	—
16 800	8 900	180	0.7	—
12 800	9 000	120	—	3.3
10 800	8 600	170	—	2.9
11 400	9 500	350	3.5	—
13 100	9 000	260	0.6	—
9 000	8 300	280	0.6	—
9 000	8 000	220	0.8	—
14 100	8 600	230	1.1	—
12 800	8 800	200	0.4	2.6
10 800	8 600	210	0.9	6
—	—	200	1.5	10
9 600	8 500	100	1.5	2.1
9 000	6 900	90	1	2.1
12 800	8 300	130	0.7	2.1
16 000	8 300	100	1.6	3.6
12 800	8 600	80	1.5	4.1
—	—	140	—	2.9
		4.7*	3.7*	4.7*

* Ratio of the maximum value to the rated value.

From Table 1 it can be seen that deformations and vibrations of the frontal part of the generator type SV (1160/180)–72 are greater than those of the generator type AT-I-W--72. It can be explained by a better mounting and assembling of the stator active steel and a better quality of binding of the winding frontal parts in the generator type AT-I-W--72.

Tables 1 and 2 show the calculated values of the maximum relative extensions of the copper of the winding frontal parts, which are caused by electrodynamic forces, acting in the plane of minimum rigidity. As can be seen from these tables, the values calculated give deformations of the same order of magnitude or slightly greater than the experimental values.

It has already been said that deformations were measured in the insulation

surface of the frontal part. Laboratory investigations have shown that, for bending of the winding bar in the plane of minimum rigidity, deformations on the surface of the individual wires are smaller than the deformations of the insulation; moreover, the nearer to the surface the greater is the insulation deformation.

Let us assume that the maximum deformation on the copper surface is equal to the maximum insulation deformation; in this case, as can be seen from Table 2, the maximum stress in the copper, corresponding to the maximum insulation deformation, recorded when the generator type SV (1160/180) – 72 was switched in to the grid by the method of self-synchronization, should not exceed 85 kg/cm². But, in calculating the influence in the windings of electrodynamic forces, factories accept stresses in copper of 600 - 800 kg/cm² as permissible values. Preliminary investigations of the mechanical and electrical properties of the new continuous compound insulation for the bars of the stator winding, which was tested under a voltage of 6 kV, gave the following results.

After 1.2×10^6 vibration cycles with a frequency 100 c/s and with a double vibration amplitude of the middle of the bar of 2.5 - 3 mm; during which deformations, of a double amplitude from 4×10^{-4} to 5×10^{-5} relative units were recorded on the insulation surface, no lowering of the insulation puncture voltage was recorded. The bars were 900 mm long, and a bending moment of constant magnitude acted on their middle portion which was 340 mm long.

Tests of electrical motors

On starting electrical motors, the character of the deformations and vibrations of the frontal parts of the stator winding was the same as that which occurs in generators switched in to the grid by the method of self-synchronization, only the duration of these deformations is considerably shorter, (Fig. 3). Deformations of windings were investigated on eight high-voltage synchronous motors in which the construction and mounting of the frontal parts are the same as in the hydrogenerators tested.

The maximum deformation of the insulation of the frontal part, equal to 3×10^{-4} was registered on starting an electrical motor made by Metro-Vickers, of 2600 kVA, 6.6 kV, 228 A, 1000 rev/min. Vibrations of the frontal part head (at the projecting part 340 mm long) were 450 μ. With an electrical motor type MS - 395 - AV - 8/28, 3500 kVA, 6.6 kV, 306 A, 214 rev/min, the maximum insulation deformation was 1.3×10^{-4} and the vibrations of the frontal part head (at the projecting part 310 mm long) were 0.24 μ.

The tensometric method and high speed cine-photography gave the same values of the vibrations.

All electrical motors which were tested had been in service for a long time,

many of them having been restarted two or three times a day. Nothing abnormal during starting, operation or overhaul of these motors was recorded.

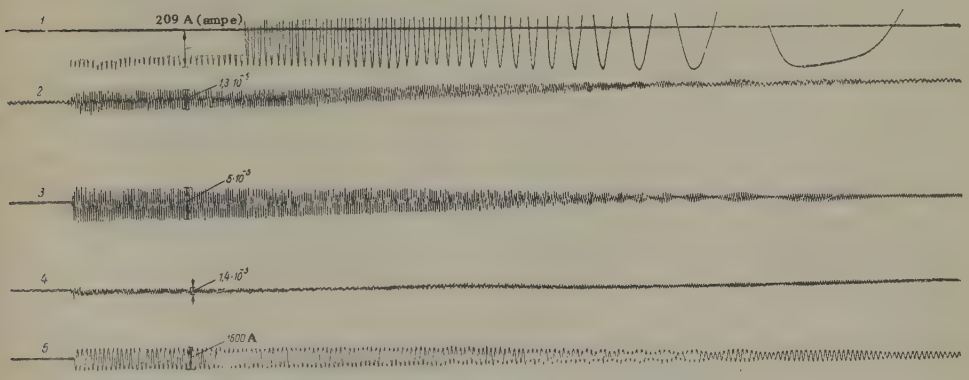

FIG. 3. Starting of an electrical motor type MS-395-AV-8/28 directly from the grid
1 — rotor current; 2—4 deformations (relative extensions) of the insulation of the frontal part on the wide side of the coil; 5 — stator current.

Conclusion

1. Investigations show the usefulness of supplementing a mathematical analysis by experimental data, which allows us to collect more complete and concrete information about the character and magnitude of deformations of windings of the generators in various operating conditions.

2. For investigation of these deformations and vibrations tensometric apparatus can be used. Besides strain gauges it is advisable to use high-speed cine-cameras. Further improvement of methods and apparatus for the research in question is needed.

3. Deformations of insulation and vibrations of the frontal parts of the stator windings, which are recorded in various operating conditions of hydro-electric generators, are insignificant: they are smaller than or of the same order as those which occur during the starting of synchronous motors directly from the grid.

4. Taking into account the individual properties of the mechanical properties of the insulation it is advisable to continue work in collecting experimental data on deformations of the hydro-electric generators windings and to extend analogous research on turbo-generators.

5. It is necessary to carry out special investigations on the mechanical properties of insulation and of bars, and to establish criteria specifying the permissible deformations of windings.

Appendix

Table 2 gives the values of the maximum electrodynamic forces calculated for 1 cm of length; of bending moments and stresses in the copper of the frontal parts of the stator winding for the three-phase short-circuits on the terminals behind the step-up transformer of hydro-electric generators; it also gives the experimental values of the maximum vibrations of the frontal part heads and the maximum stresses in the copper calculated from the insulation deformations.

In calculating the electrodynamic forces only the influence of currents in the conductors of the phase in question and of those of the adjacent phases was considered; the influence of currents in conductors located in another layer of the winding was ignored.

To determine the stresses, the frontal part was considered as a beam freely supported at its two ends, and loaded with a uniformly distributed load equal to the electrodynamic force. The span of the beam was taken as equal to the distance between two adjacent distance spacers. In the generator type SV (1160/180)-72 on the bars, where deformations were measured, the distance spacers between the two adjacent frontal parts were of insufficient thickness, and in certain places were absent. In this case, in calculating the maximum stresses in the copper, the span of the beam was taken as equal to the maximum distance between the two adjacent spacers which closely adjoined the adjacent frontal parts.

The voltage before the short-circuit was taken as equal to the rated voltage. The reactance of transformers was taken as equal to that in existing installations and is given in relative units, reduced to the rated power of the generator.

Translated by S. Szymanski

REFERENCES

1. M.P. Kostenko; *Elektricheskiye mashiny (spetsialnaia chast). (Electrical machines, special section).* Gosenergoizdat (1940).
2. E. Weber; *Veroffentlichen aus dem Siemens-Konzern,* Vol. VIII, part 3, 166 (1930).
3. J.B. Young and D.H. Tompsett; *Proc. I.E.E.* vol. 102, part A, 101-120, No. 2 (1955). Further discussion on the article, vol. 102, part A, No. 6, 856-859, 1956 and vol. 103, 449-452, No. 10 (1956).
4. *Eksperimentalnoe izuchenie mekhanicheskikh usilii v gidrogeneratorakh.* Sbornik trudov kursov-sovyeshchaniia pod redaksiyei Iu. M. Elkinda. *(Experimental investigation of mechanical stresses in hydro-generators.* Symposium of works of courses and conference under the editorship of Iu. M. Elkind). Gosenergoizdat (1957).
5. *Izmerenie napriazhenii v detaliakh mashin.* Sbornik rabot pod redaksiyei N.I. Prigorovskogo. *(Measurements of stresses in machine elements,* symposium of works under the editorship of N.I. Prigorowskii). Mashgiz G N T I Moscow Leningrad (1955).

6. Iu. I. Skanavi; *Sviaz' mezhdu mekhanicheskimi svoistvanu' statornoi obmotki nepreryvnoi izoliatsii turbo-igidrogeneratarov i ee probivnym napriazheniem.* Sbornik "Elektricheskaia Izoliatsiia". *(Relationship between mechanical properties of the continuous insulation of the stator windings of turbo and hydro-electric generators and its puncture voltage).* Symposium "Electric Insulation", part II, NKM, U.S.S.R (1938).

7. I.A. Syromiatnikov; *Rezhimy raboty sinkhronnykh generatov. (Operational conditions of synchronous generators.)* Gosenergoizdat (1952).

8. L.G. Mamikoniants; *Toki i momenty vrashcheniia, voznikaiushchie v sinkhronnoi mashine pri vkliuchenii ee sposobom samosinkhronizatsii. (Currents and driving torques occurring in a synchronous machine, when switched on by the method of self-synchronization).* Trud. Ts N I E L M E S, part IV, Gosenergoizdat (1956).

9. I. Biermans; *A.f.E.*, vol. IX, issue 7, 326-334 (1920).

10. N.A. Kozyrev; *Kontrol' sostoianiia izolatsii elektricheskikh mashin po ee mekhanicheskim kharakteristikam. (Control of the state of the insulation of electric machines on the basis of its mechanical characteristics).* Electric stations, No. 2 (1957).

11. A. Ia Berger; *Turbogeneratory peremennogo toka. (A.C. turbo-generators),* part I, United Scientific and Technical Press (1935).

CALCULATION OF LOSSES IN THE SLIDING CONTACT OF ELECTRIC MACHINERY*

P.S. LIVSHITS

(Received 21 April 1958)

The formulation of a proven method of calculating losses in the sliding contact of electrical machines is an extremely important problem in modern electrical machine design. The different aspects of this problem have been studied in a considerable amount of research. However, because of insufficient knowledge of the properties of electrical brush materials none of the work carried out has been able to produce a conclusive result. Every calculation has been completed by recommendations propounding the use of approximate data, the basis of which has not usually been quoted. Such is the exposition of the question of losses in an electrical sliding contact given in the technical literature at present available, [1-3].

The methodical study of the properties of electrical brush materials [4-6], has enabled us to establish that the numerical values of the technical characteristics of these materials can be distributed according to the standard rule (or not far short of it), that each characteristic of each type of material has its own nominal (the most probable) value and that their volt-ampere and frictional characteristics can be described by means of the following formulae:

$$2\Delta U = A + Bj; \qquad (1)$$

$$\mu = C - Dv, \qquad (2)$$

where $2\Delta U$ – Intermediate drop in voltage in a pair of electrical brushes of different polarity V;

A – a free term in the equation of the volt-ampere characteristic†,

* *Elektrichestvo* No. 7, 55-58, 1958.

† Detailed information on the magnitudes of A, B, C and D can be found in [6]. Their numerical values for a number of types of electrical brush material also appear in the appendix to this article.

B – angular coefficient of the equation of the volt-ampere characteristic;

J – current density (apparent) in an electrical brush, A/cm²

μ – coefficient of friction of electrical brushes on the sliding surface of a (ring) commutator;

C – a free term in the equation of the frictional characteristic;

D – angular coefficient of the equation of the frictional characteristic;

v – peripheral speed of the sliding surface of the (ring) commutator, m/sec.

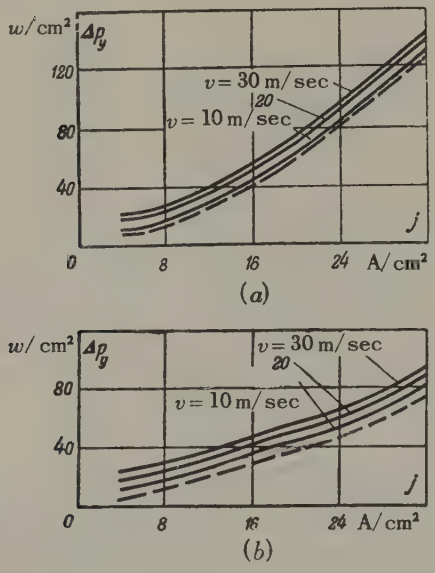

FIG. 1. Curves of dependence of specific losses in the sliding contact of electrical machines on current density. a – EG-4 type of electrical brush material; b – the same for the MGS-7 type; ------ specific electrical losses; ——— total (electrical and mechanical) specific losses with various v.

The utilization of new information which has been obtained about the properties of electrical brush materials enables one to come near to the calculation of losses in a sliding contact with more foundation than previously. As is known, these losses generally accumulate from mechanical losses in friction ΔP_m; electrical losses dependent on the intermediate drop in voltage, ΔP_e and losses dependent on sparking, ΔP_s. Just as the third kind of losses in machinery working normally need not occur, it is customary to confine oneself to the

determination of volumes ΔP_m and ΔP_e, in the corresponding calculations, and the expression for ascertaining losses is utilized in the following way:

$$\Delta P = \Delta P_m + \Delta P_e. \tag{3}$$

Each of the terms which comprise the last expression are in their turn determined by means of the well-known formulae:

$$\Delta P_m = 9.81 qF\mu v; \tag{4}$$

$$\Delta P_e = 2\Delta UI, \tag{5}$$

where q – individual pressure (apparent) on electrical brushes kg/cm²

F – area of the cross-section (apparent) of every electrical brush, cm²;

I – current, passing through sliding contact, A.

Taking into consideration the special features of the constructional formation of the elements of the brush-commutator nodes of electrical machines by which the relationship between the area of all electric brushes of both polarities F and the magnitudes of j and I is presented in the following form:

$$F = \frac{2I}{j}, \tag{6}$$

we find the loss which refers to a unit of the area of a sliding contact produced by electrical brushes of both polarities. After conversion it is possible to obtain from formulae (1)-(6) an expression for specific losses in the following form:

$$\Delta P_{sp} = \frac{\Delta P}{\frac{1}{2}F} = 2 \cdot 9\,81 qv\,(C - Dv) + \\ + j\,(A + Bj)\ [w/cm^2]. \tag{7}$$

By substituting in the last formula the values of A, B, C and D it is possible to calculate the volume of the specific losses for the majority of cases encountered in practice where a sliding contact is employed.

Results of calculations obtained for electric brushes of types EG-4 and MGS-7 are represented in Fig. 1. The figure produced gives an entirely definite picture of the role of separate components in the overall specific losses and of the influence exerted by the operating conditions of sliding contact elements (speed, current density) on the character of the variation of these losses.

By using formula (7) we can also solve the problem of expediently selecting the area of a sliding contact, i.e. the total area of the brushes in a machine when the current load is given.

By examining formula (7) and Fig. 1, it can seem at first sight, that just as specific losses vary in proportion to the current density, so a reduction of total losses can be reached by selecting the low value of this density. In actual fact such a deduction proves to be inaccurate. In order to throw light upon this question from a correct point of view, it is essential to transform formula (7), having solved this in reference to total losses:

$$\Delta P = [2 \times 9.81 qv(C - Dv) + j(A + Bj)] \frac{I}{j} [w]. \tag{8}$$

By analysing the last formula it is possible to discover that certain optimum current densities exist, at which the losses in a sliding contact will be at a minimum, for the different values A, B, C and D, i.e. for the different types of electrical brush materials.

For an illustration of such a case let us determine the losses in the sliding contact of an electrical machine for any given current, e.g. $I = 100$ A. The results of appropriate calculations for electrical brush types EG-4, EG-14, M-3 and MGS-7 are shown in Fig. 3. It is evident from the figure that electrical losses continuously increase with the growth of current density in a sliding contact. As for the overall losses, they drop initially, reach a minimum, and only then begin to increase.

The nature of the variation of total losses which has been described is explained by the fact that a reduction of the necessary sectional area of electrical brushes and also, in conjunction with that, a reduction of the losses which depend on mechanical friction, occurs in accordance with the degree of increase in current density at a given I. While the reduction ΔP_m is more rapid than the growth of ΔP_e, total losses decrease. When the indicated relationship varies the total losses begin to increase and the appropriate curves take on a U-like form.

The regularity of the variation of total losses, strictly speaking, depends on the relationship of the volumes A, B, C and D (see formulae (1) and (2)). The influence of the term B is particularly important. In the case where $B > 0.02$, i.e. when the volt-ampere characteristic has a large gradient, the curves of total losses have a more or less clearly expressed minimum. If, however, $B < 0.02$, the growth of electrical losses cannot compensate for the diminution of mechanical losses and the graphs of total losses assume the shape described in Fig. 3*a*, *b* and *c*. The constructions shown here concern electrical brush materials of types MG-2, MGS and MG-6 in which the angular coefficient values of the volt-ampere

characteristic equation prove to be: $B = 0.01$; 0.008 and 0.01 respectively. In these instances it is no longer possible to observe the minimum points of the total losses. A similar effect also takes place for materials of the types MG, MG-4 and MGS-6.

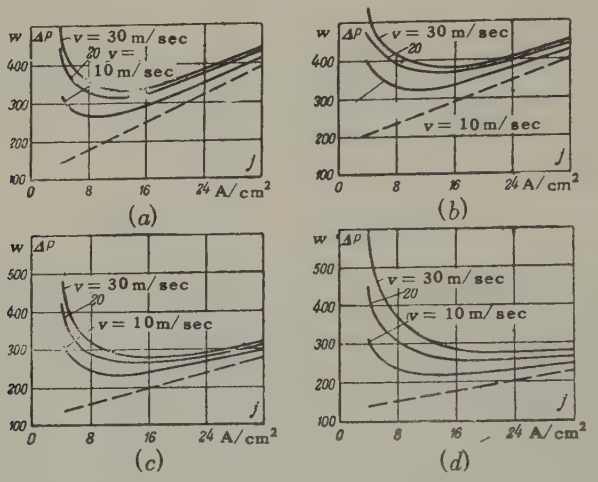

FIG. 2. Curves of dependence of total losses in the sliding contact of an electrical machine of a given output on current density.

a – EG-4 type of electrical brush material; *b* – EG-14 type; *c* – M-3 type; *d* – MGS-7 type. ------ electrical losses; ——— total (electrical and mechanical) losses with various *v*.

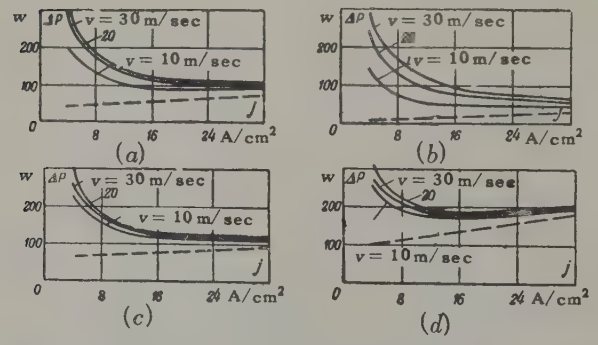

FIG. 3. Curves of dependence of total losses in the sliding contact of an electrical machine of a given output on current density.

a – MG-2 type of electrical brush material; *b* – MG-S type; *c* – MG-6 type; *d* – MGS-5 type. ------ electrical losses; ——— total (electrical and mechanical) losses with various *v*.

One more possible abnormality in the arrangement of curves of total losses is shown in Fig. 3*c* and *d*. Here a variation in the sequence of the arrangement of curves is implied, where the line representing $v = 30$ m/sec is lower than the line representing $v = 20$ m/sec. Such a case depends on the gradient angle of frictional characteristics. It arises in cases where $D < 0.005$ (materials of types EG-8, MG, MG-6 and MGS-5

The question of the minimum points of curves of total losses in a sliding contact of electrical machines has a practical value. The position of these can determine the nominal current density for each type of electrical brush, for only on this condition it is possible to talk about complete and expedient utilization of the potentialities of electrical brush materials.

Up to the present time no physical basis of the conception of a "nominal current density in the sliding contact of electrical machines" has existed. The values of appropriate magnitudes quoted in literature have been derived from the All-Union State Standard on brushes for electrical machines, [7], where they were established in 1943. It is natural that these values reflect the standard of utilization of electrical brush materials attained up to that time.

The new data set forth in this work has enabled us to contribute a definite physical significance to the idea of a nominal current density. By nominal current density in the sliding contact of electrical machines it is suggested that one should mean that current density at which the curve of total losses at a certain speed v will have its minimum value. The results of calculations of current density values, subject to the condition formulated where $v = 20$ m/sec, are shown in Table 1.

It follows from the table that for the "ferrous" (non-metal) types of electrical brush materials the nominal current density varies between 11 and 15 A/cm^2. For the "non-ferrous" (containing metal) types these increase to between 15 and 20 A/cm^2.

The results which have been obtained give a basis for a certain stepping-up of the current densities in the sliding contact of electrical machines in comparison with those which are standardized, GOST 2332-43. Such a recommendation primarily concerns machines having a small number of brushes operating in parallel.

TABLE 1

Type of electric brush materials	Current density according to All-Union state standard 2332-43 A/cm²	Nominal current density, determined from the condition of the minimum of total losses A/cm²
G-3	10...11	15
G-8	11	15
EG-2A	10	12
EG-4	12	12
EG-8	10	11
EG-14	10...11	14
M-1	15	18
M-3	12	16
M-6	15	16
M-20	12	15
MG	20	—
MG-2	20	—
MG-4	15	—
MG-6	18	—
MGS	20	—
MGS-5	15	16
MGS-6	15	—

Total loss curves for MG, MG-2, MG-4, MG-6, MGS and MGS-6 do not have a minimum.

TABLE 2

Values of volumes A, B, C and D in formulae for calculating the volt-ampere and frictional characteristics of electric brush materials.

Type of electric brush materials	A	B	C	D
G-3	1.20	0.05	0.23	0.005
G-8	1 00	0.08	0.20	0.002
EG-2A	1.50	0.10	0.21	0.003
EG-4	1.10	0.09	0.20	0.003
EG-8	1.90	0.07	0.21	0.005
EG-14	1.80	0.07	0.23	0.004
M-1	1.30	0.03	0.23	0.004
M-3	1.20	0.05	0 20	0.003
M-6	0.80	0.04	0.20	0.003
M-20	1.20	0.04	0.19	0.003
MG	0.16	0.007	0.22	0.005
MG-2	0.40	0.01	0.22	0.004
MG-4	0.50	0.02	0.21	0.004
MG-6	0.62	0.01	0.22	0.005
MG-5	0.04	0.008	0.18	0.002
MGS-5	0.90	0.03	0.21	0.005
MGS-6	1.20	0.02	0.17	0.001
MGS-7	1.30	0.03	0.17	0.001

Appendix

Instructions for the choice of brushes*

Type	Type of m/c
G 1, G 2, G 3, EG 4	Normal generators and motors of 110, 220 and 440 V
MG 2	Generators to 6 - 12 V
M 1, M 3, M 6, M 20, M 22	Generators and motors 25 - 60 V
EG 2, EG 6, EG 8, EG 10	Motors for rolling mills
G 3, EG 4	Generators for electrical welding
EG 2, EG 6, EG 8, EG 10	Traction motors
EG 2, EG 4, EG 8, EG 14, EG 83	Turbogenerators d.c.
G 3	Exciters of synchronous generators and motors
G 3, EG 4	Hydro-electric generator exciters
EG 4, EG 83	Turbogenerator exciters
MG, MG 2, M 1	Induction motors
G 3, MG 2	Synchronous generators and motors
EG 14, EG 83	Turbogenerators 3000 rpm

NB

G = Graphite
M = Copper
E = Electro-graphited
S = Silver

* Electrotechnical Handbook.

Translated by J.F. Boyland

REFERENCES

1. M.A. Shatelen, V.F. Mitkevich and V.A. Tolvinskii; *Spravochnaia kniga dlia elektrotekhikov (Handbook of Electric technology)* Vol. 5, pp. 84 - 86, 90 and 100 - 101 (1934).
2. M.P. Kostenko; *Elektricheskie mashiny (Electrical Machines)* pp. 135 - 136, Gosenergizdat (1949).
3. V.A. Tolvinskii; *Elektricheskie mashiny postoiannovo toka (Direct Current Electrical Machines)* pp. 381 - 382 and 394 - 395, Gosenergizdat (1956).
4. P.S. Livshits; *Tekhnicheskie kharakteristiki elektroshchetochnykh materialov, opredelennye statisticheskimi metodami. (Technical Characteristics of Electrical Brush Materials, Determined by Statistical Methods)* No. 5, VEP (1956).
5. P.S. Livshits; *Primenenie metodov matematicheskoi statistiki k izucheniiu svoistv metallokeramicheskikh kompozitsii. (Application of Mathematical Statistics' Methods to the study of the properties of Metallic-ceramic Compositions).* Sbornik "Poroshkovsia Metallurgia, 4, (1956).
6. P.S. Livshits; *Vol't-ampernye i friktsionnye kharakteristiki elektroshchetochnykh materialov (Volt-ampere and Frictional Characteristics of Electrical Brush Materials)* VEP, No. 2, (1958).

7. GOST 2332-43. *Shchetki dlia elektricheskikh mashin (Brushes for Electrical Machines)* Standartgiz, (1955).

ABSTRACTS FROM PAPERS PUBLISHED IN ELEKTRICHESTVO NO. 12, 1958

Determination of the recovery voltage form in transforming installations: N.M. Maslennikov. (pp 9 - 13)

The author presents a new and simple method of determining the shape of the recovery voltage curve in d.c. converter installations. The frequency and damping of the recovery voltage can be quickly determined in simple installations. Where the installations are more complex, it is advisable to use an oscillograph and a low powered equivalent circuit in which oscillations are excited. The results produced by the method have coincided well with experimental data. Damping oscillations due to losses in larger power installations were not taken into account. Five examples of the calculations are given and seven diagrams of circuits and oscillograms.

Electrical arc in longitudinal slits: O.B. Bron and L.A. Rodshtein. (pp 14 - 18)

Arc-extinction devices with narrow longitudinal slots are widely used in high- and low-voltage switchgear. The author considers new processes which have not yet been discussed and states more precisely and generally the results which have already been obtained. He considers the arc in a slot with flat parallel walls and in a ribbed slot. The results of the calculations point to the advantage of arc-extinction chambers with ribbed slots over slots with flat parallel walls. The author asserts that earlier works incorrectly used the photographic method of determining the speed of the arc in longitudinal slots. By making a cut in the walls of the slot they unsuspectingly raised the average longitudinal voltage gradient in the arc. This was discovered as the method of probes has been used for this investigation and not the photographic method.

Resonance transformer: A.A. Kosovskii. (pp 22 - 26)

High-voltage testing at line frequency of the insulation of objects such as hydro-electric generators and cables with great electrical capacitance involves difficulties due to the great reactive power required. It is therefore advisable to utilize the resonance between the capacitance of the test object and the inductance of the testing device, using the inductance of the resonance transformer without applying additional chokes (reactors). The author describes the design of this

transformer. It is characterized by its little weight, low consumption of current from the network, convenient tuning to resonance and by the sinusoidal shape of the secondary voltage.

Investigation of electrical circuits with non-linear inductance: S.P. Pivovarov. (pp 27-29)

When regulating and stabilizing voltage in relay, non-linear bridge starting and counting schemes etc, electrical circuits are employed which contain reactive coils with a ferromagnetic core, autotransformers and transformers, (i.e. elements with non-linear characteristics), the inductance of which depends on the amount of current. The author proposes a method of calculating the current and voltages of the basic and of the third harmonics.

Voltage regulation in low-voltage networks: N.K. Arkhipov. (pp 30-33)

A distribution transformer is a possible means of regulating voltage. The electrical industry is producing two types of distributor transformer with an output of from 20 to 560 MVA and automatic voltage regulation on load. The author considers the conditions in which these transformers can be applied with single and multi-step control. The degree of regulation in multi-step regulators determines the degree of accuracy of operation of the sensitive element (relay). The greater the accuracy, the less should be the degree of regulation. The author argues that a decrease of the degree of regulation is more economical, especially in metal. He uses a transformer with a 5 per cent degree of regulation to examine these questions and considers that the range of insensitivity of the switching device should be greater than the degree of regulation for stable operation. After considering such transformers he recommends the application of distribution transformers with two stage automatic voltage regulation, (5 per cent each stage) where practicable, and distribution transformers with multi-stage regulation (a larger number of finer stages). Transformer works should therefore produce 35 and 110 kV transformers of all dimensions with regulatable voltage on load and also additional-voltage transformers for 6-35 kV and low voltage.

A criterion of synchronous machine stability: I.D. Urusov. (pp 34-38)

The author considers that the usual methods of investigating rotor stability in the presence of small changes of angle θ using linearized equations ignore certain important physical factors which makes it difficult to evaluate their effect on stability and to investigate the process qualitatively. He therefore proposes a criterion of stability and a method of finding the roots of the characteristic equation which is directly based on the use of the "moment frequency characteristic" of a salient pole synchronous machine. This machine is provided (in order to improve

its damping properties, in addition to damping windings), with a stabilizing device called the "swing damping block" in which the first and second derivatives of angle θ are realized. An example of the calculations is given.

Investigation into the heating of series *A* and *OA* induction motors with a capacity ranging from 0.6 - 100 kW at the intermittent-duty conditions of their operations: P.A. Suiskii. (pp 44 - 45)

Average established temperature rises in the windings of induction motors are analysed by the method of "equivalent heating losses" for the case when the motors are being operated intermittently whereas the existing regulations in GOST 7217 - 54 provide for the use of the "resistance method" during half the subsequent period of operation. Average equivalent heating losses can be found from the relationship

$$P_{e.a} = P_{m1a} + k_{st\,a} P_{st\,a} + k_{m2a} P_{m2a} + k_{d\,a} P_{d\,a},$$

where P_{m1a}, $P_{st\,a}$, $P_{m2\,a}$ and $P_{d.a}$ are the average heating losses in the stator winding, in the stator steel, in the rotor and the additional losses on load W; $k_{st.a}$, $k_{2.a}$ and $k_{d.a}$ are the average heating loss factors. Formulae are also introduced for determining these coefficients. Examples of calculations carried out on motors are given. The difference in the results of the two methods is ± 5 per cent.

Change in load characteristics of magnetic amplifiers: V.S. Vysochanskii. (pp 49 - 51)

The author points to the disadvantages of magnetic amplifiers and the choice between expensive magnetic materials (permalloy, supermalloy, mumetal and so on) and special circuits to overcome there difficulties. The existing materials and circuits only partly overcome these difficulties. He therefore proposes a scheme for connexion of a magnetic amplifier on load with a standard voltage in the circuit and usual electro-technical steel which overcomes these difficulties completely. This scheme is represented diagrammatically. The scheme enables the load current of the amplifier to be equated to zero in any desired zone of change of input signals. The input current of the amplifier can pass through the load only after it attains a definite value because of the counter action of the standard voltage in the load circuit. In the presence of control signals outside the operating zone of the amplifier, all the current of the load windings is closed through a ballast resistance. In order to prevent the passage of the current through the load resistance when the voltage on the ballast resistance is less than the standard voltage, a semiconductor rectifier is connected in the load circuit. The author discusses the tests made on this device and its construction.

Maximum output of energy by induction motors when feeding the network: V.S. Mogilnikov. (pp 52-55).

When there is a short circuit in the network or a sudden voltage drop for other reasons, the induction motors are temporarily converted into a generating system and supply power to the network owing to the partial power decrease of the rotating rotor mass and mechanism. On the fault section, the power generated by the induction motors is added to the power which can be supplied from the network during the short circuit with the result that certain elements in the system are more stressed. The author sets out the conditions in which induction motors can supply maximum power to the network and proposes a formula for determining this power by a simplified method. Tests results on 'Ural' type motors are tabulated. An example of the calculation is given. He concludes that the power supplied to the network by induction motors decreases when the inductive resistance of the stator is increased. If the resistance of the stator circuit is increased, the power supplied first increases and then decreases. In the case of standard small and medium motors, the maximum power supplied is on average equal to the kinetic energy of the motor rotor at synchronous speed independently of the power of all the rotating masses of the drive.

Improved characteristics of arc-type steel furnaces: N.V. Okorokov. (pp 58-61)

A large number of works deal with the application of circular diagrams and operating characteristics to determine the optimum electrical conditions of an arc-type steel smelting furnace but these do not take into account one source of inaccuracy. Usually an equivalent network is used for the phase of the furnace, according to which, the usual resistance of the phase is merely the arc resistance, R_a. Therefore in the presence of a short-circuit of the arc, the useful resistance of the furnace R_u and the resistance of the arc are zero $R_u = R_a = 0$. Likewise the active power introduced into the furnace is zero.

$$P_u = P_a = 0$$

Accordingly, diagrams are shown for the circular diagram of one phase and the operating characteristics, both of which take the heat losses of the furnace into account and are true for a symmetrical circuit. In effect, the larger part of the electrode is inside the furnace and an active power is produced there which must be included in the active furnace power P_u, but the resistance of this section of the electrode r_e must be regarded as part of the useful resistance of the furnace R_u:

$$R_u = R_a + r_e$$

The equivalent network for one phase changes and the furnace power P_u equals the sum of the arc power P_a and the power produced in the resistance r_e:

$$P_u = P_a + I^2 r_e$$

Thus R_u can vary from infinity on no load to r_e (but not to zero) in the presence of a short circuit of the arc. The ramifications of this refinement are considered mathematically and diagrammatically and tests on ore reduction furnaces (iron smelting, carbides etc) are considered.

Method of studying power distribution in ore-refining furnaces: B.M. Strunskii. (pp 62-66)

The author reviews the existing differences of opinion on how to determine the amount and distribution of power in the hearth of an electrical ore-reduction furnace. He concentrates his attention on electrical schemes of the hearths of ferrosilicium and carbide furnaces and describes an experimental method of determining the distribution of power in the hearth. The tests made to verify this method are also described. He shows the scheme of a furnace when the position of the electrode is normal and the load is 20,000 A. When the electrode is raised to a high position and the load is reduced he shows the new scheme that would be necessary. The arcs burn between the side surface of the electrode and the hearth walls independently of the position of the electrode. There is no arc between the face of the electrode and the melt. When the electrode is in a lower position and the load is raised, the electrode sinks into the melt.

Measures for reducing the currents branching off into ground: A.S. Skuratov. (pp 67-71)

A survey is made of measures to be taken to reduce stray earth currents in underground metal equipment. The problem of protecting underground equipment from corrosion is not tackled. The author points to the increase of stray currents accompanying the increased length of railway lines in the presence of supply at one end and considers decentralized supply, parallel operation of substations, normalized voltage drop in the rails and increased transient resistance of the rails-earth (by insulation e.g. bitumin, water repellent earth covering), but finds none of these measures satisfactory. The author then advocates the two-conductor contact network for tramlines and the Underground with doubled supply voltage. He considers the pros and cons of this system and compares the capital and operating cost and power losses of single and double conductor contact networks. The conclusion is drawn that it is worthwhile to lay an experimental two conductor contact network and to see if any great operating difficulties arise.

Automatic arrangement for mutual reservation of low-voltage power supply sources I.I. Zhigachev. (pp 71 - 76)

Present day trends favour the extensive use of automatic reclosure. Continuity of supply is improved by automatic mutual reservation of two supply sources. The author describes certain schemes developed with a two-end automatic reclosure device. The schemes are applicable to any configurations of a network with sources operating separately at a different power. The different schemes are said to be simple and the apparatus can be employed on existing gear. The schemes are represented diagrammatically.

Hysteresis coupling for frequency stabilization: A.N. Larionov and V.G. Morozov. (pp 76 - 78)

The results are given of tests on asynchronous and hysteresis couplings without windings for stabilizing the frequency of a low-power synchronous generator excited by permanent magnets. The problem was to stabilize frequency at an output of 300 VA with an accuracy of ± 0.5 per cent, when the speed of the drive varied ± 5 per cent and in the presence of a possible 30 per cent load reduction. In fact the use of a resonance frequency stabilizer obtained frequency stability of ± 0.2 per cent. Compared with the d.c. generator-converter system, the hysteresis coupling method is 20 per cent lighter in weight and has a higher efficiency (70 per cent compared with 40 per cent). The hysteresis coupling system can be used for an output of 500 VA, in the presence of a 30 - 40 per cent load reduction and at speeds over 600 rev/min.